Experimental studies of turbulent flames at gas turbine relevant burners and operating conditions

Liu, Xin

2021

Document Version:
Publisher's PDF, also known as Version of record

Experimental studies of turbulent flames at gas turbine relevant burners and operating conditions

XIN LIU
DEPARTMENT OF PHYSICS | FACULTY OF ENGINEERING | LUND UNIVERSITY

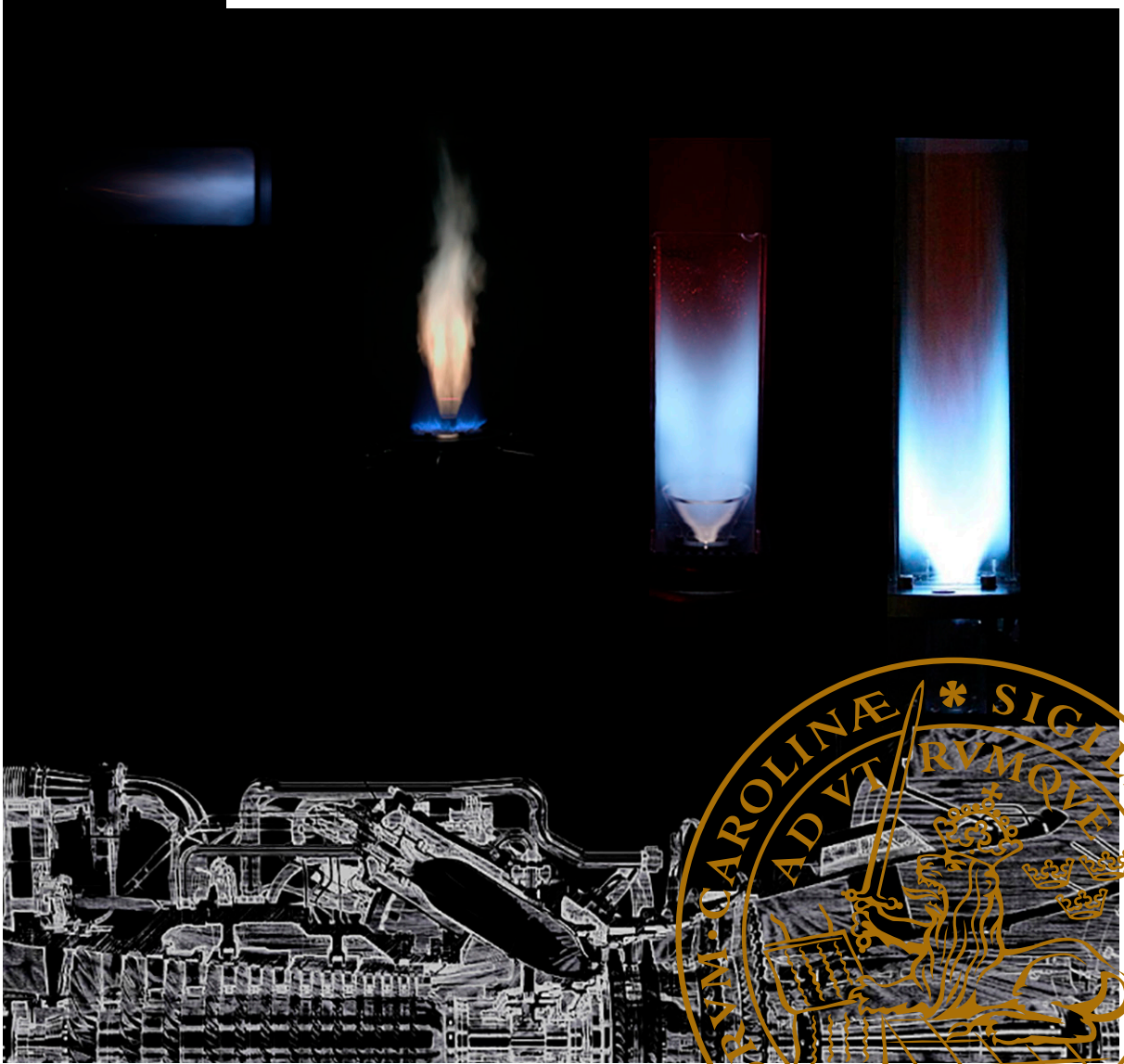

Printed by Media-Tryck, Lund 2021 NORDIC SWAN ECOLABEL 3041 0903

Faculty of Engineering
Department of Physics
Division of Combustion Physics

Lund Reports on Combustion Physics: LRCP-229
ISRN LUTFD2/TFCP-229-SE
ISBN 978-91-7895-824-5
ISSN 1102-8718

Experimental studies of turbulent flames at gas turbine relevant burners and operating conditions

Experimental studies of turbulent flames at gas turbine relevant burners and operating conditions

Xin Liu

LUND
UNIVERSITY

DOCTORAL DISSERTATION
by due permission of the Faculty of Engineering, Lund University, Sweden.
To be defended at Rydbergssalen, Professorsgatan 1, Lund. Date 23rd Apr. 2021, at 13:15.

Faculty opponent
Dr. Nabiha Chaumeix
CNRS-ICARE, Orléans, France

Organization LUND UNIVERSITY Division of Combustion Physics P.O.Box 118 SE-221 00 Lund, Sweden	**Document name** DOCTORAL DISSERTATION **Date of issue** 2021-04-23
Author(s): Xin Liu	Sponsoring organization

Title and subtitle: Experimental studies of turbulent flames at gas turbine relevant burners and operating conditions

Abstract

With the increasing demand of using alternative and renewable fuels, it becomes of vital importance to consider the fuel flexibility when designing a new burner for gas turbines. Hydrogen-enriched fuel and ammonia are two of these potential fuels, and they can significantly change the operability range of the gas turbines. Thus, it is necessary to enhance both the fundamental understanding on turbulent combustion of these fuels and their combustion performance in practical combustors. Due to its advantages of in-situ measurement, non-intrusiveness and high spatial and temporal resolution, laser-based diagnostics technology has been regarded as one of the best measurement methods for researching combustion processes and phenomena. In this thesis work, experimental studies have been conducted to investigate the turbulent flames of different fuels at various gas turbine related burners, employing laser diagnostics measurement. The measurement methods include planar laser-induced fluorescence (PLIF) for various species, particle image velocimetry (PIV), laser doppler anemometry (LDA), etc.

A newly designed gas turbine model combustor had been developed at the Swedish National Centre of Combustion and Technology, so it was named the CECOST burner. One of the main objectives of this thesis is to improve the premixing effect of the CECOST burner by changing part of its internal configuration and investigate its fuel flexibility by using natural gas and hydrogen-enriched methane mixtures as fuels. The experiment was conducted at an atmospheric rig, and high-speed OH^* chemiluminescence imaging, simultaneous OH-/CH_2O PLIF, and PIV were employed. The operability range and flame structures were investigated for different fuels at various Reynolds numbers (Re). The operability range was found to be highly sensitive to Re, as well as the fuel. For natural gas/air flames, the lean blowout (LBO) limit was approximately independent of Re, while flashback showed obvious dependence on Re and no flashback was observed for higher Re. For hydrogen-enriched methane/air flames, a comparison of combustion characteristics between pure methane and hydrogen-enriched methane with two mixing ratios, 25% and 50% in volume, was investigated. It was found that the flame stabilized in an M shape for all pure methane/air flames, whereas the flame shape transits to a Π shape at a specific equivalence ratio (ϕ) for hydrogen-enriched methane flames. Besides, the flashback events with two different mechanisms, combustion-induced vortex breakdown (CIVB) and boundary-layer flashback, were observed. By statistical analysis, we can get that the CIVB flashback took place only for pure methane flames with M shape, while the boundary-layer flashback happened for all hydrogen-enriched flames with Π shape.

Aiming to achieve stable combustion in lean conditions, a plasma-assisted flame control system is a potential way to help stabilize the flame. An industrial gas turbine combustor, known as Siemens dry low emission (DLE) burner, was modified to place a high-voltage electrode in the rich-pilot-lean (RPL) section and was used for investigation of a rotating gliding arc (RGA) discharge effect on swirl flames stabilized in the gas turbine combustor. In the unmodified DLE burner configuration, fuel and air are injected into the RPL to hold a premixed flame which can help stabilizing the main flame, but in the modified configuration, only air/O_2 was injected into the RPL. The flame emissions were measured by a gas sampling probe and emission analyzer. The CO emission results were used to identify the improvement of the LBO limit with plasma assistance. NO_x emissions were slightly increased by the RGA plasma, but still, less than the same main flame with RPL flame assisted. Flame emission spectra were also measured.

Ammonia combustion is recently one of the hot research topics due to its promising future of carbon-free emission. To deepen our knowledge on turbulent ammonia flames, a jet burner with a large scale was constructed and used to investigate the flame structure of premixed ammonia/air flames, by employing simultaneous OH-/NH-PLIF and LDA measurements. Most of the studied flames are located in the regime of the distributed reaction zone (DRZ), determined by their Karlovitz numbers that are larger than 100. Results of simultaneous OH-/NH-PLIF show that the NH and OH layer can coexist in a thin boundary and the NH signal appears evolving to the reactants side.

In addition, the practical gas turbine combustors are all operated at elevated pressure conditions, but it is not easy to perform an experiment at elevated pressure in the lab. A co-axial jet burner was installed and studied in the high-pressure combustion rig (HPCR) at Lund University to investigate the characteristics of methane/air inverse diffusion flames (IDF) at elevated pressure (up to 5 bar). The flame structure and its lift-off height influenced by pressure increasing were discussed. More wrinkles and larger curvature of the flame front were found in the inner flame structure at higher pressure.

Key words: Turbulent combustion, gas turbine, laser diagnostics, fuel flexibility, plasma-assisted combustion, ammonia flames, high-pressure

Classification system and/or index terms (if any)

Supplementary bibliographical information		**Language** English
ISSN and key title 1102-8718		**ISBN** 978-91-7895-824-5 (print) 978-91-7895-823-8 (pdf)
Recipient's notes	**Number of pages** 212	Price
	Security classification	

Signature Xin Liu Date 2021-03-17

Experimental studies of turbulent flames at gas turbine relevant burners and operating conditions

Xin Liu

LUND
UNIVERSITY

Coverphoto by Xin Liu

Faculty of Engineering, Department of Physics
Division of Combustion Physics

Lund Reports on Combustion Physics: LRCP-229
ISBN 978-91-7895-824-5 (print)
ISBN 978-91-7895-823-8 (pdf)
ISSN 1102-8718
ISRN LUTFD2/TFCP-229-SE

Printed in Sweden by Media-Tryck, Lund University
Lund 2021

To my late maternal grandpa, for encouraging me to pursue science and the endless love for me

To my beloved mom and dad, for always supporting and taking good care of me with your unconditional love.

草木本心

無問西東

Abstract

With the increasing demand of using alternative and renewable fuels, it becomes of vital importance to consider the fuel flexibility when designing a new burner for gas turbines. Hydrogen-enriched fuel and ammonia are two of these potential fuels, and they can significantly change the operability range of the gas turbines. Thus, it is necessary to enhance both the fundamental understanding on turbulent combustion of these fuels and their combustion performance in practical combustors. Due to its advantages of in-situ measurement, non-intrusiveness and high spatial and temporal resolution, laser-based diagnostics technology has been regarded as one of the best measurement methods for researching combustion processes and phenomena. In this thesis work, experimental studies have been conducted to investigate the turbulent flames of different fuels at various gas turbine related burners, employing laser diagnostics measurement. The measurement methods include planar laser-induced fluorescence (PLIF) for various species, particle image velocimetry (PIV), laser doppler anemometry (LDA), etc.

A newly designed gas turbine model combustor had been developed at the Swedish National Centre of Combustion and Technology, so it was named the CECOST burner. One of the main objectives of this thesis is to improve the premixing effect of the CECOST burner by changing part of its internal configuration and investigate its fuel flexibility by using natural gas and hydrogen-enriched methane mixtures as fuels. The experiment was conducted at an atmospheric rig, and high-speed OH^* chemiluminescence imaging, simultaneous OH-/CH_2O PLIF, and PIV were employed. The operability range and flame structures were investigated for different fuels at various Reynolds numbers (Re). The operability range was found to be highly sensitive to Re, as well as the fuel. For natural gas/air flames, the lean blowout (LBO) limit was approximately independent of Re, while flashback showed obvious dependence on Re and no flashback was observed for higher Re. For hydrogen-enriched methane/air flames, a comparison of combustion characteristics between pure methane and hydrogen-enriched methane with two mixing ratios, 25% and 50% in volume, was investigated. It was found that the flame stabilized in an M shape for all pure methane/air flames, whereas the flame shape transits to a Π shape at a specific equivalence ratio (ϕ) for hydrogen-enriched methane flames. Besides, the flashback events with two different mechanisms, combustion-induced vortex breakdown (CIVB) and boundary-layer flashback, were observed. By statistical analysis, we can get that the CIVB flashback took place only for pure methane

flames with M shape, while the boundary-layer flashback happened for all hydrogen-enriched flames with Π shape.

Aiming to achieve stable combustion in lean conditions, a plasma-assisted flame control system is a potential way to help stabilize the flame. An industrial gas turbine combustor, known as Siemens dry low emission (DLE) burner, was modified to place a high-voltage electrode in the rich-pilot-lean (RPL) section and was used for investigation of a rotating gliding arc (RGA) discharge effect on swirl flames stabilized in the gas turbine combustor. In the unmodified DLE burner configuration, fuel and air are injected into the RPL to hold a premixed flame which can help stabilizing the main flame, but in the modified configuration, only air/O_2 was injected into the RPL. The flame emissions were measured by a gas sampling probe and emission analyzer. The CO emission results were used to identify the improvement of the LBO limit with plasma assistance. NO_x emissions were slightly increased by the RGA plasma, but still, less than the same main flame with RPL flame assisted. Flame emission spectra were also measured.

Ammonia combustion is recently one of the hot research topics due to its promising future of carbon-free emission. To deepen our knowledge on turbulent ammonia flames, a jet burner with a large scale was constructed and used to investigate the flame structure of premixed ammonia/air flames, by employing simultaneous OH-/NH-PLIF and LDA measurements. Most of the studied flames are located in the regime of the distributed reaction zone (DRZ), determined by their Karlovitz numbers that are larger than 100. Results of simultaneous OH-/NH-PLIF show that the NH and OH layer can coexist in a thin boundary and the NH signal appears evolving to the reactants side.

In addition, the practical gas turbine combustors are all operated at elevated pressure conditions, but it is not easy to perform an experiment at elevated pressure in the lab. A co-axial jet burner was installed and studied in the high-pressure combustion rig (HPCR) at Lund University to investigate the characteristics of methane/air inverse diffusion flames (IDF) at elevated pressure (up to 5 bar). The flame structure and its lift-off height influenced by pressure increasing were discussed. More wrinkles and larger curvature of the flame front were found in the inner flame structure at higher pressure.

Popular science

Until now, more than 80% of the global total energy is still derived from the combustion of fossil fuels. Combustion is widely used and plays vital roles in human's modern life, industrial production, aerospace engineering, etc. Most of the heating in life comes from combustion or electricity generated by combustion. And almost all of the transportation systems are driven by the energy from combustion. However, the downside brought by combustion is environmental pollution and fire hazard. The main pollutants from combustion include unburned hydrocarbon (UHC), nitrogen oxides (NO_x), sulfur oxides (SO_x), carbon monoxide (CO), carbon dioxide (CO_2), and particulates. These pollutants are the main source of the acid rain and greenhouse effect, which harm human health as well as the growth of animals and plants, and even affect the ecological balance. Besides, the combustion process heavily depends on fossil fuels, which sources are limited and non-renewable. To meet the huge energy needs of society, the demand for developing and using more alternative renewable energy resources and improving existing combustion devices with higher combustion efficiency and low emissions has increased dramatically.

In most practical devices, e.g., internal engines and gas turbines, combustion is no longer just an oxidation reaction process but is a complicated process involving turbulent flow, heat transfer, and mass transfer. Furthermore, combustion does not occur at room temperature and atmospheric pressure, but under more severe conditions with high temperature and elevated pressure. The gas turbine is a versatile industrial combustion device, which can be used in power generation, aviation, and other related industries. It consists of three main modules: a compressor, a combustor, and a turbine, which are connected by one or more shafts. The gas turbine transfers the chemical energy in the fuel into the rotational mechanical energy of the turbine shaft. Considering the higher requirement on the performance of modern gas turbines, such as high combustion efficiency, low emissions, and fuel flexibility, acquiring comprehensive knowledge and conducting in-depth research on the combustion process in combustors relevant to gas turbines are very important. Especially, it is challenging to perform the experimental investigation in a practical gas turbine combustor.

Due to the severe environment for taking measurements inside the combustor, laser diagnostics are regarded as the best method because of their in-situ, non-intrusive, and high spatial and temporal resolution. By advanced laser techniques, many parameters are available to measure, e.g., temperature, various species

concentration, velocities. Simply put, for most laser diagnostics, a laser source with high intensity is used shooting through an area/point in the objective flame. Then a specific signal, which comes from the photonic activity excited by the laser and has somehow mathematical correlation to the parameter that we want to measure, can be captured by a detector (such as a camera). The duration of the laser pulse is short enough to provide us the information on what happened in a freezing moment. The development and application of laser techniques in the combustion process provide not only a lot of possibility for taking the measurement in complicated combustion devices, but also the data for validating the combustion model in the numerical study.

In this thesis work, experimental studies were performed in several different burners, which are related to gas turbine combustor or under gas turbine relevant operating conditions. Various laser diagnostics were employed to measure different parameters in flames, e.g., planar laser-induced fluorescence (PLIF), particle image velocimetry (PIV), and laser doppler anemometer (LDA). A gas turbine model combustor with a swirler in the cone shape, named after the CECOST burner, was utilized to investigate its optimal performance and fuel flexibility. The mixing of this burner has been improved through lots of tests, and the fuel flexibility was studied by using natural gas and hydrogen-enriched methane mixtures as fuels. Completely new research has been conducted on an industrial gas turbine combustor, named after Siemens Dry Low Emission burner, aiming to achieve stable lean combustion and low emission by introducing a plasma source in the burner. This experiment is a brand-new attempt, and no one has seen it before. Besides, the characteristics of turbulent premixed ammonia combustion were studied on a large-scale jet burner. Ammonia is a potential carbon-free fuel in the future, and a fundamental understanding of its combustion process and characteristics in the turbulent flow are still needed. This experiment was believed to fill part of the gap in this field. I also got a short opportunity during my PhD study to conduct research at the high-pressure rig, in which experiment was challenging than that in the atmospheric rig and rarely reported in the literature. Achievements from all of my works are attached in the list of papers, many of them have been published in academic journals or proceedings of international conferences.

List of papers

I. E. Hodzic, S. Yu, A. A. Subash, **X. Liu**, X. Liu, R. Z. Szasz, X. S. Bai, Z. S. Li and M. Aldén. Numerical and experimental investigation of the CECOST swirl burner.

In Proceedings of the ASME Turbo Expo 2018, Volume 4A: Combustion, Fuels and Emissions, GT2018-75760

II. A. A. Subash, S. Yu, **X. Liu**, M. Bertsch, R. Z. Szasz, Z. S. Li, X. S. Bai, M. Aldén and D. Lörstad. Flame investigations of a laboratory-scale CECOST swirl burner at atmospheric pressure conditions.

Fuel, Vol. 279, 118421, 2020

III. **X. Liu**, M. Bertsch, A. A. Subash, S. Yu, R. Z. Szasz, Z. S. Li, P. Petersson, X. S. Bai, M. Aldén and D. Lörstad. Investigation of turbulent premixed methane/air and hydrogen-enriched methane/air flames in a laboratory-scale gas turbine model combustor.
Accepted for publication in International Journal of Hydrogen Energy

IV. Q. S. Fan, **X. Liu**, A. A. Subash, C. Brackmann, M. Aldén, X. S. Bai and Z. S. Li. Flame structure and burning velocity of ammonia/air turbulent premixed flames at extreme conditions.
Manuscript to be submitted.

V. **X. Liu**, A. A. Subash, Y. P. Bao, T. Hurtig, Z. S. Li, A. Ehn, J. Larfeldt, D. Lörstad, T. Nilsson and C. Fureby. Experimental investigation of plasma discharge effect on swirl flames at a scaled Siemens Dry Low Emission burner.
In Proceedings of the AIAA SciTech Forum, 2021.

VI. A. A. Subash, **X. Liu**, Y. P. Bao, T. Hurtig, A. Ehn, J. Larfeldt and C. Fureby. Experimental investigation of the influence of plasma discharge on flame characteristics at a Siemens Dry Low Emission industrial burner under atmospheric conditions.
Manuscript to be submitted.

VII. **X. Liu**, A. A. Subash, Q. S. Fan, C. Brackmann, J. Evers, M. Aldén and Z. S. Li. Visualization of turbulent inverse diffusion flames at elevated pressure using OH-PLIF and OH^* chemiluminescence imaging.
In Proceedings of the 9th European Combustion Meeting, Lisboa, Portugal, 2019.

Related work

A. Q. S. Fan, J. L. Gao. **X. Liu**, B. Li, E. Kristinsson, M. Aldén and Z. S. Li. Sensitive CH3 imaging for flame front structure visualization in premixed flames over broad stoichiometric ratios.
Manuscript to be submitted.

B. D. Kong, Q. S. Fan, **X. Liu**, A. A. Subash, T. Hurtig, A. Ehn, M. Aldén and Z. S. Li. Non-thermal gliding arc discharge assisted turbulent combustion (up to 80 kW) at extended conditions: phenomenological mechanism.
Manuscript to be submitted.

C. Q. S. Fan, **X. Liu**, X. Cai, C. Brackmann, M. Aldén, X. S. Bai and Z. S. Li. Flame structure of ammonia/air premixed flames under high Ka number conditions.
Manuscript to be submitted.

D. S. Yu, A. A. Subash, **X. Liu**, M. Bertsch, R. Z. Szasz, X. Liu, X. S. Bai, Z. S. Li, M. Aldén and D. Lörstad. Numerical and experimental studies on blow-off and flashback process of lean-premixed swirl flames.
Manuscript to be submitted.

E. A. A. Subash, **X. Liu**, Y. P. Bao, T. Hurtig, A. Ehn, J. Larfeldt and Christer Fureby. A rotating gliding arc (RGA) discharge in a scaled Siemens dry low emission (DLE) burner.
Manuscript to be submitted.

F. C. Brackmann, **X. Liu**, S. J. Xu, Y. Qian, Z. S. Li and M. Aldén. Investigation of NO formation in DME-NH_3 combustion at elevated pressure
Manuscript in preparation.

Abbreviations

BLF	Flashback in the boundary layer	**LUPJ**	Lund University Piloted Jet
CCD	Charge-coupled device	**MCP**	Micro-channel plate
CECOST	Swedish National Centre for Combustion and Technology	**NDF**	Normal diffusion flame
CIVB	Combustion-induced vortex breakdown	**Nd: YAG**	Neodymium-doped Yttrium Aluminium Garnet
CMOS	Complementary metal-oxide semiconductor	**ORZ**	Outer recirculation zones
CRZ	Center recirculation zone	**OSL**	Outer shear layer
DLE	Dry low emission	**PAC**	Plasma-assisted combustion
DRZ	Distributed reaction zone	**PDF**	Probability density function
GTMC	Gas turbine model combustor	**PIV**	Particle image velocimetry
HPC	High-pressure combustion	**PLIF**	Planar laser-induced fluorescence
HV	High voltage	**PM**	Possibility map
IA	Interrogation areas	**POD**	Proper Orthogonal Decomposition
ICCD	Intensified charge-coupled device	**PVC**	Precessing vortex core
IDF	Inverse diffusion flame	**RGA/GA**	Rotational gliding arc
IDJ	Inverse diffusion jet	**RMS**	Root mean square
IRZ	Inner recirculation zones	**RPL**	Rich-Pilot-Lean central-body sector
LBO	Lean blowout	**SLR**	Single-lens reflex
LDA	Laser doppler anemometer	**UHC**	unburned hydrocarbon
LIF	Laser-induced fluorescence		

Nomenclature

C_K	Kolmogorov constant	τ_{flow}	flow resident time
Da	Damköhler number	τ_η	Kolmogorov time scale
f	Focus	$\overline{U_y}$	average axial velocity
h	enthalpy	$\overline{U_t}$	average tangential velocity
I	Turbulence intensity	**u'**	turbulent fluctuated velocity
Ka	Karlovitz number	u	fluid velocity
κ	wavenumber	μ	dynamic viscosity
L	characteristic length scale	u_η	Kolmogorov velocity scale
l_0	Integral scale	**V**	Volume
P	Pressure	$\mathbf{V_r}$	velocity ratio
ρ	Density	ν	kinetic viscosity
R	equivalent nozzle radius	ϕ	Equivalence ratio
Re	Reynolds number	λ_t	Taylor length
Re_t	Turbulent Reynolds number	ε	spectral transfer per unit time
S	Swirl number	η	Kolmogorov length scale
$\mathbf{S_L}$	Laminar flame speed	δ_L	Laminar flame thickness
T	Temperature	$\delta_{L,NH}$	NH layer thickness
τ_{chem}	chemical time scale		

Table of Contents

1 Introduction

1.1 Motivation

Nowadays, more than 80% of the world's total energy is supplied by combustion. Combustion plays an indispensable role in our daily life, such as heating, transportation (road, rail, and air), aerospace propulsion, electricity generation, industrial processing, waste incineration, etc. But in the meantime, exhaust emissions from the combustion process are the main source of global air pollutions. Following the latest data from the International Energy Agency [1], Figure 1.1 (source from [2]) presents the global energy needed in 2019 and the forecast until 2040. It can be seen that fossil fuels e.g., oil, natural gas, and coal, are still dominant in the energy source for the future 20 years as in the past, while a significant increase can be found in the demand for renewable energy as well as other clean energies, such as nuclear, solar, and hydrogen. Since fossil fuels are limited and non-renewable, it is crucial to improve combustion efficiency and look for alternative renewable energy sources to meet the energy demand.

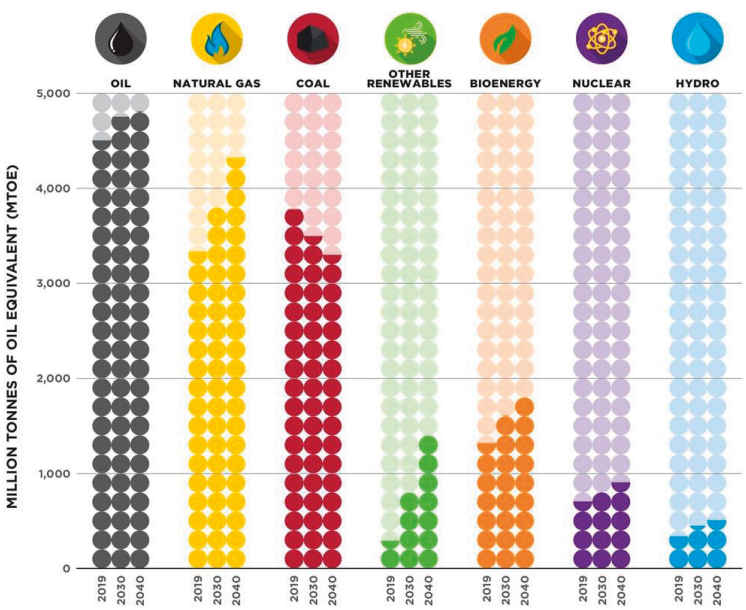

Figure 1.1: Changes in the global energy demand in 2019-2040. [2]

Combustion commonly occurs in turbulent flows in most practical combustion devices, such as gas turbine combustors and internal engines. Turbulence can accelerate the combustion process by rapid heat and mass transfer which further enhance the mixing of fuel and air and enables combustion to take place in a smaller combustor. As a versatile industrial combustion device, gas turbines are widely used in power generation, aviation, etc. Increasing concerns about more severe global environmental issues and the depletion of fossil energy sources have put forward higher requirements for the design and development of modern gas turbines, including high combustion efficiency, low emissions, and fuel flexibility.

Lean premixed combustion has been developed for gas turbine combustors to achieve a significant decrease in flame temperature and thus thermal NO_x emissions. But problems that come with it are unstable combustion, decreased combustion efficiency, lean blowout, and flashback. To stabilize the lean premixed combustion and ensure a lower NO_x emission level, adding a diffusion pilot flame and a pre-chamber combustor in the burner design are efficient ways [3] and applying a plasma-assisted flame control system can be another potential method [4].

In addition, improving the fuel flexibility for the gas turbine combustors is of great importance, by which gas turbines can operate safely with cleaner or renewable fuels, such as using gaseous fuel with a high proportion of hydrogen, or even applying ammonia as fuel.

1.2 Objectives

This thesis work aims to investigate typical turbulent flames in gas turbine relevant combustors or flames at gas turbine related conditions by using various laser-based measurements. Laser diagnostics techniques have great advantages in studying combustion phenomena, providing measurements featured as in-situ, non-intrusive, and high temporal-spatial resolutions.

The primary objective of this thesis is to study the characteristics of turbulent flames stabilized in a gas turbine model combustor and to develop the fuel flexibility of the burner. Natural gas and hydrogen-enriched methane mixtures are to be used as fuels to investigate the burner stability regime, flame structures, and flame in the transition process. Also, the application of the gliding arc discharge plasma in a scaled gas turbine combustor is another objective. A modified Siemens DLE burner equipped with an electrode in the RPL section was used to generate the discharge in the burner and to study the effect of plasma on the flame stabilization, LBO limits as well as emissions. Besides, the turbulent premixed ammonia/air flames stabilized in a large-scale piloted jet burner were investigated to gain a deeper understanding on the characteristics of ammonia flames and the flame behaviours, especially when pushing to the regime of the distributed reaction zone.

1.3 Thesis outline

This doctoral thesis consists of six chapters:

Chapter 1: Introduction on the motivations and objectives of the thesis.

Chapter 2: An overview of the experimental methods and equipment involved in the work of this thesis, including the laser diagnostics techniques and equipment systems.

Chapter 3: Descriptions of the experimental test rigs, burner component, and flow path. An atmospheric pressure test rig, a high-pressure combustion rig, as well as four different burners, are included.

Chapter 4: Discussions on flame investigations at gas turbine relevant combustors. A brief overview of the fundamentals of gas turbine combustion is included. Results of the work reported in Paper I-III and Paper V-VI are summarized.

Chapter 5: Discussions on applications of diagnostics on the investigations of turbulent jet flames. Fundamentals of turbulent flames are briefly introduced. Results of the work reported in Paper IV and Paper VII are summarized.

Chapter 6: Summary of the concluding remarks in the thesis and suggestions on the future work.

2 Measurements and optical diagnostics

An overview of the experimental methods and equipment involved in the work of this thesis is presented in this chapter. The measurement techniques employed in the experiments include planar laser-induced fluorescence (PLIF) on various species, particle image velocimetry (PIV), laser Doppler anemometer (LDA), flame chemiluminescence imaging, optical emission spectroscopy, and combustion emission sampling. The optical equipment used in these measurements, including lasers, detectors, and laser sheet forming optics, are also demonstrated.

2.1 Measurement techniques

2.1.1 Planar laser-induced fluorescence (PLIF)

Laser-induced fluorescence (LIF) is an optical spectroscopic technique, being widely used in combustion diagnostics. It is capable of detecting the concentrations of flame radicals, other combustion intermediates, and pollutant species down to sub-ppm level due to its high sensitivity, as well as monitoring parameters such as temperature, velocity, etc [5]. Generally, the principle of the LIF process includes two steps. Firstly, the specific kinds of atoms or molecules at the ground state are excited to higher energy levels by a laser excitation where the beam wavelength is tuned to a fixed specific resonant frequency. This absorption process is followed by an emission process from the fluorescence emitted by the excited atoms or molecules as they are unstable at the excited state and then returning to their ground state. A schematic representing the LIF process with the typical energy diagram of a diatomic molecule (e.g., OH, NH, etc) is shown in Figure 2.1. More details about the LIF technique can be found in reference [6].

For two-dimensional (2D) visualization, the planar laser-induced fluorescence (PLIF) has been employed, in which the incident laser beam is made into a laser sheet through a set of optical lenses to illuminate the measured area. The fluorescence signal is collected by a gated, intensified CCD camera, locating perpendicular to the laser sheet plane. A filter is set in front of the camera lens to

block spurious scattered light. Since PLIF has a high temporal resolution in the nanoseconds level and the spatial resolution is usually in the order of ~ some hundreds μm, it becomes a powerful tool for combustion studies in practical applications.

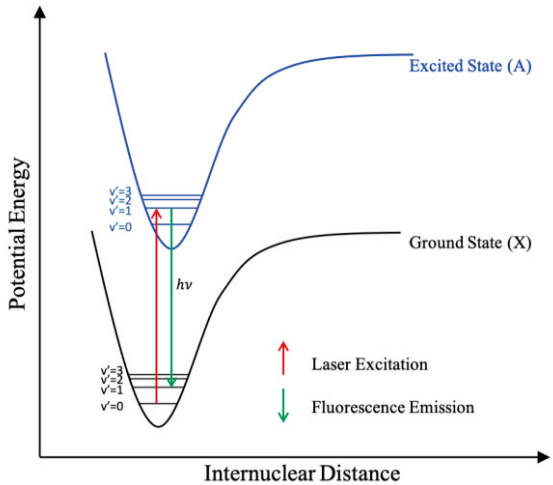

Figure 2.1: Schematic of a typical energy diagram for a diatomic molecule and presentation of LIF process.

For employing the PLIF technique, crucial radicals with proper fluorescence properties are to be selected to provide useful information in combustion. Visualization of the reaction zone in the flame provides a better understanding of turbulent combustion. Based on the well-known results from chemical kinetics, several intermediate species have been chosen as proper markers of the flame front (i.e., reaction zone), such as OH, CH, HCO, and $CH_2O \times OH$. In addition, one of the most important parameters needed to be measured in a gas turbine combustor is the fuel concentration distribution [7]. For gaseous flows, acetone (CH_3COCH_3) can be regarded as an ideal tracer due to its high vapor pressure and proper optical properties. In this thesis, PLIF measurements on different species, in which some are measured simultaneously, were conducted in different turbulent flames. The strategies of PLIF measurement for different species involved in this thesis are summarized in Table 2.1.

Table 2.1: Summary of the PLIF measurement on different species involved in this thesis work.

Species	Excitation wavelength	Lasers	Pulse energy	Fluorescence wavelength	Filter
OH	~283 nm	Dye laser (Rh590)	14~16 mJ	~310 nm	UG11 & WG305
CH_2O	355 nm	3rd harmonic of Nd:YAG	~120 mJ	380 – 550 nm	GG395
NH	~303.6 nm	Dye laser (Rh610+Rh640)	~8.5 mJ	>335 nm	WG335
Acetone	266 nm	4th harmonic of Nd:YAG	~60 mJ	350 – 500 nm	-

2.1.2 Particle image velocimetry (PIV)

For the study of turbulent flames, visualization of the flow-field provides a better understanding of the flame-flow interaction. The particle image velocimetry (PIV) is a widely adopted technique in fluid dynamic investigations to provide instantaneous velocity vectors in a cross-section of a flow.

Figure 2.2 shows the schematic of a PIV measurement. Trace particles are carried by the gas flow and illuminated by a laser sheet of a sequence of two laser pulses. The tracer particles used for PIV measurement need to be small enough to follow the gas flow closely, but big enough to scatter detectable light. The delay time between the two pulses is short enough to enable acquiring instantaneous information. With a highly sensitive CCD camera, the scattered signals from particles by a set of two pulses are captured in two separate image frames. The movements of particles during the period of two frames are tracked, by which the velocity can be derived. When processing the signal, the recorded image pairs are firstly divided into small sub-windows, which are called interrogation areas (IA). For each frame of the image pairs, their IA is cross-correlated pixel by pixel, and the correlation generates a peak that identifies the particle displacement. By repeating the correlation of IA over image frames, the velocity distribution in the target area can be obtained. [8]. In a PIV system, the data-processings are usually completed by the software that comes with it.

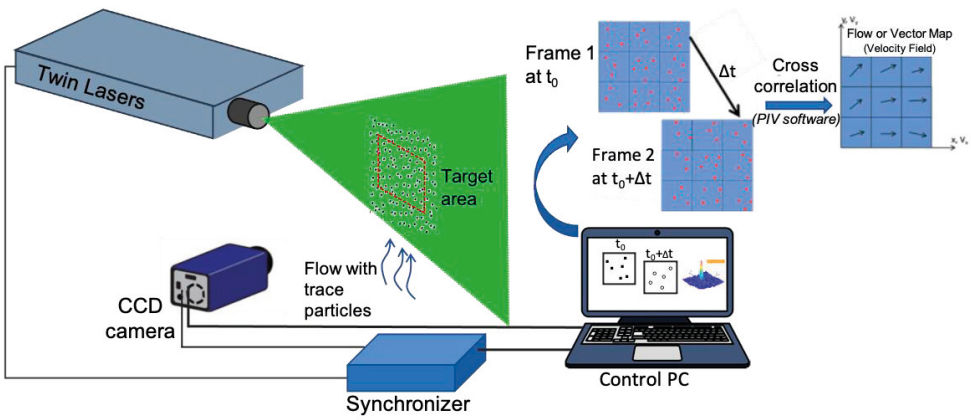

Figure 2.2: Schematic of a PIV setup.

In this thesis, a high-speed PIV system was employed for measuring velocity distributions in both gas turbine model combustor and jet burner. Titanium dioxide (TiO_2) particles with a diameter of around 2.5 μm were used as tracer particles. The captured image frames were processed by the software named DynamicStudio 6.3 (Dantec Dynamics). To optimize the local particle densities and flow gradients, the adaptive PIV method was selected to calculate the velocity vectors, in which the size and the shape of IA are adjusted to the best performance.

2.1.3 Laser Doppler anemometer (LDA)

LDA is a well-established technique which has been widely used for measuring flow velocity for gases or liquids. The advantages of LDA measurement include non-intrusiveness, high spatial and temporal resolution, free of calibration, and the ability to measure in reversing flows. An LDA system comprises a continuous wave laser, transmitting optics, receiving optics, a signal conditioner, and a signal processor. In this thesis, a 2D LDA measurement system was employed in the experiment. As shown in Figure 2.3, a laser with a two-component probe and a 2D traversing system is used to enable 2D measurement. For each component probe, two parallel coherent laser beams, generated by a Bragg cell, are focused by a lens intersecting at a probe volume. In the probe volume, interference fringes are produced by these two crossed beams. The spacing distance between two fringes can be determined by the wavelength of the laser beam (λ) and the angle between two beams (θ):

$$d_f = \frac{\lambda}{2\sin(\theta/2)}$$

When the fluid carries the seeding particles passing through the probe volume, the particle scatters light to the photodetector, and then the light intensity signal is converted into the electric signal. Due to the Doppler effect, the scattered light has a shifted signal frequency, f_D, which is proportional to the corresponding velocity component. For example, the scattered light signal from the dual beams with red colours shown in Figure 2.3 corresponds to the velocity component along the z-axis. The velocity component U_z can be calculated as:

$$U_z = d_f \cdot f_D = \frac{\lambda}{2\sin(\theta/2)} \cdot f_D$$

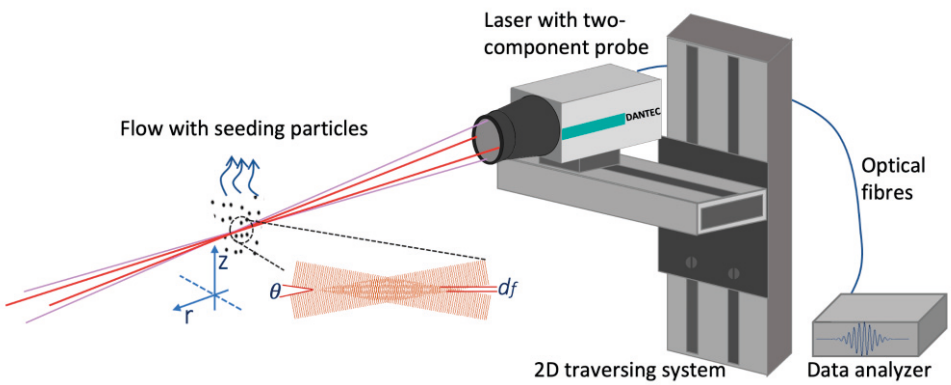

Figure 2.3: Principle of a 2D LDA measurement.

In a 2D LDA system, the other dual-beam laser coming out from a plane orthogonal to the first dual-beam plane. They are focused on the same probe volume. The wavelengths of these two dual-beam lasers are different to separate the measured components. More detailed information about the LDA principle can be found in [9].

In this thesis, two lasers with wavelengths of 660 nm and 785 nm, were focused in the probe area by a lens with a focal length of 500 mm. The probe volume for the red beams is $0.162 \times 0.162 \times 2.698$ mm with a fringe spacing of 5.628 μm, and the probe volume for the infrared light beams is $0.192 \times 0.192 \times 3.209$ mm with a fringe spacing of 6.512 μm. TiO_2 particles with a diameter of around 2.5 μm were used as seeding particles. During the measurement, a burst mode sampling was used for the data collection, which can provide high temporal resolution. Two LDA channels corresponding to two velocity components were operated in a coincidence way. A commercial software *BSA Flow* was used to complete the data processing and analysis like moments, correlation, and spectrum. Further details on algorithms of data processing can be found in the user's guide of BSA Flow [10].

2.1.4 Flame chemiluminescence

Generally, the flame can spontaneously emit electromagnetic radiation in the following ways [11]: (1) the black-body spectrum from soot or char particles, which is continuous and mainly observed in a diffusion flame; (2) the rotation-vibration emission bands generated by high-temperature gas molecules, so that the radiative heat transfer mainly results from the H_2O and CO_2 which radiations appear more obvious in a particle-free flame; (3) 'chemiluminescence', which means that the radiation emitted from excited species (atoms, molecules, or radicals) generated by a chemical reaction when they are returning to the ground state. Unlike the PLIF technique, flame chemiluminescence imaging is excited by the chemical reaction instead of the external excitation of laser light, and it provides line-of-sight integrated information across the imaged volume.

Since chemiluminescence originates in the reaction zone of the flame, it is generally believed to characterize the heat release rate of the flame [12]. However, it is difficult to get a reliable value of the heat release rate of turbulent flames due to line-of-sight integrated information. Nevertheless, flame chemiluminescence is still a suitable tool to represent the overall flame position, the fluctuation in the flame's overall heat release, and the fluctuation in the flame structure in an unstable condition. A typical chemiluminescence spectrum from a turbulent methane/air flame at atmospheric pressure is presented in Figure 2.4. It shows that the narrowband emissions from radicals (OH^*/CH^*) superimposed on the broadband emissions from CO_2^*.

In this thesis, high-speed chemiluminescence imaging for OH^* is employed, which shows a peak at 310 nm in the emission spectrum. With the high sampling rate, it is also possible to observe the flame dynamics.

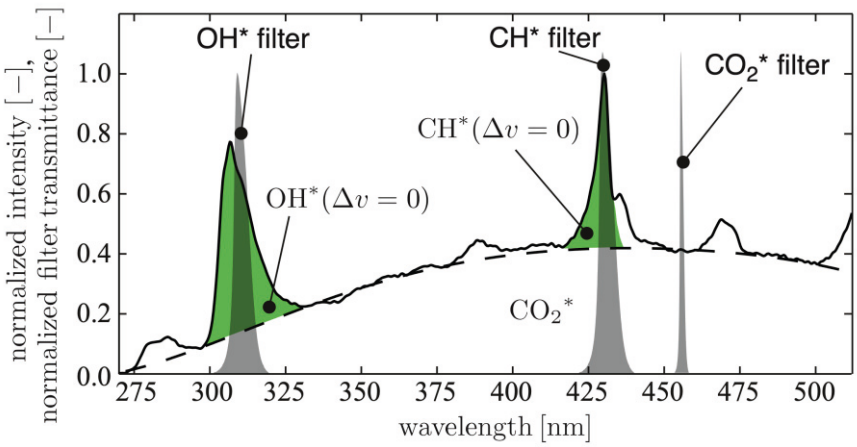

Figure 2.4: A typical chemiluminescence spectrum of the turbulent methane/air flame at atmospheric conditions [12].

2.1.5 Optical emission spectroscopy

Optical emission spectroscopy is a powerful analytical technique that has been widely used in element determination. This technique is based on a simple principle of studying the radiation emitted from the atoms or molecules returning from the excited states to their ground states, in which the excitation sources can come from either flames or a discharge. The emission spectrum produced by each specific excited atom or molecule is unique. The intensity of the emission is proportional to the concentration of the analyzed species. The most important instrument for performing optical emission spectroscopy is the spectrometer, in which the spectral lines are focused onto a detector by an optical system consisting of slits, mirrors, and gratings [13].

In this thesis work, two spectrometers with different spectral resolution and sensitivity were used to investigate the flame emission from the turbulent combustion with and without the assistance of gliding arc discharge in an industrial gas turbine combustor. One was a fibre spectrometer (AvaSpec-ULS2048XL-EVO-RS-UA) used in the range between 200 nm to 1160 nm. Another one was a Czerny-Turner spectrometer (Andor Shamrock 750, 1200 l/mm blazed at 300 nm) with an ICCD camera (Andor iDus 420-OE) with higher resolution and sensitivity, which was used at around 590 nm and 770 nm.

2.1.6 Combustion emission sampling

A water-cooled multi-hole gas sample probe (PSP4000-H/C) with a sampling rate of 1 Hz was employed for the extraction of emission gases after combustion. It provides direct in-situ ultra-fine filtration during continuous gas sampling for analytic measurements. More detailed information about this electrically heated and portable gas sample probe can be found in the product manual [14]. In this thesis, the sampling probe was arranged at the exit of the combustor liner to collect the combustion emissions. The sample gas passes through a condenser to remove the water, then reaches a custom-built emission analysis system to complete the emission data processing. The emission analysis system needs calibration with standard calibration gas bottles every day before measurements. Figure 2.3 shows photos of the gas sample probe and the emission analyzer.

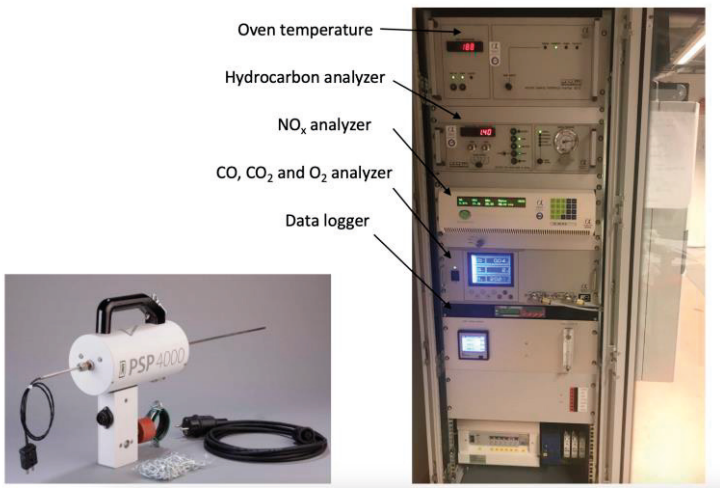

Figure 2.3: Photographs of the gas sample probe (Left) and the custom-built emission analyzer (Right).

2.2 Optical equipment

As described above, various laser diagnostics measurements were employed in this thesis work. In this section, the optical equipment including lasers, detectors, and laser sheet optics involved in these techniques will be introduced.

2.2.1 Lasers

1) Nd: YAG laser

One of the most common laser equipment available for laser combustion diagnostic applications is Nd: YAG laser, in which 'Nd' means neodymium ions (Nd^{3+}) and

'YAG' means Yttrium Aluminium Garnet ($Y_3Al_5O_{12}$). It is a typical four-level solid-state laser system of the neodymium ions hosted in Nd: YAG crystal act as the laser medium. The lasing principle of Nd: YAG laser is based on the population inversion after the lower energy level electrons of Nd3+ being excited to the higher level. After reflecting the photons many times inside the laser cavity, an optical switch called Q-switch is open to allow the light to escape from the cavity while the maximum population inversion is achieved. Typically, the fundamental laser beam emitted from a Nd: YAG laser is in the infrared region with a wavelength of 1064 nm. This wavelength can be converted into 532 nm, 355 nm, and 266 nm by second, third, and fourth harmonic generation, respectively. The laser beam with a wavelength of 532 nm is commonly used to pump a dye laser for generating a laser beam with a tunable wavelength.

In the thesis, different Nd: YAG lasers were employed in various PLIF measurements. The second harmonic of a Quantel YG980 YAG laser with a wavelength of 532 nm was used as the pump laser for OH-PLIF measurement. The third harmonic (355 nm) and fourth harmonic (266 nm) of a Brilliant B pulsed YAG laser were used to perform the CH_2O-PLIF and acetone-PLIF, respectively. Besides, the dye laser was pumped by the second harmonic (532 nm) of a Quanta-Ray Lab-Series pulsed Nd: YAG laser for the NH-PLIF measurement. The Nd: YAG lasers involved here all have a repetition rate of 10 Hz and a pulse duration of ~10 ns.

2) Dye laser

Unlike the Nd: YAG laser, which only generates a laser beam at a fixed wavelength, the output from a dye laser is tunable, and the lasing wavelength can be tuned over a wide range. In a dye laser, the organic dye dissolved in solvents (e.g., ethanol, benzene, water, etc) is used as the lasing medium. The dye solution absorbs light at a certain wavelength then it reemits fluorescence in a specific range. Typically, the dye laser needs a pumping laser to provide the energy exciting the dye, such as a Nd: YAG laser.

In the thesis, a Continuum ND60 dye laser was used to provide a laser beam for performing the OH-PLIF. The dye solution is a mixture of Rhodamine 590 and ethanol, and it can generate the 576 nm laser by a pumping 532 nm laser. The second harmonic generation of this wavelength provides the 283 nm laser beam, which excited the OH radicals at the $Q_1(8)$ transition in the $A^2\Sigma^+$- $X^2\Pi$ (1-0) band. For the NH-PLIF, a Cobra Stretch-G-2400 (PrecisionScan, Sirah) dye laser was employed, using a dye mixture of Rhodamine 640/610 and ethanol. The output of this dye laser with a wavelength of 607 nm was frequency-doubled to 303.6 nm and tuned to the $R_1(4)$ transition in the $A^3\Pi$ - $X^3\Sigma^-$ (1-0) band.

3) High-speed Nd: YLF laser

The Nd: YLF laser is a solid-state laser based on neodymium-doped (Nd^{3+}) yttrium lithium fluoride ($YLiF_4$) crystals and typically is diode-pumped. Compared with the

Nd: YAG laser, a diode-pumped Nd: YLF laser has better beam quality, significant anisotropic thermal expansion, and a longer upper-state lifetime, resulting from its lower thermal conductivity and weaker thermal distortions [15]. In this thesis, a high-speed dual-cavity diode-pumped Nd: YLF laser (Litron LDY304-PIV) was employed to generate the 527 nm wavelength laser pulses for performing the PIV measurement. The output energies of this laser were up to 30 mJ (at 527 nm at 1 kHz) and the pulse repetition rates were in a range of 1 kHz to 20 kHz.

2.2.2 Detectors

1) ICCD camera

The ICCD camera, standing for the intensified charge-coupled device, is the most common detector employed for both spectroscopy and imaging applications in laser diagnostics. In an ICCD camera, the intensifier enables low light signals to be amplified sticking out from the noise level of the CCD array and allows photodetection with a high temporal resolution by its fast-gating capability. Based on the photoelectric effect, the incident photons are transformed to electrons by the photocathode in the intensifier. These emitted electrons are accelerated by a micro-channel plate (MCP), and then be converted back to photons by a phosphor screen. After this, the output of the intensifier is coupled to a CCD image sensor, which reads out the pixels by a way of the horizontal shift-register like a 'Bucket-Brigade' and has advantages of high sensitivity and fidelity. In either PLIF or spectroscopy measurement involved in this thesis, the PIMAX II/III ICCD camera produced by Princeton Instrument was employed as the detector.

2) High-speed CMOS camera

Unlike the CCD sensor, the complementary metal-oxide-semiconductor (CMOS) sensor gains advantages in high frame rates and lower power consumption due to the different way of readout. In a CMOS sensor, the charge of the emitted electrons is converted into a voltage signal directly at the pixel sensor [16], which makes the readout faster. Benefiting from this, the CMOS sensors are usually used in high-speed cameras. In this thesis, a high-speed CMOS camera (Phantom V7.1, Vision Research) equipped with a gated image intensifier (Hamamatsu) was used for high-speed chemiluminescence imaging with frame rates of 1 kHz. Another high-speed CMOS camera (Phantom V311, Vision Research) was employed for the PIV measurement.

2.2.3 Laser sheet optics

As described above in Section 2.1, both PLIF and PIV measurements require a laser sheet for illuminating the target area. The laser sheet was formed using sheet-forming optics. For the PLIF measurements in this thesis, the laser sheet was formed

by a -40/-75 mm cylindrical lens and a +500 mm spherical lens, and for the PIV measurement, a wider laser sheet was needed which formed by a -40 mm cylindrical lens and a +500 mm cylindrical lens.

3 Test rigs and combustors

Turbulent flames operating in gas turbine relevant combustors or research jet burners have been experimentally investigated at either atmospheric or high-pressure conditions. This chapter provides an overview of the experimental test rigs and combustion devices that were utilized in the thesis. The design, configuration, and assembly are presented and discussed briefly here. Detailed information on different research works at various combustors, including experimental setups, diagnostics, and results can be found in Chapter 4.

3.1 Experimental test rigs

Experimental studies on various turbulent flames were performed at both an atmospheric pressure test rig and a high-pressure combustion rig in the Division of Combustion Physics, Lund University. A brief description of these two rigs is given in the following sections.

3.1.1 Atmospheric pressure test rig

For the work involved in Paper I – VI, all of the experiments were performed at the atmospheric pressure test rig at Lund University. A photo of the test rig illustrating the main components is shown in Figure 3.1. Looking at the picture from left to right, there are air blowers, mass flow meters, heaters, an optical bench, a burner stand, as well as a ventilation system which is on the top of the burner exit and shown outside the picture. The bulk airflow is supplied by two air blowers (Rietschle SAP 300) and the flow of air is controlled by adjusting the motor speed of the blowers. The two blowers have total capability of providing an air mass flow in the range of 0 – 110 g/s at non-reaction cases. To monitor the mass flow of air, a thermal mass flow meter (Eldridge MPNH-8000) is mounted downstream of each blower, with an accuracy ±1% reading and ±0.5% full load. Every mass flow meter is followed by an inline heater (Leister), which provides a preheating temperature of up to 750 K for the bulk air. For an experimental campaign with maximum airflow lower than 55 g/s, one of the blowers, i.e., one air passage, can be used alone to provide higher accuracy by blocking the other air passage. After passing through these passages, the bulk airflow into the plenum chamber over a series of meshes to

break up the large flow structures [17]. The plenum and burner are mounted vertically at a burner stand and an optical bench was used to arrange optics holders for diagnostics. At the top of the burner stand, there is a powerful ventilation system to suck away the exhaust gas efficiently. Besides, the fuel flows are usually controlled using mass flow controllers (Alicat Scientific MC-100SLPM, with accuracy ±0.8% reading and ±0.2% full load).

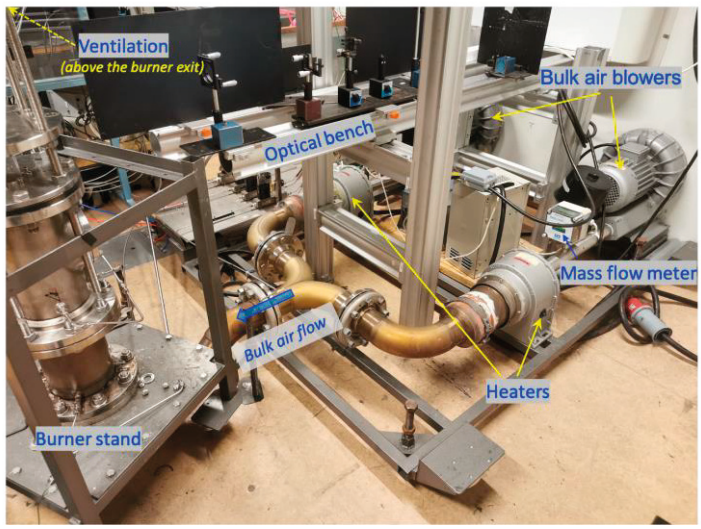

Figure 3.1: Photograph of the atmospheric pressure test rig.

3.1.2 High-pressure combustion rig

Combustion in gas turbines and most internal combustion engines are operated at elevated pressures. Performing experimental combustion studies at high-pressure and high-temperature conditions, relevant to gas turbine applications is always challenging. The high-pressure combustion (HPC) rig at Lund University was designed for phenomenological and applied studies of gas turbine and jet engine related combustion at elevated pressures. The HPC rig provides a maximum airflow of 1.2 kg/s with a preheated temperature of up to 800 K and a maximum chamber pressure up to 16 bar.

Figure 3.2 shows a 3D sketch of the whole infrastructure of the HPC rig. It can be seen that the HPC rig is a complex system, which consists of the air compressor, the resistance heater, the test-section, the afterburner, the exhaust system, and the lab operation room. The air supplied by an air compressor (750 kW) is first introduced into the outer pressure vessel, which flows in a direction opposite to the flow inside the chamber and plays a role in cooling down the combustion chamber. Then the air is preheated by an electrical heater (1 MW) and passes through a Coriolis mass flow meter and the plenum of the burner before entering the combustion chamber [18].

Two fuel lines are used to supply fuel to the main and pilot respectively, which are controlled by the high-pressure fuel mass flow meters. The afterburner downstream to the test-section enables the research on fuel evaporation to be conducted. The photos and a zoom-in schematic of the test-section are shown in Figure 3.3, including the burner, combustion chamber, cooling chamber, etc. The burner is mounted horizontally in the rig inside a plenum. To enable optical access, the combustion chamber has quartz windows on four sides with a square cross-section of 100×100 mm and thickness of 5 mm. Due to the complexity of the HPC rig, professional operators are needed to operate the HPC system when performing the experiment. The experimental work presented in Paper VII was carried out in Lund HPC rig.

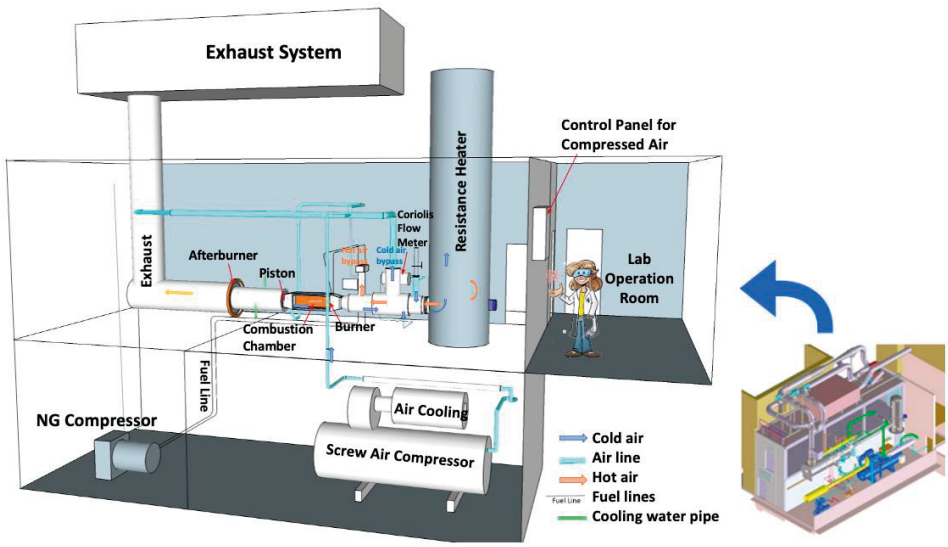

Figure 3.2: A 3D sketch of the whole infrastructure of the high-pressure combustion rig.

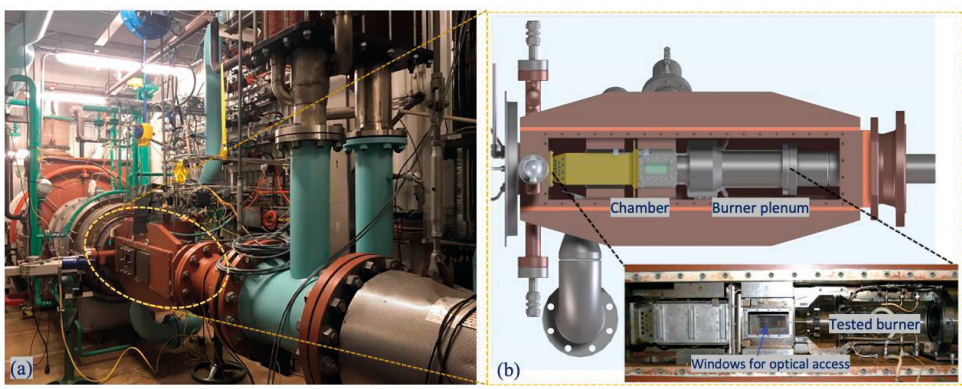

Figure 3.3: (a) Photograph of the HPC rig; (b) A schematic and a photo zooming in the test-section of the HPC rig.

3.2 Gas turbine related combustors

Experimental studies in practical gas turbine combustors can provide valuable information not only for in-depth understanding and CFD validation but also serves the design and optimization of practical devices. To facilitate these experiments, gas turbine-related combustors, e.g., the gas turbine model combustors and downscaled industrial gas turbine combustors, are usually employed.

3.2.1 The CECOST lab-scale swirl burner

A gas turbine model combustor (GTMC), named CECOST swirl burner, has been developed under the Swedish National Centre for Combustion Science and Technology (CECOST) research programme. The design concept of the CECOST swirl burner is inspired by the EV/AEV burner, which has advantages of robustness, simplicity, high flame stability, and broad fuel flexibility, etc [19-22]. More information on the development process of the CECOST swirl burner can be found in Paper I and in Ref. [23].

Figure 3.4 shows the cross-section and photos of the CECOST swirl burner. A swirl generator consists of four quarter-cone vanes in a counterclockwise direction, with the half-angle of 25° and the blade thickness of approximately 2 mm. The swirler is connected to and held by a lance and assembled inside a metallic mixer-pipe of 220 mm in length and 54 mm in diameter. A honeycomb is mounted inside the mixer-pipe upstream of the swirler to break up the large eddy structures of the flow. At the nozzle exit of the swirler, there is a cylindrical premixing tube with an outer diameter of 50 mm and a length of 100 mm. Downstream of the premixing tube, two types of liner both with 400 mm in length are placed on a metal plate. One is in a cylindrical shape with a circular cross-section of 100 mm in diameter, and another one is in a cuboid shape with a square cross-section of 100×100 mm^2. To provide optical access, both the premixing tube and the liner are made of quartz. Over the top of the liner, a quartz flange with a circular hole of 55 mm in diameter acts as a contraction outlet. As shown in Figure 3.4 (b), the CECOST swirl burner is installed vertically in the atmospheric pressure test rig. In the original setup, the fuel inlets are two simple pipes upwards. However, the strategy of fuel injectors was changed for improving the mixing performance of the CECOST burner, which will be described in Chapter 4. The experimental works involved in Paper I-III in this thesis were performed at the CECOST swirl burner.

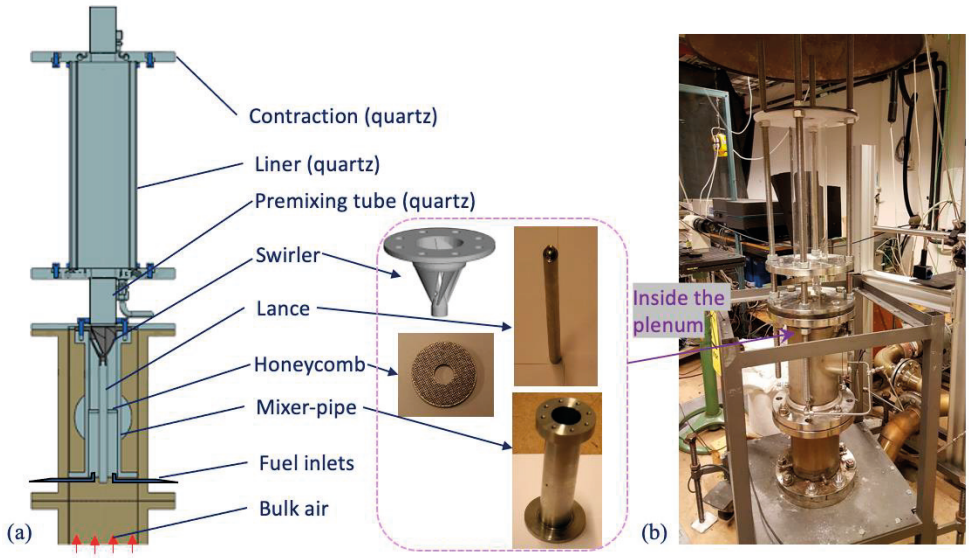

Figure 3.4: (a) Cross-section of the CECOST swirl burner; (b) Photographs of the CECOST burner and some key components.

3.2.2 The scaled Siemens Dry Low Emission burner

The flame was investigated in a scaled industrial gas turbine combustor, named a prototype 4th generation of Dry Low Emission (DLE) burner, which was designed by Siemens Energy AB for developing the SGT-750 DLE burner. The cross-section of this burner assembly is shown in Figure 3.5 (from the Ref. [24]). The scaled Siemens DLE burner consists of three concentric sectors: the Main (a radial swirled outer sector), the Pilot (the intermediate sector with an axial swirler), and the RPL (the Rich-Pilot-Lean central-body sector). Compared to the SGT-750 burner, the 4th generation prototype DLE burner has the one-third (1/3) downscaled Main and Pilot sectors and the same scale RPL sector. For the Pilot and Main sectors, the fuel is supplied by an individual line, but the air is divided as a ratio of 21%:79% from the bulk airflow according to the flow path areas. The RPL owns separate fuel and air lines. Downstream of the burner throat, a quartz conical section, termed as Quarl, is placed to smooth the flow. Outside of the Quarl, a rectilinear quartz combustor with a cross-section of 100×100 mm^2 and a length of 400 mm is mounted. More detailed descriptions on this burner can be found in Ref. [25].

In this thesis work, the configuration of the scaled Siemens DLE burner was modified aiming to apply the gliding arc discharge in the RPL sector. As shown in the schematic of the cross-section, before and after the modification in Figure 3.6, a high voltage (HV) electrode was designed and mounted inside the RPL sector. To generate the gliding arc plasma discharge in the burner, the HV electrode is charged by a 35 kHz AC power supply (Generator 9030 E, SOFTAL Electronic GmbH). The

outer shell of the RPL together with the remaining part of the burner is grounded. This modified Siemens DLE burner was utilized for the investigation involved in Paper V and VI.

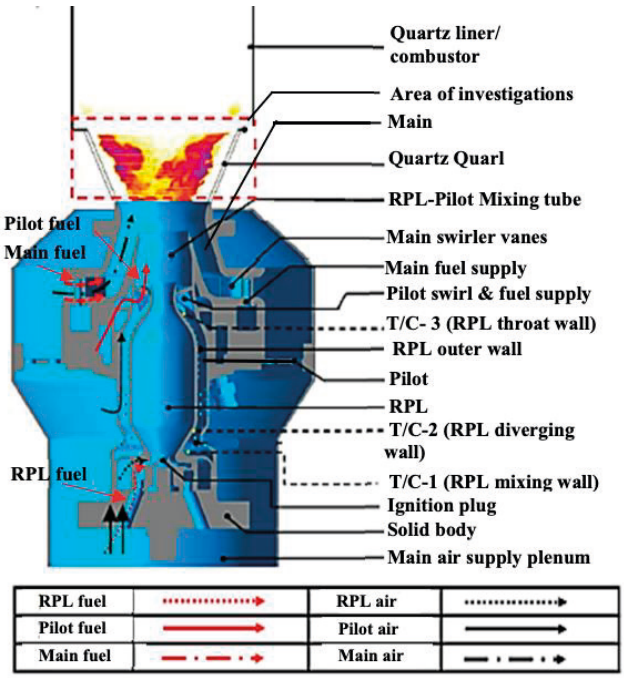

Figure 3.5: Cross-section of the prototype 4th generation DLE burner assembly [24].

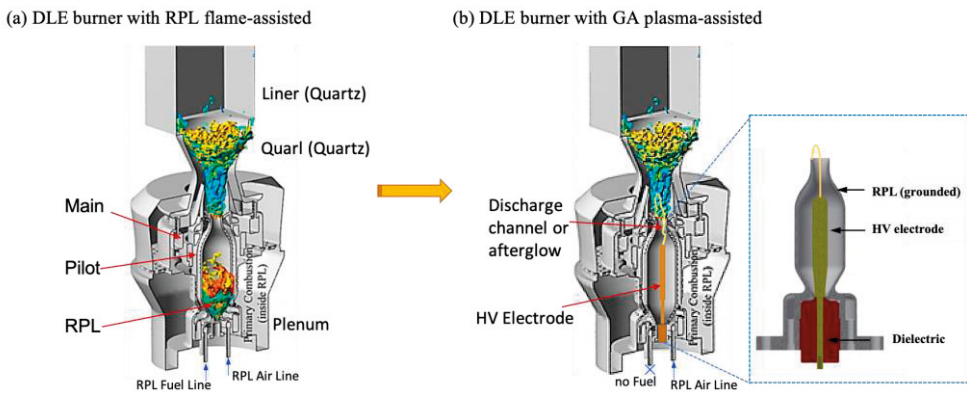

Figure 3.6: Schematic of the cross-section of the DLE burner before (a) and after (b) modification, (a) is from Ref. [26].

3.3 Research jet burners

Research jet burners are commonly employed in laboratory studies to deepen the fundamental understanding of turbulent flames. Due to the simple geometry, easy deployment, and possibility to achieve high turbulence levels, research on jet burners provides measurements with broader parameters and enables a detailed discussion on flame structures and covers a large region of the regime diagram.

3.3.1 The DRZ burner

To investigate turbulent premixed flames which are mainly located at the regime of the distributed reaction zone (DRZ), a jet burner with large integral scale, called DRZ burner, was developed inspired by both the Michigan Hi-Pilot burner [27] and the hybrid Mckenna-type burner (LUPJ) [28].

The cross-section of the DRZ burner and a photo of it are shown in Figure 3.7 (a) and (b), respectively. The DRZ burner consists of two parts: the central jet and the co-flow pilot. To enable the large flow rate, there are eight fuel inlets evenly distributing in two circles upstream of the plenum. The mixture of air and fuel is further blended by passing through a metallic meshed cylinder being filled with glass balls and uniformized by a perforated plate. After this, the homogenized reaction mixtures are obtained before passing through a turbulent generator and a contracting-expanding nozzle. This kind of nozzle can prevent flashback of the flame. As the mixture leaving the nozzle exit, a jet flow with high velocity and intense turbulence is generated. The diameter of the nozzle exit is 22 mm. For the co-flow pilot, the air and methane are premixed prior to injecting into the pilot chamber. A porous plug plate is used to generate a quasi-one-dimensional laminar flame surrounding the jet flame. The cooling water is supplied through a pipe made of brass, which is arranged under the porous plug to prevent overheating.

Besides, there are also four more inlets getting through the nozzle pass way, which can generate the impinging jets when it is needed to further increase the turbulence. Upstream the turbulent generator, two seeding inlets as shown in Figure 3.7 (a) are used to supplying seeding particles when performing PIV or LDA measurements.

Figure 3.7 (c) presents an image of a premixed methane/air flame stabilized on the DRZ burner, in which the pilot flame provides a large hot ambient area to support the central jet flame. In this thesis, an investigation of turbulent premixed ammonia/air flames at the DRZ burner is conducted and results are analyzed and discussed in Paper IV.

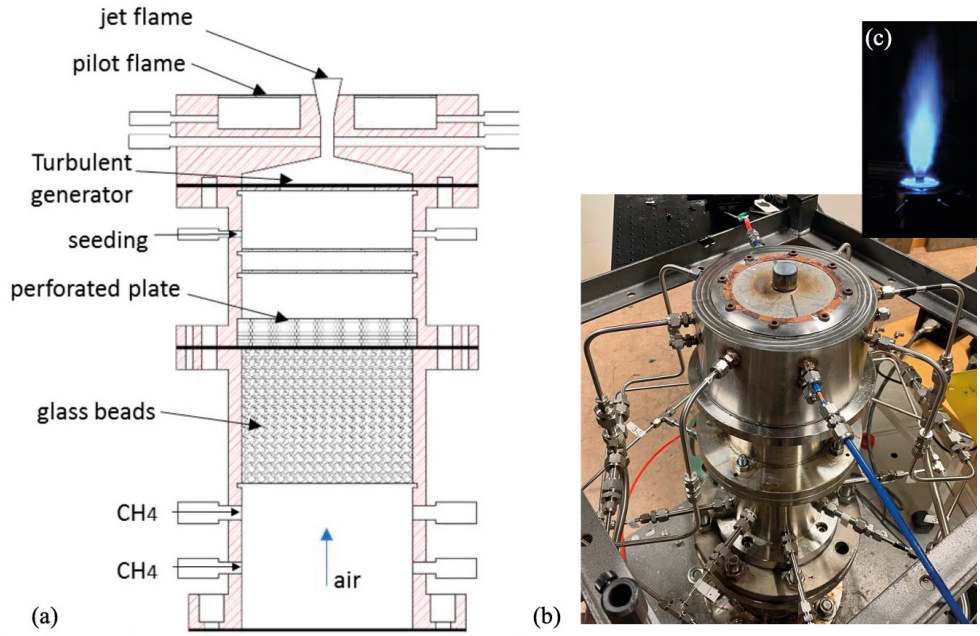

Figure 3.7: (a) Cross-section of the DRZ burner; (b) Photograph of the DRZ burner; (c) An image of a premixed methane/air flame tested in DRZ burner, which taken with a digital camera.

3.3.2 The inverse diffusion jet (IDJ) burner

The turbulent non-premixed/partially premixed flames are widely employed in practical combustors, e.g., gas turbines and rocket engines. A burner consisting of two coaxial tubes was designed to form an inverse diffusion flame, thus the burner is named inverse diffusion jet (IDJ) burner in this thesis. A sketch of the cross-section of the IDJ burner is shown in Figure 3.8 (a). In the IDJ burner, the air is supplied through an inner tube with a diameter of 1.6 mm, while the fuel is supplied through the outer tube with a diameter of 30 mm. Outside of these two coaxial tubes, a plenum with an exit diameter of 90 mm is mounted to allow the co-flow air to pass through it. To perform the experiment on the IDJ burner at high-pressure combustion rig at Lund University, an outer plenum is used to install the burner in the test-section and connect the exit of the inner plenum to the entrance of the combustion chamber, which is shown in Figure 3.8 (b). An image of a methane inverse diffusion flame stabilized on the IDJ burner at high pressure is presented in Figure 3.8 (c).

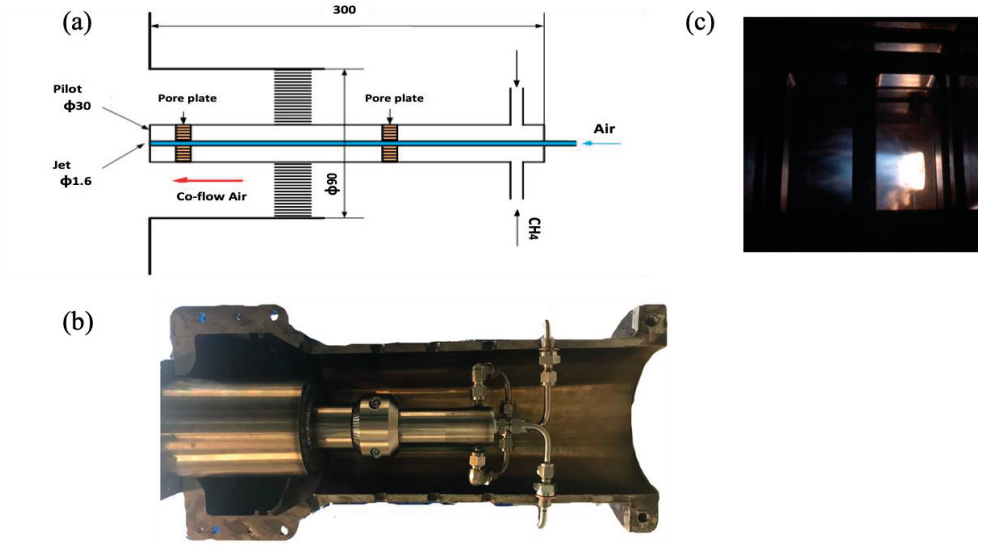

Figure 3.8: (a) A sketch of the cross-section of the IDJ burner; (b) Photograph of the IDJ burner mounted in an outer plenum; (c) An image of a methane inverse diffusion flame at the high-pressure chamber.

4 Flame diagnostics in gas turbine relevant combustors

Experimental investigation on turbulent flames in gas turbine relevant combustors is the major research objective of this thesis. This chapter begins with an overview of the fundamentals of combustion in gas turbines. Then the results of experimental studies on the CECOST swirl burner and Siemens DLE burner are discussed. The results and discussion presented in Section 4.2 are from Paper I – III, while contents presented in Section 4.3 are from Paper V and VI.

4.1 Combustion in Gas turbines

As one of the 'youngest' energy converter, gas turbines have been widely used in stationary, marine, and aviation applications and have various advantages: (1) capability of producing high power from the relatively small size and weight; (2) long mechanical life resulting from pure rotational motion of main components; (3) ability to reach a full-load condition in minutes; (4) utilizing a wide variety of fuels; (5) free of liquid coolant [29].

4.1.1 Gas turbine thermodynamics

Typically, a gas turbine consists of three main components: a compressor (to compress the air), a combustor (to burn the fuel and compressed air), and a turbine (to drive the compressor or to generate power). For the aircraft gas turbine, the exhaust gas flow is accelerated to the atmosphere by an exhaust nozzle after leaving the turbine, which produces the thrust for the aircraft. But for a land-based or marine gas turbine, except driving the compressor, the remaining power from the turbine is an output as shaft power to drive an electric generator or a ship's propeller. Figure 4.1 (a) presents a schematic of a typical gas turbine system. The principle of most industrial gas turbines is based on a thermodynamic process, termed the Brayton cycle. A simple open Brayton cycle is composed of three processes, including fluid compression, heat addition (combustion), and expansion. Commonly, these processes are presented as diagrams of pressure vs. volume (P-V) or temperature vs.

entropy (T-S) shown in Figures 4.1 (b) and (c). Based on the assumption of an ideal thermodynamic process, i.e., no losses, when the ambient air is compressed by passing through the compressor, its pressure (P), temperature (T), and enthalpy (h) are increased by such an isentropic process shown as 1-2 in Figure 4.1. Then in an isobaric expansion process 2-3, the volume (V) increases at a constant P when the air is heated in the combustor. After leaving the combustor, the exhaust gas with high temperature is isentropically expanded in the turbine, thus P decreased as well as T and h, as shown in process 3-7 in Figure 4.1. Unlike the open cycle, in which the air is taken from the atmosphere and passed through the engine only once, the exhaust gas is continuously recirculated and cooled by a heat exchanger in a closed gas turbine cycle during process 7-1. [30, 31]

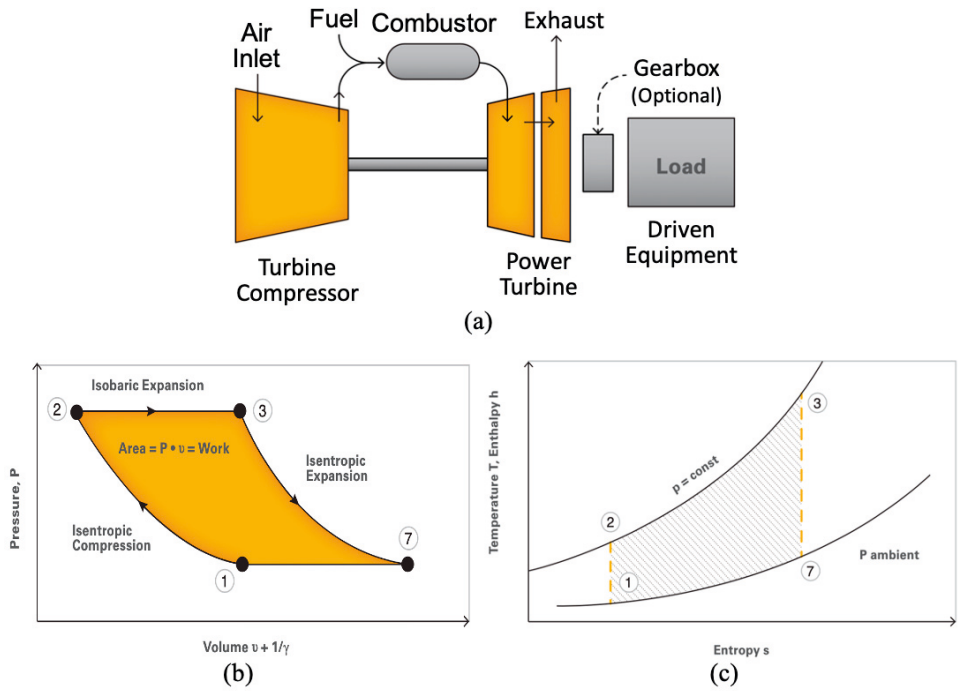

Figure 4.1: (a) A schematic of a typical gas turbine system; (b) The Pressure-Volume (P-V) diagram for the Brayton cycle; (c) The Temperature vs. Entropy (T-S) diagram for the Brayton cycle. [30]

4.1.2 Swirl stabilized premixed flame

In conventional gas turbine combustors, diffusion (non-premixed) flames are used, which have high flame stability but with the drawback of high flame temperature and high NO_x emission. Besides, the fuel-pockets presented in hot regions can also lead to increased soot production. To meet the increasingly stringent requirement on emission, gas turbines with low emission combustion systems have been

developed by employing the lean premixed flames concept, in which fuel and air are premixed before entering the combustor chamber. The lean premixed combustion features lower flame temperature and reduced NO_x emission by limiting the chemical pathways of producing thermal NO_x [32, 33].

For the low emission combustion system, one of the major design challenges is the flame stability. The most common method to solve this issue is creating low-velocity regions in the combustor by, for example, employing a bluff body or a swirler. Particularly, swirl stabilization has been used as the preferred flame stabilization mechanism in modern industrial combustors [34-36]. The main characteristics of the swirl stabilized flame are reduced flame lengths, good flame stability resulting from better mixing, and long-life expectancy of the combustor hardware due to no direct contact with the high-temperature flame [34, 37, 38]. A typical flow structure in the gas turbine combustor with a swirler is shown in Figure 4.2. In a swirling flow, the center recirculation zones (CRZ), also called inner recirculation zones (IRZ), are created aerodynamically by the spiral motion. Meantime, the outer recirculation zones (ORZ), also called corner recirculation zone, are formed. It can be also seen that shear layers are generated and located between the main flow and the CRZ/ORZ. The mechanism of the swirl-stabilized flame is dominated by the flow region of the vortex breakdown [39]. During the vortex breakdown, a three-dimensional large-scale unsteady motion arose is the precessing vortex core (PVC). This PVC is usually located on the boundary of the CRZ between the zero velocity and zero streamline [40] (as shown in Figure 4.2) and is found to be highly correlated to the strength and position of the CRZ [38, 41]. Figure 4.3 from Ref. [42] shows the topology of a PVC. More details of the occurrence of the PVC are reviewed in Ref. [43].

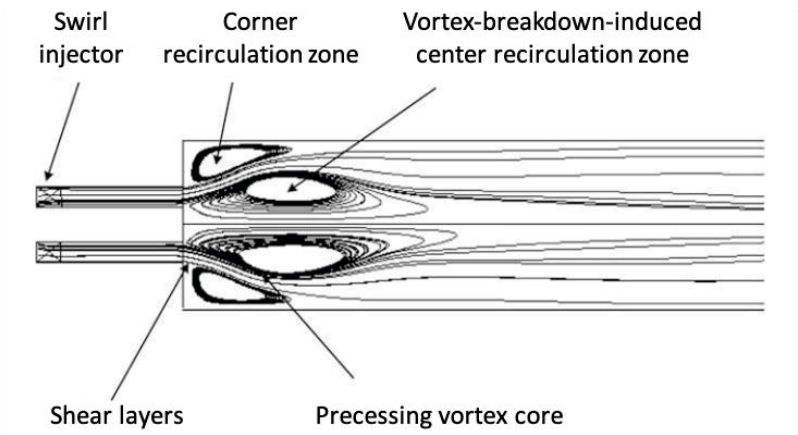

Figure 4.2: Flow structure of a typical gas turbine combustor with a coaxial swirl injector [39].

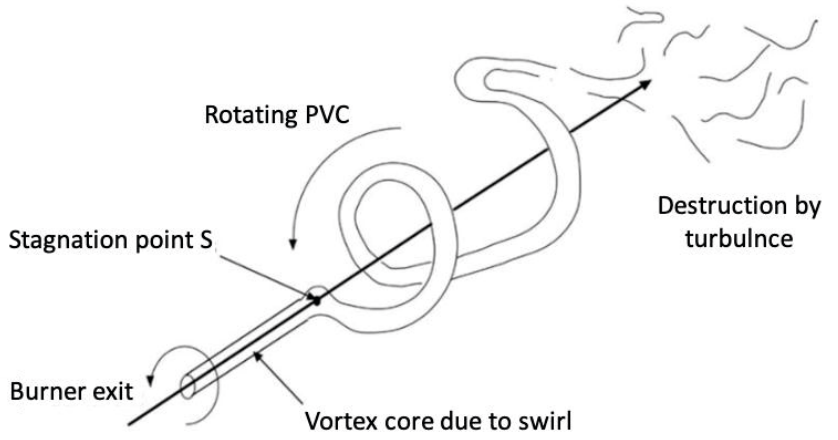

Figure 4.3: Topology of a precessing vortex core [42].

The most important parameter relevant to the swirling flows is the swirl number (S), which represents the degree of swirl and is defined as the axial flux of tangential momentum divided by the axial flux of axial momentum [44],

$$S = \frac{\int_0^R \overline{U_y}\,\overline{U_t}\,r^2\,dr}{R\int_0^R \overline{U_y}^2\,r\,dr}$$

where, $\overline{U_y}$ is the average axial velocity, $\overline{U_t}$ is the average tangential velocity, and R is the equivalent nozzle radius.

4.1.3 Combustor operability

Being able to operate in a wide range of parameters is one of the most important features when designing qualified gas turbine combustors. The lean premixed gas turbine combustion system, as the most adopted concept, generally faces four critical operability issues, i.e. lean blowout (LBO), flashback, combustion instability, and autoignition [45]. In this thesis discussion, the LBO and flashback issues will be the main focus.

Lean blowout (LBO) refers to the phenomenon of flame extinction occurring when the equivalence ratio is lower than the lean flammability limit, which manifests a flame detached from the anchoring position and blown out of the combustor. When the flame close to the LBO limit, combustion instability generally becomes a major issue, and the flame extinction is easily triggered by small perturbations. The occurrence of LBO can be recognized with an exponential increase in the carbon monoxide (CO) emission level. It is because the local quenching of the flame releases unburned hydrocarbons (UHC) into the post flame region, which

subsequently oxidized into CO [46]. The LBO limit is strongly influenced by the fuel properties and it can be significantly extended by using hydrogen (H_2) enriched fuels.

Another undesired operability issue is the flashback, where the flame propagates upstream into the premixing tube. The flashback event increases the risk of overheating of the combustor material as the flame is anchored in the nozzle. Four basic mechanisms of flashback have been described and studied in numerous studies [45, 47, 48]: a) turbulent flame propagation in the core flow, b) flashback resulting from combustion instabilities, c) flashback due to combustion induced vortex breakdown (CIVB), and d) flashback in the boundary layer (BLF). In swirl stabilized gas turbine combustors, CIVB is driven by the interaction of the chemical reactions and swirling flow, leading to the upstream propagation of the vortex breakdown [49, 50]. In contrast, the BLF is mainly driven by the flame propagation processes. In the case of BLF, the upstream propagation of flame is initiated from the flame speed exceeding the local flow velocity, which occurs along the wall due to the existence of the non-slip condition in the wall boundary. Since the risk of BLF for fuels with low quenching distance is high, the BLF becomes one of the most dominant mechanisms for gas turbine combustion using highly reactive fuels such as hydrogen or hydrogen-enriched hydrocarbons.

4.1.4 Emissions

To achieve the increasing demand for low pollution and high energy efficiency in the gas turbine, comprehensive studies on the ways to control the emission levels in the combustion process become critical. The major exhaust species from gas turbines include nitrogen (N_2), oxygen (O_2), carbon dioxide (CO_2), and water vapor (H_2O). Among these, CO_2 is the main concern because it leads to a greenhouse effect which contributes to global warming. There are also minor species that are harmful pollutants to the environment and human health, e.g., nitrogen oxides (NO_x), CO, sulphur oxides (SO_x), UHC, and particulate matter. Figure 4.4 listed the typical concentration and source of the different exhaust species from conventional fuel combustion in a gas turbine.

CO and NO_x emissions are of primary concerns in gas turbine combustion. CO is a toxic gas and CO poisoning is fatal since the oxygen-carrying capacity of the blood is reduced by the formation of carboxyhaemoglobin. Commonly, CO is formed by incomplete combustion of the fuel, resulting from [51]:

- Insufficient burning velocity in the primary zone of the flame, due to too lean combustion or too short residence time
- Inadequate mixing of the fuel and air, causing local over-rich yields
- Quenching of the postflame products by ambient air entrainment

Major Species	Typical Concentration (% Volume)	Source
Nitrogen (N_2)	66 - 72	Inlet Air
Oxygen (O_2)	12 - 18	Inlet Air
Carbon Dioxide (CO_2)	1 - 5	Oxidation of Fuel Carbon
Water Vapor (H_2O)	1 - 5	Oxidation of Fuel Hydrogen
Minor Species Pollutants	**Typical Concentration (PPMV)**	**Source**
Nitric Oxide (NO)	20 - 220	Oxidation of Atmosphere Nitrogen
Nitrogen Dioxide (NO_2)	2 - 20	Oxidation of Fuel-Bound Organic Nitrogen
Carbon Monoxide (CO)	5 - 330	Incomplete Oxidation of Fuel Carbon
Sulfur Dioxide (SO_2)	Trace - 100	Oxidation of Fuel-Bound Organic Sulfur
Sulfur Trioxide (SO_3)	Trace - 4	Oxidation of Fuel-Bound Organic Sulfur
Unburned Hydrocarbons (UHC)	5 - 300	Incomplete Oxidation of Fuel or Intermediates
Particulate Matter Smoke	Trace - 25	Inlet Ingestion, Fuel Ash, Hot-Gas-Path Attrition, Incomplete Oxidation of Fuel or Intermediates

Figure 4.4: Gas turbine exhaust emissions burning conventional fuels [52].

NO_x expresses the sum of nitric oxide (NO) and nitrogen dioxide (NO_2). Excessive emission of NO_x can cause great damage to the environment, manifested as acid rain, photochemical smog, depletion of the stratospheric ozone layer, etc. There are four chemical pathways of producing NO_x [53]:

- Thermal NO: produced in flame regions with a high temperature of greater than 1800K, and the reaction pathway is based on the extended Zeldovich mechanism.
- Nitrous oxide (N_2O) pathway: formed by a combination reaction that preferred at low temperature ($N_2 + O + M = N_2O + M$)
- Prompt NO: found in the flame region very early, which is initiated by the HCN/CN reaction pathways.
- NNH route: NO is produced by the reaction between an intermediate species NNH and the oxygen atom, which is particularly viable at low flame temperatures.

These major pathways of NO_x formation and their interconnections are summarized and shown in Figure 4.5.

In summary, the temperature of the combustion zone has a great influence on the CO and NO_x emissions. NO_x is mainly formed by the thermal NO pathway at high flame temperature, while much of CO is formed at lower temperatures. Therefore, to control the emissions of CO and NO_x both to a relatively low level, the flame temperature needs to be maintained within a narrow low-emissions window, as shown in Figure 4.6.

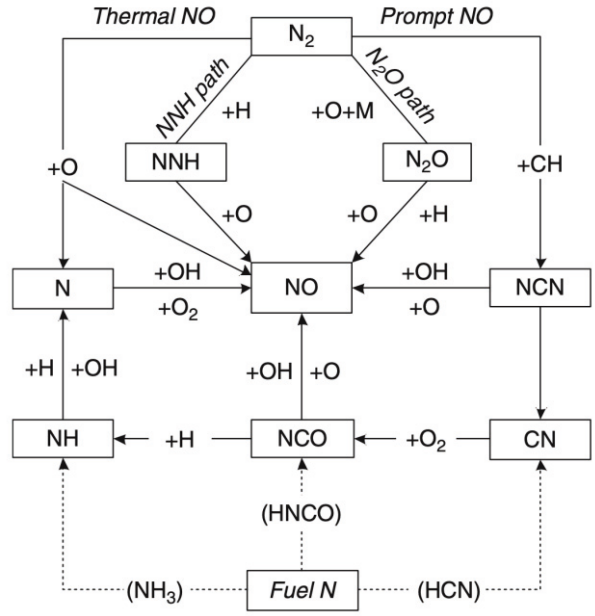

Figure 4.5: Major reaction pathways of NO_x formation and their relationships [53].

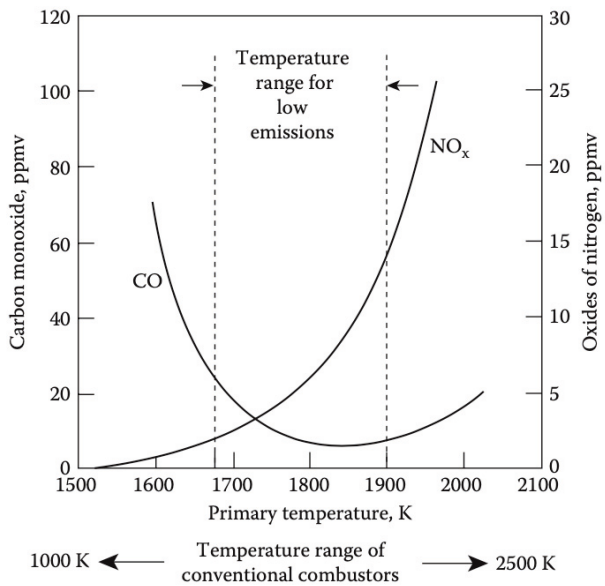

Figure 4.6: Influence of temperature in combustion zone on CO and NO_x emissions [51].

4.2 Investigation of the CECOST swirl burner

The experimental studies were performed to understand the operability range, flame stabilization, flame structures, and fuel flexibility in a gas turbine model combustor, i.e., the lab-scale CECOST swirl burner (described in Section 3.2.1). This section will discuss the results of investigations on flames in the CECOST burner with different fuels, which are presented in Paper I-III, as well as the improvement in degrees of mixing of the CECOST swirl burner.

4.2.1 Flame investigation of the CECOST swirl burner

Investigation of the natural gas/air flames in the CECOST swirl burner was conducted both experimentally and numerically. This work aims at identifying the LBO and flashback limits at various Reynolds number (Re) and equivalence ratios (ϕ), deepening the understanding of the flame dynamics, characterizing the flame structures at different conditions, and preliminarily providing the validation for the CFD modelling. In the experiments, the CECOST swirl burner was mounted on the atmospheric pressure test rig (described in Section 3.1.1) and various optical diagnostics measurements were employed. Figure 4.7 shows a schematic of the experimental setup applied in the work presented in Paper I-II.

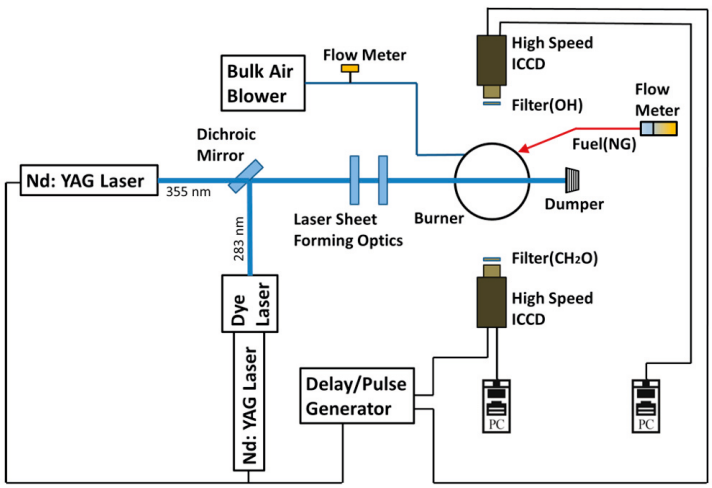

Figure 4.7: Schematic of the experiment setup in work presented in Paper I-II.

Simultaneous OH- and CH_2O-PLIF measurements, as well as high-speed OH^* chemiluminescence imaging were performed. Two laser beams with wavelengths of 283 nm for the OH excitation and 355 nm for the CH_2O excitation were superimposed and then formed into a thin laser sheet with a height of 50 mm. The pulse duration of both lasers was around 10 ns and the time separation between them

was 100 ns. Two ICCD cameras were used to detect the OH- and CH_2O-PLIF signal, respectively. For each measured case, 1000 single-shot images were collected at a frequency of 10 Hz and with a camera gate width of 30 ns. PLIF measurements were carried out at two positions in the burner: one is located at the central vertical plane of the combustor closing to the bottom of the liner; another one is inside the premixing tube. However, only OH-PLIF was possible to perform to capture the flame structure in the premixing tube, as the strong reflection by the 355 nm laser causing severe difficulties for the CH_2O-PLIF measurements. Moreover, the OH^* chemiluminescence images were acquired by a high-speed CMOS camera equipped with a gated intensifier, which is described in Section 2.2.2. For each measured case, 1000 single-shot images were collected at a frequency of 1 kHz and with an exposure time of 50 μs.

Results of the experiments are discussed in the following aspects:

1. Stability regime and flame states

The burner stability regime for the natural gas/air combustion is shown in Figure 4.8, which demonstrates the effect of ϕ and Re on the flame states. There are three regimes presented in the figure, referring to the LBO limit, stable flame (flame in the combustion chamber, abbreviated as FIC), and flashback (flame in the mixing tube/attached to the swirler, abbreviated as FIMT/FIS). The stability regimes were mapped for both the cylindrical liner and the cuboid liner, which shows slight differences as the geometry of the liner was changed.

We observed that the LBO limit keeps almost constant at around $\phi = 0.49$ for all conditions with different Re. One possible reason for this observation is that the imbalance between the rate of reactant entrainment and rate of reaction, which is determined by the Damköhler number criterion (Da < 1) [54, 55]. The Damköhler number (Da) is defined as the flow resident time (τ_{flow}) divided by the chemical time scale (τ_{chem}). LBO occurs when the residence time is too short to complete reactions for the reactants, or the heat release from the reactions is insufficient for igniting unburned reactants. Since τ_{chem} at the LBO condition is insensitive to Re, τ_{flow} should also be insensitive to Re (suggested by Da criterion). The LES results presented in Paper II show the vortex breakdown (induced CRZ) being insensitive to Re, so that τ_{flow} should decrease as Re is increasing. The LBO limit appears to depend only on the lean flammability limit of the fuel/air mixture, due to the sufficient long τ_{flow} for all Re conditions in the CECOST burner. In contrast, flashback limits are strongly influenced by Re. For lower Re conditions ($Re < 10000$), FIMT occurs at $\phi = 0.58$ and FIS occurs as further increasing ϕ. For moderate Re conditions, in the range of $10000 \leq Re \leq 17000$, only FIMT events were observed. While for higher Re conditions, ($Re > 17000$), no flashback occurs even when ϕ was close to the stoichiometric ratio. This observation reveals a trend of less prone to flashback at higher Re.

The time averaged OH^* chemiluminescence images are shown in Figure 4.9, which reveal the overall flame behaviours. Stable flames were both observed for $\phi = 0.52$ at Re = 10000 and 20000, as shown in Figure 4.9 (a) and (c). While for $\phi = 0.60$ cases, a flame propagating inside the premixing tube (FIMT) was observed at Re = 10000 (shown in Figure 4.9 (b)), but the flame at Re = 20000 still keeps stable (shown in Figure 4.9 (d)). Besides, the OH^* signal is relatively weak at lower ϕ and becomes stronger as ϕ increasing for both Re.

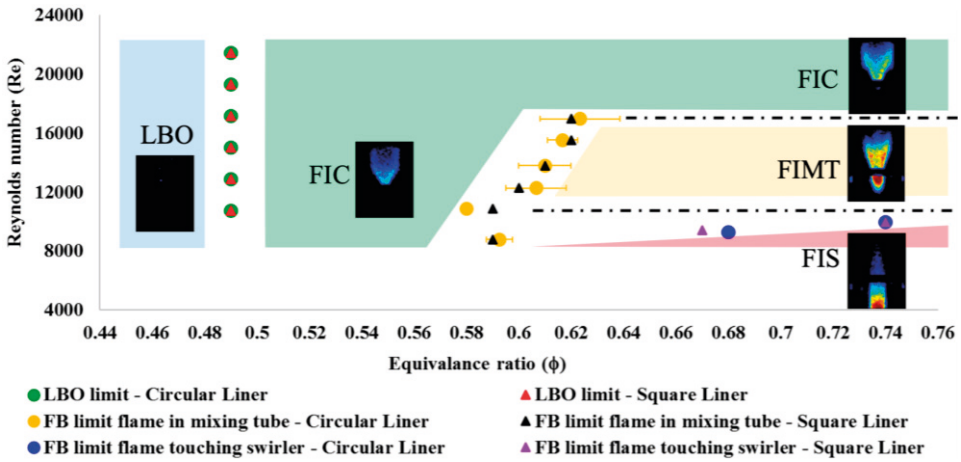

Figure 4.8: Burner stability regime, including LBO limits, stable flame, and flashback.

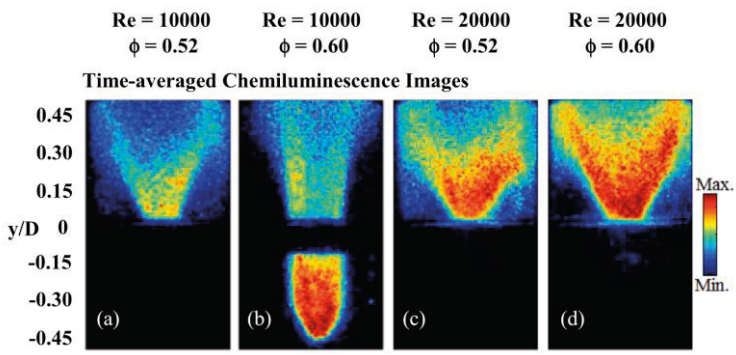

Figure 4.9: Time-averaged OH* chemiluminescence images for ϕ = 0.52 and 0.60 at Re = 10000 and 20000.

2. Flame structures

OH- and CH_2O-PLIF were carried out simultaneously to visualize the flame structures and to identify the heat release zones in this work. The distribution of OH radicals is regarded as a proper marker of the reaction zone and the post-flame zone of the flame, whereas the CH_2O distribution is often used to represent the preheat

zone of the flame. Thus, the overlap of the OH- and CH_2O-PLIF signals have been extensively employed for indirectly marking the heat release zone in many studies [56, 57]. The results of OH- and CH_2O-PLIF measurements for flames with $\phi = 0.52$ and 0.60 at Re = 10000 and 20000 are shown in Figure 4.10, including single-shots, heat release zone, and probability maps (PM) of both species (the processing method of PM is described in Paper II).

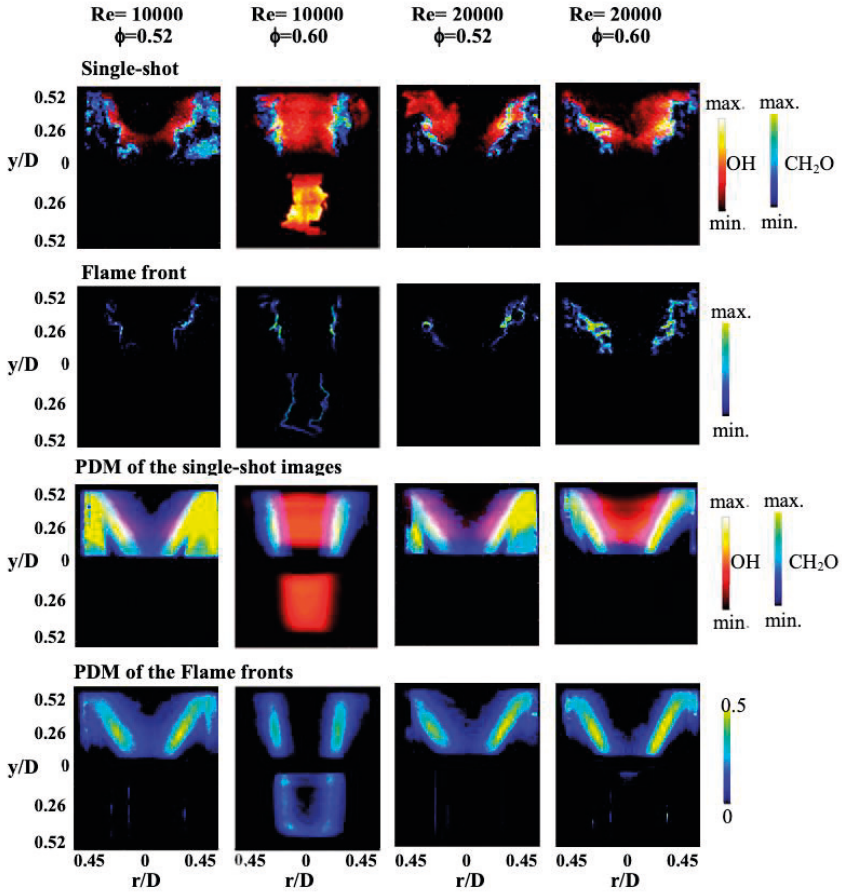

Figure 4.10: Images of simultaneous OH- and CH_2O-PLIF for $\phi = 0.52$ and 0.60 at Re = 10000 and 20000: single-shot images shown in the first row, heat release zone estimated by [OH]×[CH_2O] and gradient [OH] shown in the second row, PMs of single-shots shown in the third row, and PMs of the heat release zones shown in the fourth row.

The heat release zone in the combustion chamber is indicated by the product of [OH]×[CH_2O], while it is indicated by the gradient of OH-PLIF signals in the premixing tube where only OH-PLIF measurements were performed. A significant broadened CH_2O layer was observed for the case at $\phi = 0.52$ and Re = 10000 due to the low reaction rate at the condition near LBO. As the Re increased, the thickness of the CH_2O decreased rapidly. This implies the reinforcement of the chemical

reactions, which consumes more fuel with increasing bulk velocity and thus high turbulence intensity. The distribution of OH radicals was found mainly located in the premixing tube with strong signal intensity for the flashback case (ϕ = 0.60 and Re = 10000). For cases at high Re, the thin flame front (heat release zone) reveals the flame still in the flamelet or thin reaction regime. Besides, more wrinkles were found in the flame front with an increase of Re.

4.2.2 Effect of H_2 enrichment on the methane/air flames

To achieve better flame stabilization at lean operating conditions in a gas turbine combustor, the addition of H_2 is a potential strategy for practical applications. Investigations on H_2 addition to the swirl stabilized methane/air flames are of great interest and have been conducted by many researchers recently. As an alternative fuel for natural gas, H_2-enriched methane mixtures were used in the CECOST swirl burner. Since the combustion characteristics of H_2 is significantly different from hydrocarbon fuels, the operating performance of gas turbine combustors can be changed significantly for hydrogen-enriched methane mixtures.

The effects of H_2 enrichment on the methane/air flames at the CECOST swirl burner were investigated experimentally by employing different optical measurement techniques. In this experimental campaign, there were a few changes in the burner setup to further improve the mixing process. A porous plug plate was added above the honeycomb (shown in Figure 3.4) and the fuel injection pipes were arranged vertically inclined 45° in a clockwise direction, that detailed geometric layout is shown in Fig.1 in Paper III. The OH-PLIF, high-speed PIV, and high-speed OH^* chemiluminescence imaging were performed separately for fuels with different addition of H_2 at various Re. The schematic of the setup is shown in Figure 4.11 and a photo of the setup in the lab is shown in Figure 4.12. The OH-PLIF measurement and high-speed OH^* chemiluminescence imaging were performed as the experiments on natural gas/air flames, which have been described in Section 4.2.1. For the PIV measurement, a high-speed diode-dumped, dual cavity Nd: YLF laser was used to generate the 527 nm laser pulses, and the laser sheet in the measured region is approximately 60 mm wide. A CMOS camera was used to capture images, with a recording rate of 1 kHz.

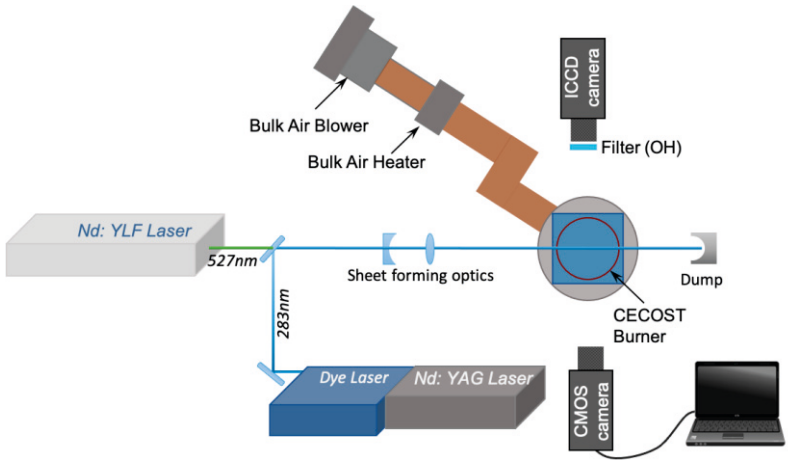

Figure 4.11: Schematic of the experimental setup.

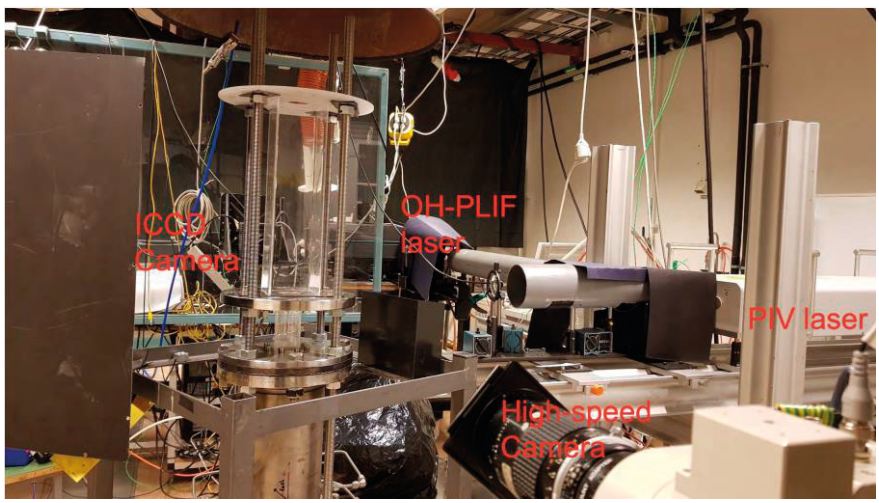

Figure 4.12: Photograph of the experimental setup in the atmospheric rig.

Three fuel mixtures of H_2/CH_4: 0/100, 25/75, and 50/50 (in vol.%) were investigated in the CECOST swirl burner and results of the experiments are discussed in the following aspects:

1. Stability regime and flame topologies

The burner stability regimes at Re = 10000, 15000, and 20000 are mapped for three different fuel mixtures in Figure 4.13. In the regime, operability limits (LBO and flashback) as well as the flame topology observed for each case, are presented. All cases are operated for three times, and the results show good repeatability. In addition, the corresponding laminar flame speed (S_L) was also plotted as the second

vertical coordinates to the right, which is calculated by the GRI-Mech 3.0 mechanism in Cantera. Typically, there are four major kinds of flame topology stabilized in a swirl-stabilized combustor as shown in Figure 4.14. Flames with a V shape, an unattached M shape, and an attached M shape are demonstrated in Figures 4.14 (a) - (c), which were reproduced from Ref. [58]. Another flame topology resembling a Π shape was reported by Reichel et al. [59] and is shown in Figure 4.14 (d). The detailed description and definition of flame stabilization with different topologies are given in Paper III. Three of these flame topologies were observed and identified in this experiment, including an unattached M-shaped flame, an attached M-shaped flame, and a Π-shaped flame, as shown in Figure 4.14 (I) – (III). These figures are time-averaged OH^* images deconvoluted by an Abel inversion (processing method described in Ref. [17]). The M-shaped flame marked in Figure 4.13 indicates flame in either unattached M or attached M shape.

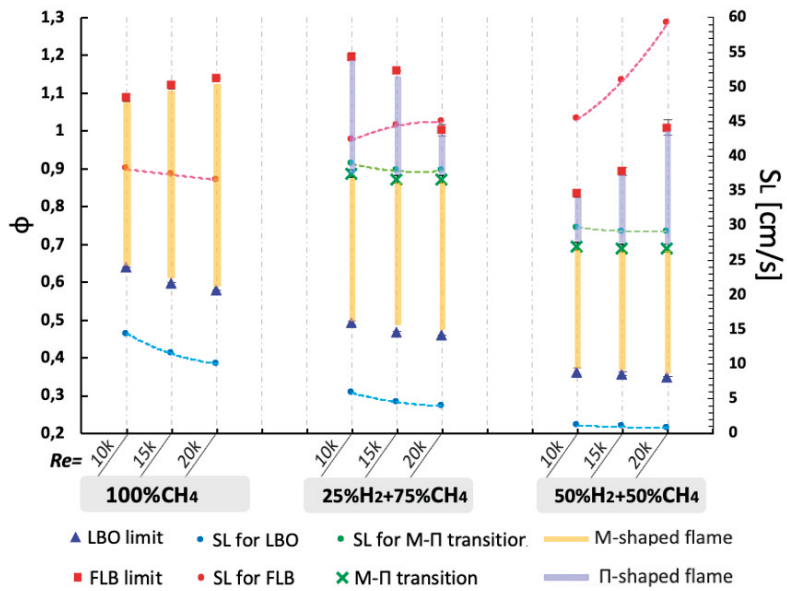

Figure 4.13: Burner stability regimes for three different fuels at various Re.

The effects of both Re and H_2 enrichment on the burner stability regimes are obvious. The LBO limits are significantly extended by the H_2 addition in methane. Compare to the pure methane cases, the ϕ of LBO limit was decreased for 25% H_2-enriched cases by around 22% and for 50% H_2-enriched cases by around 41%. This effect results from the faster reaction rate, higher diffusivity, and higher burning speed of H_2. But as Re increases, the LBO limit decreases slightly. One potential reason can be due to that the increasing volumetric heat release resulting from high Re enhances the capability of the resistance to perturbations that lead to LBO of the flame.

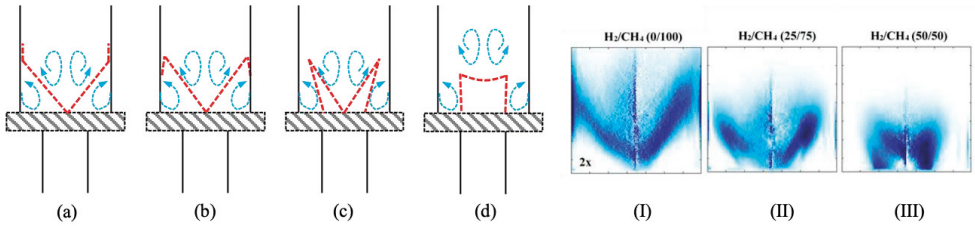

Figure 4.14: Schematics of different flame topology stabilized in the swirl-stabilized burner: (a) V-shaped flame; (b) unattached M-shaped flame; (c) attached M-shaped flame: (d) Π-shaped flame. And the representative flame topologies stabilized at the CECOST burner: (I) unattached M-shape flame; (II) attached M-shaped flame; (c) Π-shaped flame.

The flashback limit shows dependence on Re. Completely different flashback trends with Re are observed compared to the previous experiment. The flashback is proposed to occur at a comparatively leaner condition with H_2 addition in methane, but this is found to be improved by the occurrence of flame topology transition. For all H_2-enriched cases, the flame transition from M shape to Π shape takes place at a specific ϕ that is independent to Re.

2. Effect of ϕ and H_2 addition on flame structures

OH-PLIF results of pure methane/air flames at Re = 15000 for three different ϕ are presented in Figure 4.15. The cases with ϕ = 0.64, 0.80, and 0.96 represent the close-to-LBO case, a stable flame, and a flame near stoichiometric condition, respectively. The case close to LBO at ϕ = 0.64 posses comparatively low OH-PLIF signal intensity and a lifted flame root, while the stable and richer cases show higher OH signals because of the higher flame temperature and more hot products produced, and the flame root located upstream anchoring near the exit of the premixing tube. Due to the vortex breakdown induced CRZ of the swirling flow, the flame stabilized in M shape for all methane cases. As ϕ is increasing, the flame front leading point along the inner shear layer moves upstream and the flame fronts in OSL propagate further towards the dump plane of the combustion chamber.

Moreover, Figure 4.15 also shows the effect of H_2 addition on flame structures. It is evident from the figure that the flame topology transforms from M shape to Π shape for higher H_2 concentration added in the fuel mixtures (50% H_2 in vol.). The stabilization of a Π-shaped flame in the CECOST swirl burner results from the increased flame speed due to the H_2 addition into the fuel mixture, the higher resistance to the strain rate of the flame, and the change of the CRZ location due to flame/flow interaction. The location of the CRZ can be obtained by the PIV measurements.

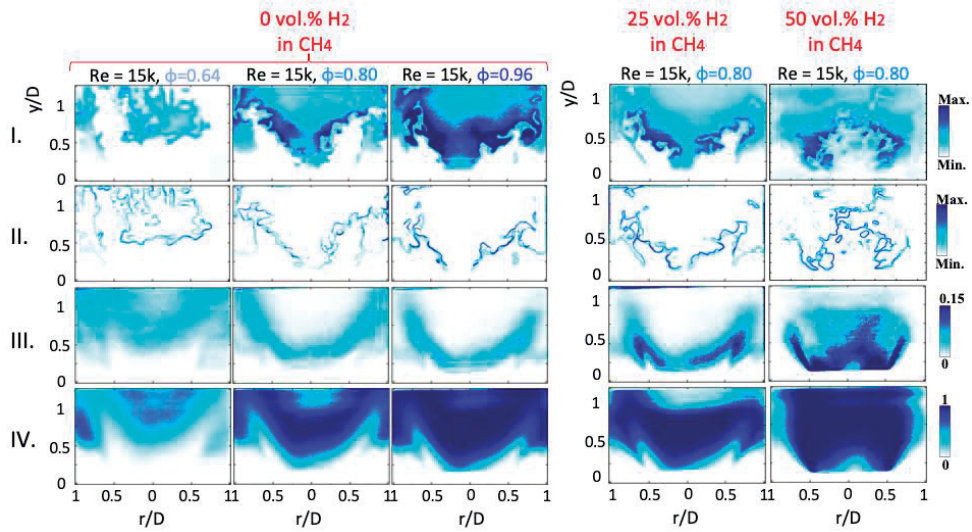

Figure 4.15: Results of OH-PLIF at different conditions presenting the effect of ϕ and H_2 addition on flame structures: I. Single-shot images; II. Gradients of OH; III. PMs of OH gradient; IV. PMs of single-shots.

3. Flow-fields of methane/air flames

PIV measurements were carried out for both cold-flows and methane/air flames to demonstrate the flow-fields in an axial/longitudinal cross-section. Figures 4.16 (a) – (c) show the comparison of mean velocity fields over 1 second (including 1000 samples) between Re = 10000 and 20000 at cold-flow cases, leaner cases at ϕ = 0.66, and richer cases near the stoichiometric conditions. In the figures of mean flow-fields, the direction of the velocity vectors is indicated by arrows and the magnitude of the in-plane velocity normalized by the bulk velocity in the premixing tube is indicated by the shades of the colour in the background. The iso-contours of the zero mean axial velocity, representing the boundaries of the CRZ, are shown in Figure 4.16 (d).

Compared to the mean velocity fields of the cold-flow cases, the centre of the CRZ approaches each other in the radial direction and moves upstream to the dump plane of the combustor at lean cases, as shown in Figures 4.16 (a) and (b). Also, increasing ϕ results in a larger maximum of velocity magnitude, and thus a larger velocity gradient. There is no CRZ appearing in the measured field only for the case close to the stoichiometric condition at Re = 10000, indicating that it is a flashback case where the CRZ is supposed to push into the premixing tube outside of the measured region. When considering the OH-PLIF results together with the flow-fields for these cases, it is evident that the flame fronts are unable to exist in the regions with a high strain rate.

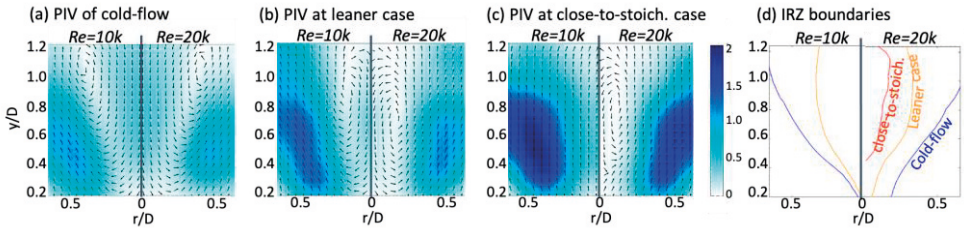

Figure 4.16: Results of PIV measurements for methane/air flames: (a) – (c) Comparison of mean flow-fields normalized by the bulk velocity of cold-flow between low and high Re for different ϕ; (d) Boundaries of the CRZ.

4. Flashback mechanisms

Flashback events occurring at various Re conditions in the CECOST swirl burner were captured by the high-speed OH^* chemiluminescence imaging system. Two types of flashback events were observed and identified in the experiments. Figure 4.17 shows the representative cases of flashback with different mechanisms through time-sequence single-shots of OH^*, in which (a) presents a flashback event driven by the CIVB and (b) presents a flashback initiated in the boundary layer.

In the process of the CIVB flashback for the pure methane/air case shown in Figure 4.17 (a), the leading flame tongue starts to propagate upstream into the premixing tube along the tube centreline. The upstream flame propagation appears a 3D helical motion caused by the swirling flow and the vertical oscillation, after which the flame approaches the bottom of the premixing tube (shown in the single-shot at 684 ms). In the CIVB driven flashback case, the flame is prevented from propagating upstream along the near-wall region, where the reactants flow being accelerated in the streamwise direction. Besides, a boundary-layer flashback (BLF) was observed for the H_2 enrichment case shown in Figure 4.17 (b). The first three single-shots in it appear distinct initiation process compared to CIVB, in which the upstream propagation of the leading flame tongue starts from the near-wall region. Since the single-shot at 163 ms, additional flame tongues can be observed and one of them is always dominating in leading the flame position. These two types of flashback events are identified by both observation and statistics methods. The probability density function (PDF) of the radial position of the leading flame tip in the premixing tube was used for this statistical analysis, which shows a clear distinction between the CIVB and BLF cases. The detailed description and histograms of the PDF in radial position can be found in Paper III.

Moreover, the flashback mechanisms are found to be related to the fuel composition and thereby the flame topology. The CIVB flashback was observed for all pure methane/air flames with an M shape, while the BLF was found to occur for all H_2-enriched methane flames with a Π shape. In this work, the propensity of flashback in the boundary layer increases by H_2 addition to the methane.

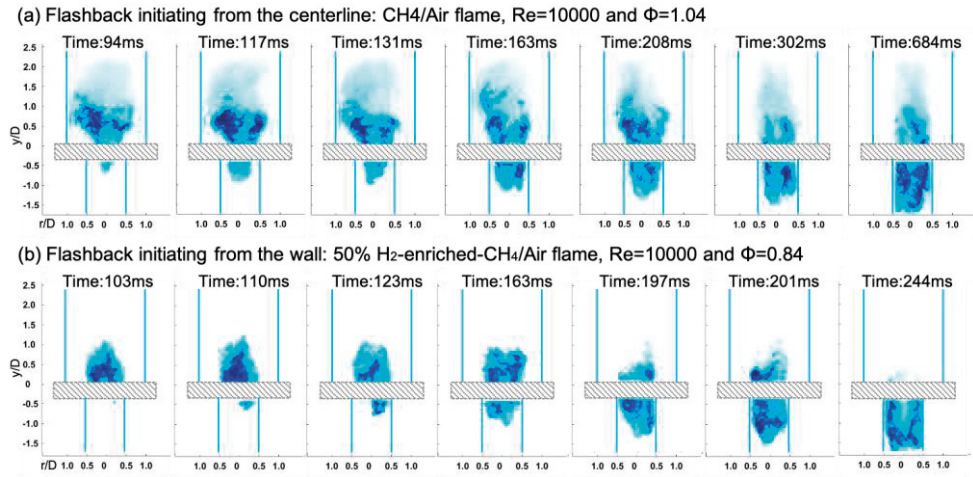

Figure 4.17: Representative flashback events occurring in the CECOST swirl burner with different mechanisms: (a) flashback due to CIVB; (b) flashback in the boundary layer.

5. Flame shape transition

As shown in Figure 4.13, the transition of flame shape from M to Π took place for H_2 enriched cases at a specific ϕ, which is almost independent of the Re. The process of this transition was also captured using high-speed OH^* chemiluminescence imaging. A representative process of the flame shape transition from M to Π occurring in the CECOST swirl burner for a H_2 enriched methane case was presented in Figure 4.18 by the time-sequence single-shots of OH^*. In the figure, an M-shaped flame was initially stabilized in the combustor, but the flame ended by a Π shape after a few seconds. During the transition process between the two flame shapes, a flame leading tip was always found to appear in the premixing tube in a way similar to the initiation of CIVB. Before completion of the transition, the upstream flame leading tip moved back to the combustor, anchoring on the exit of the premixing tube, and a more compact flame formed as a result from the radially inward motion. This phenomenon suggests that the transition of flame shape from M to Π can prevent a potential CIVB flashback and extends the flashback limit to a richer condition, which needs further in-depth investigation to come to a conclusion.

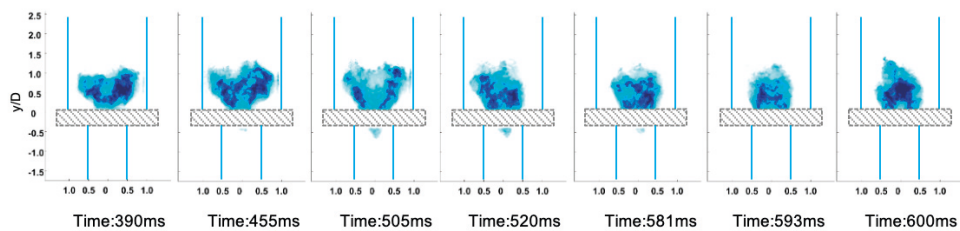

Figure 4.18: The process of the flame shape transition from M to Π.

4.2.3 Improvement of fuel/air mixing in the CECOST swirl burner

Better mixing of the fuel/air before the reaction takes place has been proven to be crucial for achieving the high performance of a gas turbine combustor. In order to advance the design and operation property of a practical combustor, acetone-PLIF has been widely used to visualize the mixture distribution and quantify the level of mixing [60, 61]. Since the fuel injection scenario strongly impacts the mixing, it also becomes a key factor for determining the performance of the burner. Therefore, the setup for fuel injections in the CECOST swirl burner was optimized and the corresponding mixing degree was investigated qualitatively by acetone-PLIF measurements.

The scheme for performing the acetone-PLIF was roughly summarized in Table 2.1, in which the laser sheet horizontally passes through a plane near to the exit of the premixing tube (~ 5 mm). Three different scenarios of fuel injections and the corresponding acetone-PLIF results are presented in Figure 4.19. Setup-1 refers to the fuel injections utilized in the investigation of the natural gas/air flames, where two vertically upward pipes, having a diameter of 6 mm, were used as fuel injectors. Setup-2 refers to the fuel injections involved in the work of Paper III, where these two pipes were vertically inclined 45° in a clockwise direction, and a porous plug plate was mounted above the honeycomb (shown in Figure 3.4 (a)) to further enhance the mixing process.

While the Setup-new is the latest improved fuel injection scenario which used spiral pipe with small holes evenly distributed along the surface instead of two pipes. From the acetone-PLIF results, it can be seen that the fuel distributions, representing the degree of mixing, have been improved in Setup-2 from Setup-1 and a further improvement in Setup-new than that for both Setup-1/2. A nearly homogeneous mixing for the fuel and air is achieved by the spiral fuel injection, which is expected to be used for further studies on the CECOST swirl burner.

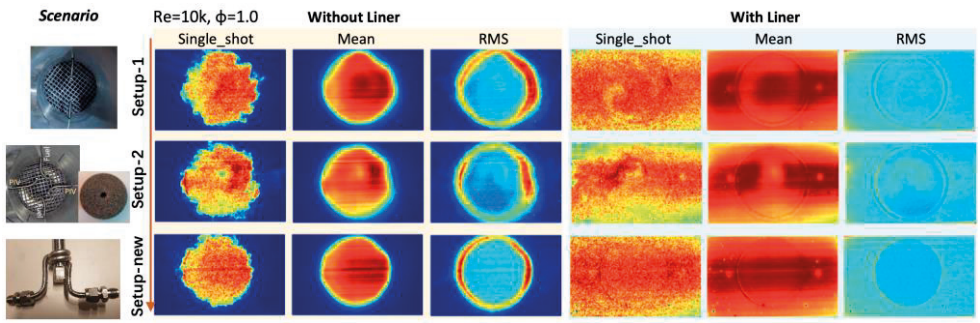

Figure 4.19: Results of Acetone-PLIF representing the mixing degree for three different setups of fuel injections.

4.3 Flame stabilization using gliding arc discharge at the scaled Siemens DLE burner

The lean premixed combustion in practical gas turbines faces issues of instability, including low combustion efficiency, local extinction, lean blowout, etc. Application of the plasma-assisted combustion (PAC) in gas turbine combustors has been demonstrated as a promising method for combustion enhancement, reduction of emissions, and improvement of the fuel reforming [62-65]. Different types of plasmas have been investigated in PAC applications. Due to various advantages: relatively low electron temperature, high power density, and easy deployment, the gliding arc discharge plasmas have been widely used in flame stabilization [66], emission control [67], and fuel reforming [68].

In this thesis work, a rotational gliding arc (RGA/GA) discharge plasma was applied at a Siemens scaled DLE burner to investigate the influence of plasma on flame characteristics. The burner was installed vertically in the atmospheric combustion test rig, and details of the setup are described in Chapter 3. Optical measurement techniques, including high-speed OH^* chemiluminescence imaging and OH-PLIF, were employed to investigate the flame stabilization and structures. The optical emission spectroscopy was used to analyze the spontaneous emissions from the flame. Besides, combustion emissions were sampled by a probe to obtain both the NO_x and CO emission levels. A schematic of the experimental setup is shown in Figure 4.20.

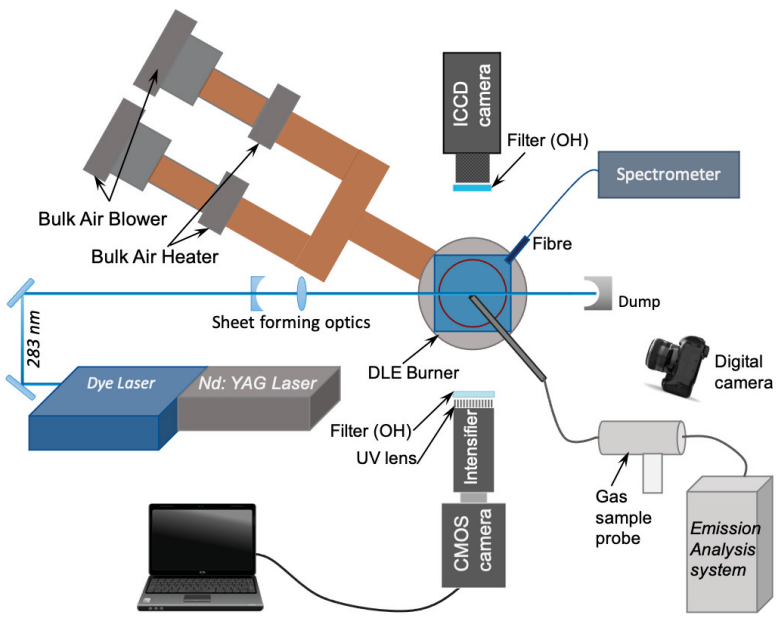

Figure 4.20: Schematic of the experimental setup in the study of the application of GA plasma in the DLE burner.

In the experiment, only air or O_2 was injected separately into the RPL section for cases with and without RGA discharge. A summary of the operating conditions and the key parameters is presented in Table 4.1. To match the practical condition of the gas turbine burner, the bulk velocity was set to 60 m/s at the burner throat, where the swirl number was around 0.7. The global ϕ was calculated by the total mass flow of the fuel and air injected into all three sections of the burner, but the ϕ of the Main and Pilot section were kept the same. Both the bulk air and the RPL flow (air/O_2) were preheated to 673 K. The flowrate of the air/O_2 injected into the RPL was determined to sustain the RGA downstream of the RPL exit. In the whole range of the operation, the average power of the RGA discharge was in a range of 75 - 82 W, which is less than 0.1% of the total thermal power. The results and discussion of this investigation are presented in Paper V and VI.

Table 4.1: Summary of the operating conditions and key parameters.

Operating Condition	RPL flow (g/s)	Global ϕ	Thermal load (kW)	Average discharge power (W)	Throat velocity (m/s)	Preheat temp. (K)
Air in RPL & RGA off	0.35	0.43-0.52	98 - 78	75 - 82	60	673
Air in RPL & RGA on						
O_2 in RPL & RGA off	0.18					
O_2 in RPL & RGA on						

4.3.1 Effect of the RPL flow and temperature on the RGA location

The location of the RGA downstream of the RPL exit is critical for the performance of the RGA. Figure 4.21 (a) shows a top view of the Siemens scaled DLE burner, in which the relative position between the main and pilot swirler is demonstrated. In Figure 4.21 (b), a photograph of the GA discharge generated in the Siemens scaled DLE burner is presented, which was taken with a standard SLR camera.

The RGA discharge is always initiated from the position with the shortest distance between the electrode and the inner surface of the RPL. A re-ignition event can be triggered by the increase of temperature when the plasma column is shortened by the reduced irregular stretch for the low turbulence. In addition, a re-ignition event can be also triggered by the too high flowrates [69, 70]. Thus, the RPL flowrate was set to 0.35 g/s for the air and 0.18 g/s for the O_2 at preheat temperature of 673 K, to avoid reignition events. A lower flowrate was needed for the O_2 injection case, as the large percentage of N_2 in the air was replaced by more reactive O_2 which leads to enhanced chemical reaction rate.

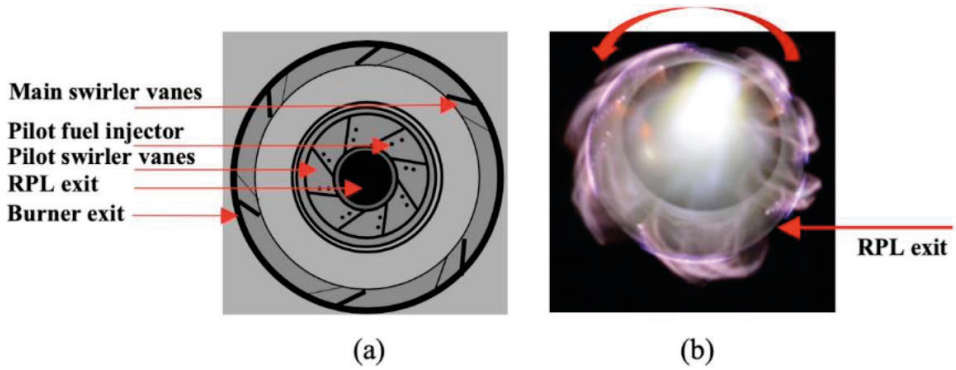

Figure 4.21: (a) Top view of the Siemens DLE burner; (b) Photograph of the GA discharge generated in the burner.

4.3.2 RGA plasma-assisted flames

The RGA plasma-assisted flames in the Siemens scaled DLE burner are discussed in this section divided into the following parts:

1. Comparison of the assistance effect by the RPL flame and plasma in RPL

In the scaled Siemens DLE burner, details are described in Section 3.2.2., the RPL flame was operated in rich conditions to assist the overall flame stabilization. Comprehensive investigations concerning the development of the DLE burner have been conducted by Subash et al. and reported in publications [26, 71-73]. As a pre-study for the work in this thesis, this burner was also tested for cases with and without RPL flame (ϕ = 1.2), in both of which the Pilot and Main flames were kept with the same ϕ = 0.47. Photographs of such two whole flames in the burner with the original design are presented in Figure 4.22 (a), which confirms that the RPL flame plays an important role in the overall flame stabilization. It is evident that the main flame approaches LBO when there is no flame in the RPL but is reattached back to the quarl as igniting the RPL flame. This is attributed to the heat and chemically active species/radicals added by the RPL flame to the main flame.

In this thesis, the RPL of this burner has been redesigned by employing a HV electrode. Photographs of whole flames with and without RGA plasma on the RPL are presented in Figure 4.22 (b), in which both the Pilot and Main flames have the same ϕ = 0.47. It can be easily found that the plasma discharge also shows the capability of improving stabilization of the main flame close to LBO. This can be explained by the fact that the RGA plasma discharge can generate large amounts of reactive species and certain thermal energy to the main flame, thus shows a similar assistance effect on the macroscopic flame stabilization as the RPL flame.

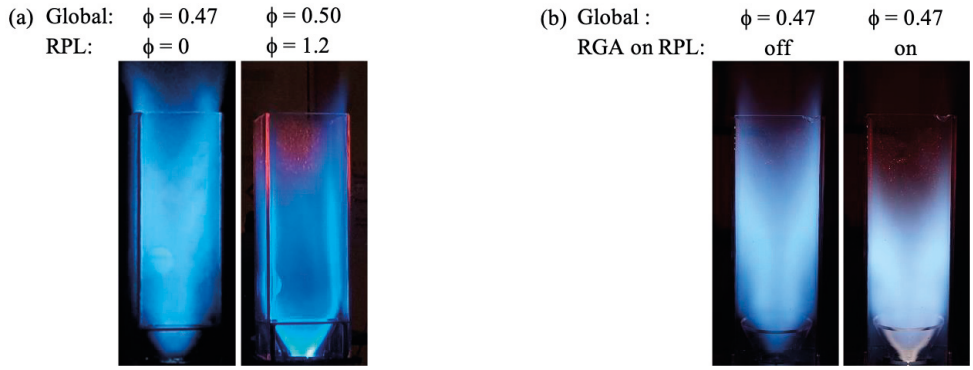

Figure 4.22: Photographs of flames (a) with and without RPL flame assistance; (b) with and without RGA plasma assistance.

2. Effect of RGA on LBO limits

Large amounts of CO species can be generated in the combustion process of a close-to-LBO case, due to the lower oxidation rates and incomplete combustion of hydrocarbon fuel [74]. Therefore, an exponential increase in CO emission is often used to recognize the occurrence of LBO. In Figure 4.23, the CO emission levels for both air and O_2 cases with and without RGA plasma are illustrated. The LBO limits for these operating conditions are also identified and presented in Figure 4.23.

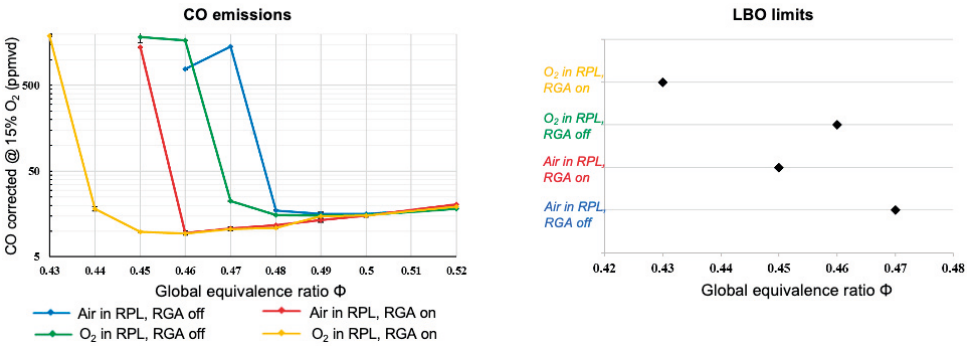

Figure 4.23: CO emission level for all operating conditions and the LBO limits which are determined by the exponential increase in CO emission.

Compared to the air injection case, the LBO is shifted towards the leaner ϕ for O_2 injection under both cases with and without RGA. This improvement is most likely due to the enhancement of the chemical reaction rate for the higher content of O_2 in the fuel/air mixture, in which the flame temperature is increased and thus the higher reactivity. This chemical reaction rate can be further increased by the plasma discharges. Flame kernels are generated after the RPL exit through the direct interaction of the Pilot fuel/air with discharge, which in a diffusion-like manner. For

O_2 injection case, flame kernels produce higher thermal energy, along with more active radicals generated by the discharge, which can significantly improve the flame stabilization. Therefore, the LBO limit is extended down to $\phi = 0.43$ for O_2 injection with RGA plasma as indicated in Figure 4.23. A similar extension of the LBO limit is also found for air injection with RGA plasma.

3. Effect of RGA on flame stabilization

Figure 4.24 presents a process of RGA assisted stabilization in the Siemens scaled DLE burner by a time-sequence OH^* single-shot images. Over a period of 24 ms, there are three distinct flame states. In the beginning, a flame without RGA shows an axially elongated shape and is no more steadily anchored in the CRZ, representing a near LBO condition. Once the RGA is applied, a flame kernel (marked by a white circle in the figure) appears from t_0+3 ms and the flame is then in a transition state, in which a re-stabilization process takes place. This transition takes around 9 ms as indicated in the figure until the flame is completely stabilized in the CRZ, which refers to the third state i.e., a stable flame. After the stable flame is achieved with RGA assistance, the flame kernel in the whole reaction zone moves in a rotational helical motion. This process can be explained as the local ignition event by the flame kernel. The typical phases of ignition by discharge in gas turbine combustors include initial kernel formation with energy deposition, early kernel growth to generate flame, flame stabilization, and propagation to the whole reaction zone [75, 76].

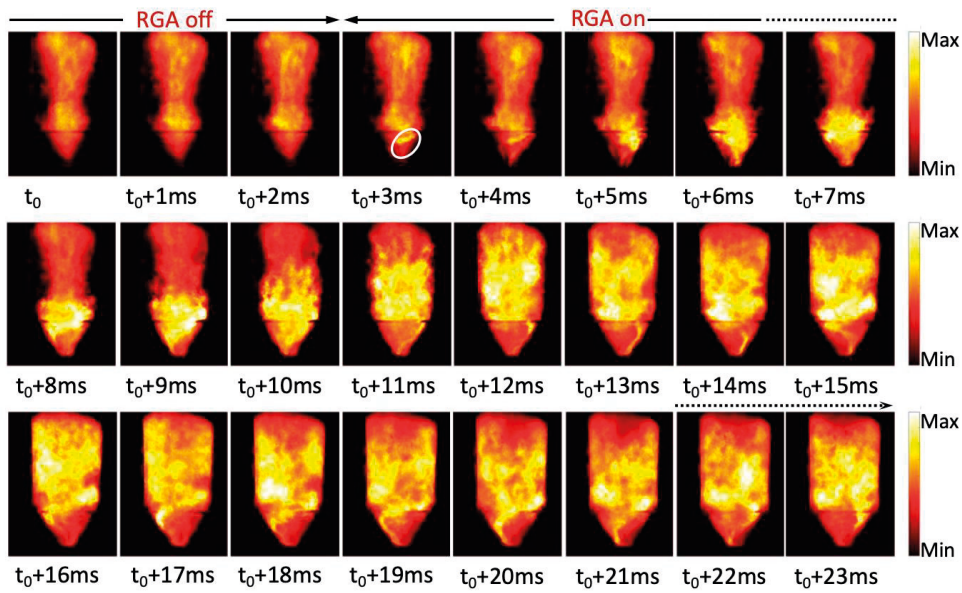

Figure 4.24: A time-sequence of OH^* chemiluminescence images showing the process of flame re-stabilization with RGA assistance.

The results of the OH-PLIF on flames at global $\phi = 0.47$ with and without RGA discharge for air/O_2 injection into the RPL are presented in Figure 4.25. For the air injection case without RGA, the flame is detached from the quarl and the flame front exhibits continuous defragmentation, due to the local extinction of the flame. The cold gas entrainment, heat loss, and high strain rate can be the reason for the local flame quenching. For the O_2 injection case without RGA, the flame is stabilized more upstream, and the flame front shows less defragmentation as compared with the air injection case. While for both air and O_2 injection cases with RGA in the RPL, the flame is expanded radially and moves slightly upstream than that without RGA, which can be explained by the improvement in flame stabilization in terms of creating CRZ by employing plasma discharge.

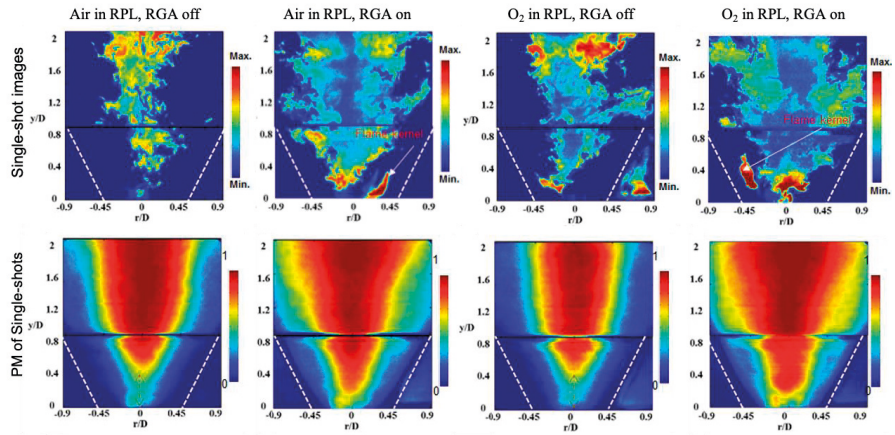

Figure 4.25: OH-PLIF results for operating conditions with air/O_2 injection at global $\phi = 0.47$, with and without RGA in the RPL. Upper row: single-shot of OH-PLIF; Bottom row: PMs of single-shots.

4.3.3 NO_x emissions

The NO_x emission levels for all operating conditions are presented in Figure 4.26. For both air and O_2 injection cases without RGA assistance, the NO_x emission levels are kept at the minimum level, while the average levels of NO_x emission increase evidently for both cases with RGA assistance. The increase in NO_x emission as RGA plasma applied can result from the NO_x produced by the plasma and/or by the more compact flame through the thermal NO pathway. Moreover, the NO_x emissions for O_2 injection cases are significantly lower than that for air injection. The drastically reduced concentration of N_2 for using O_2 in the RPL instead of air is the dominant reason for the reduced NO_x emissions. Besides, Figure 4.26 also presents the NO_x emission for the reference operating case reported in [73]. The comparison of the NO_x emission indicates the NO_x level observed in the current study for RGA assisted flames is still well below the level observed for the reference case with a rich RPL flame.

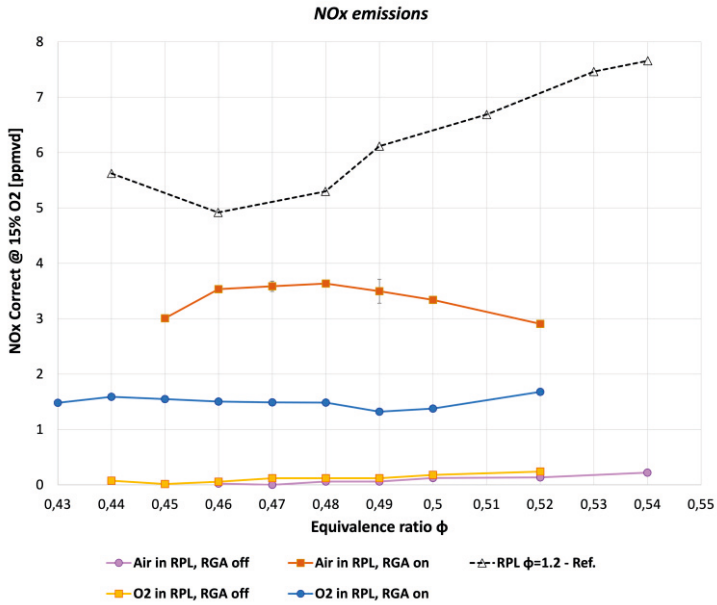

Figure 4.26: NO_x emission levels for all operating conditions with and without the RGA assistance and the comparison with the NO_x emission from a reference RPL flame assisted case.

4.3.4 Flame optical emission spectra

The optical emissions spectra from flames acquired by a fibre spectrometer are shown in Figure 4.27, presenting the average spectra from 100 measurements for different cases. In Figure 4.27 (a), the spectra for cases with and without RGA are compared between air and O_2 injection in the PRL at $\phi = 0.49$ and 0.50, respectively. Only the OH peak at around 310 nm and peaks in the near-infrared range, such as H_2O, were observed for cases without RGA plasma. When replacing the air with O_2 in the RPL, no difference was observed for the OH peak, while the infrared peaks became slightly stronger.

To observe how the flame emissions are influenced by the RGA at different ϕ, average spectra, at $\phi = 0.48$ and 0.52 for air injection, are compared between the cases with and without RGA plasma (shown in Figure 4.27 (b)). When the flame is assisted by RGA plasma, all peaks in the flame spectra become approximately 2-5 times stronger than those without plasma. This results from a large number of free electrons produced by the plasma, which further interact with the ambient species and create ironized or excited molecules/atoms. Besides, more peaks show up when the plasma is applied, which are the CH peak and two comparatively strong peaks corresponding to sodium (Na) and potassium (K). CH flame emission getting stronger with plasma can be also recognized by the photograph shown in Figure 4.22 (b), in which the flame appears much brighter with plasma on. The emissions

of Na and K are most likely due to the contaminations in the burner or plasma setup either in the RPL nozzle or the HV electrode, where the surface temperature is dramatically increased by the RGA plasma. The intensity of Na and K peaks are found to be independent of ϕ, which supports that the Na and K emissions are from the material ware rather than from the flame.

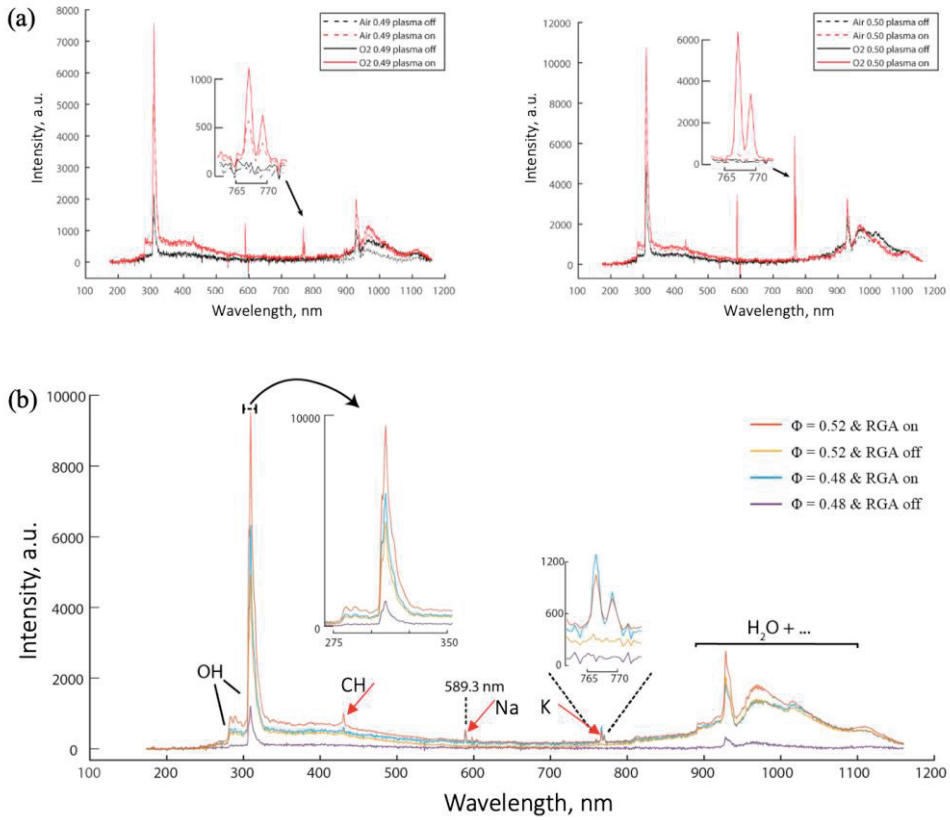

Figure 4.27: The spectra of flames: (a) for cases with and without RGA for both air and O_2 injection with global ϕ = 0.49 and 0.50; (b) for air injection cases with global ϕ = 0.48 and 0.52 with and without RGA plasma.

5 Diagnostics in turbulent jet flames

To gain a deeper understanding of turbulent combustion, investigations of turbulent jet flames were performed. In this chapter, a brief introduction of the fundamentals of turbulent flames is firstly described. Then the results of diagnostics applied to the two types of turbulent jet flames are mainly presented: 1) turbulent premixed ammonia/air flames at the DRZ burner; 2) turbulent inverse diffusion flames at elevated pressure conditions. More results and detailed discussions can be found in Paper IV and Paper VII, respectively.

5.1 Fundamentals of turbulent flames

Combustion in most practical applications occurs in turbulent flows. Turbulent flow is a random, chaotic, and irregular flow, which features high Re, 3D vorticity fluctuations, dissipation, etc. Turbulent combustion benefits from the enhanced mixing effects of the turbulence. Due to the complexity of the turbulent flames, much more special features of turbulent flames are to be defined than those for laminar flames. This section tries to briefly introduce some fundamental concepts about turbulent flames.

5.1.1 Turbulent scales

Turbulent flows always occur at high Re, which is a useful dimensionless parameter used to characterize the flow. Re is defined as the ratio of the convective forces and viscous forces, which is expressed as

$$Re = \frac{uL}{\nu}$$

where u is the fluid velocity, L is the characteristic length scale, and $\nu = \mu/\rho$ is the kinetic viscosity (μ is the dynamic viscosity and ρ is the fluid density).

The turbulent flow contains a wide range of eddies, which are characterized by their length, characteristic time, and velocity scales. Through a so-called cascade process, turbulence kinetic energy contained in the largest scales is transformed to the smaller scales, until that is transformed to the smallest scales which ends by

dissipating into thermal energy. Figure 5.1 presents the energy cascade process of the turbulence flow. In the energy containing range, large eddies carry most of the kinetic energy, which is extracted from the mean flow. Integral scale, l_0, is the length scale of large eddies. Then the large eddies continuously break up into smaller eddies in the inertial subrange, which the eddy size is given by the Taylor length λ_t. The eddies in this region can be characterized by:

$$E(\kappa) = C_K \varepsilon^{2/3} \kappa^{-5/3}$$

where $C_K \simeq 1.5$ is the Kolmogorov constant which is determined by experiments, ε is the spectral transfer per unit time, and $\kappa = 2\pi/l$ is the wavenumber. This equation represents the Kolmogorov spectrum law or the -5/3 law [77, 78], which indicates that the energy spectra should exhibit a -5/3 slope in the inertial region for the flow that is fully turbulent, corresponding to a high Reynolds number. In the end, the dissipation occurs in the viscous subrange. The scales of these smallest eddies are described by the Kolmogorov scales, which can be expressed as [79]:

$$\text{Length scale: } \eta = \left(\frac{\nu^3}{\varepsilon}\right)^{1/4},$$

$$\text{Time scale: } \tau_\eta = \left(\frac{\nu}{\varepsilon}\right)^{1/2},$$

$$\text{Velocity scale: } u_\eta = (\nu\varepsilon)^{1/4}$$

in which turbulence is only determined by ν and ε (energy dissipation rate).

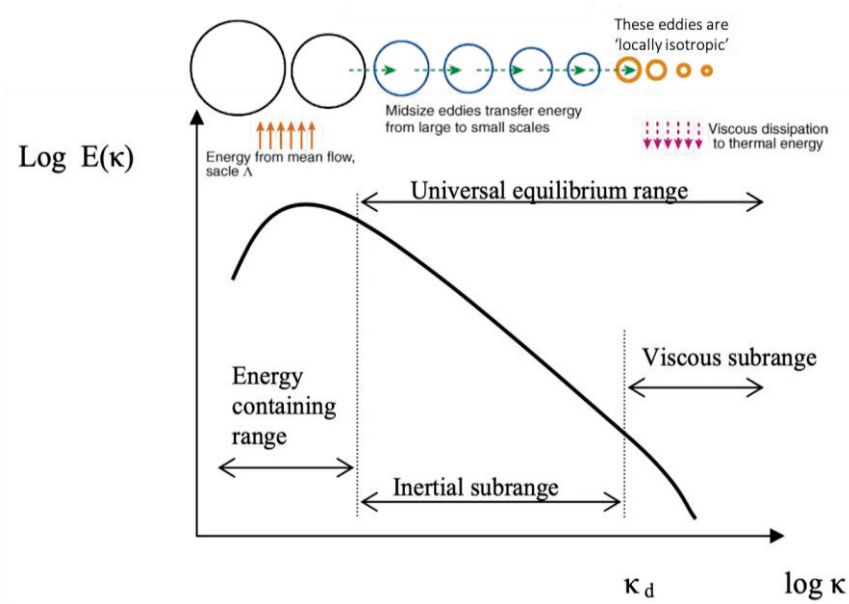

Figure 5.1: Energy cascade (spectra) of turbulence. Adapted from [80, 81].

5.1.2 Flame and turbulence interaction

The interaction between flame and turbulence in turbulent premixed flames is most commonly classified into different regimes, in which the ratio of turbulence and chemistry time scales are used as boundaries. Figure 5.2 presents a regime diagram that is mostly used, known as the Borghi diagram, which was proposed by Borghi [82] and modified by Peters [83]. In the Borghi diagram, five different regimes are divided by the value of dimensionless numbers. Therefore, it is necessary to introduce two other dimensionless numbers here to understand the Borghi diagram and quantify the extent of the flame/turbulence interaction.

The ratio of the integral time scale (τ_0) to the chemical time scale (τ_c) is defined as the Damköhler number (Da), which is expressed as:

$$Da = \frac{\tau_0}{\tau_c} = \frac{l_0 S_L^0}{u' \delta_L^0}$$

The Karlovitz number (Ka) is the ratio of the chemical time scale (τ_c) to the Kolmogorov time scale (τ_η), and can be expressed as:

$$Ka = \frac{\tau_c}{\tau_\eta} = \frac{(\delta_L^0)^2}{\eta^2} = \frac{u_\eta^2}{(S_L^0)^2}$$

where δ_L is the thickness of the laminar flame and S_L is the laminar flame speed. The turbulent Re_t can be written as [83]:

$$Re_t = Da^2 Ka^2$$

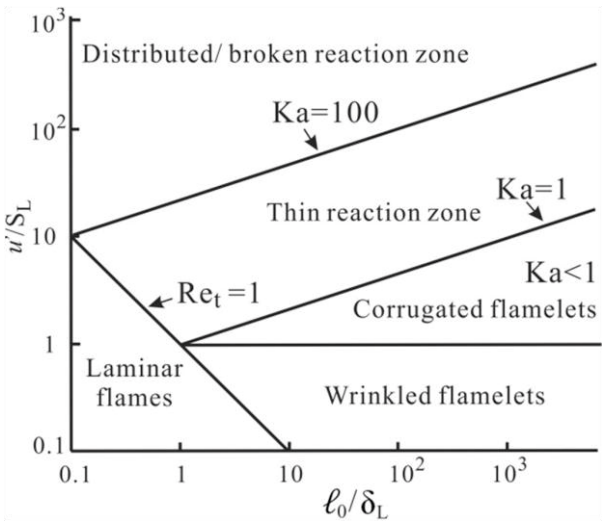

Figure 5.2: The Borghi diagram of turbulent premixed flames [82, 83].

Based on definitions of these dimensionless numbers, one can characterize a clearer understanding on the flame/turbulence interaction belonging to different regimes in the Borghi diagram. The different turbulent regimes are separated from the laminar flames with a line of $Re_t = 1$. The flamelets regimes are characterized by $Ka < 1$, where the Kolmogorov scale is larger than the chemical time scale, i.e., the smallest eddies are too large to interfere with the flame structure, resulting in a quasi-laminar flame front. But for the flame with $1 < Ka < 100$, the smallest eddies are smaller enough to penetrate the preheat zone but not able to disturb the reaction zone. Consequently, a flame with a broadened preheat zone but retaining a thin reaction layer can be observed, so that the regime is named as a thin reaction zone. As increasing the Ka further exceeding 100, the Kolmogorov eddies are smaller than the thickness of the reaction layer, thereby are able to penetrate the reaction layer and subsequently disrupt the chemistry therein. Therefore, it is expected to possess either the distributed or broken reaction zone (DRZ).

5.2 Investigation of premixed turbulent flames at DRZ burner

As a potential carbon-free renewable energy source, which is an alternative to fossil fuels, ammonia combustion researches have received increasing attention in recent years [84, 85]. But ammonia combustion in turbulent flows, close to the conditions related to practical combustors, is still lacking comprehensive studies employing optical diagnostics.

Investigations on turbulent premixed ammonia/air flames at extreme conditions were performed at the DRZ burner, which is a piloted jet burner with larger geometric scales than the LUPJ burner [28]. Details on the DRZ burner assembling are described in Section 3.3.1. In this experiment, the DRZ burner was mounted vertically at the atmospheric pressure test rig (described in Section 3.1.1), where advanced laser diagnostics measurements were employed. A schematic of the current experimental setups is shown in Figure 5.3. To characterize the reaction zone and the structure of ammonia flames, simultaneous OH- and NH-PLIF were employed. For the NH-PLIF measurement, a dye laser operated with dye mixtures of Rhodamine 640 and 610 was pumped by a frequency-doubled Nd: YAG laser. The output of the dye laser was precisely tuned to 607.15 nm and frequency-doubled to 303.576 nm, which probe the NH radicals in the $R_1(4)$ $A^3\Pi$ - $X^3\Sigma^-$ (1-0) transition. Studies on the strategy for NH-PLIF used in the current experiments can be found in Ref. [86]. The OH-PLIF measurement was performed by exciting the $Q_1(8)$ $A^2\Sigma^+$- $X^2\Pi$ (1-0) transition of OH radicals using 283.93 nm laser radiation. After passing through a prism, the OH excitation laser was superimposed with the NH laser. Then, an approximately 50 mm wide laser sheet was formed for both laser

beams by using the sheet forming optics (a -75 mm cylindrical lens and a +500 mm spherical lens). Two ICCD cameras with proper filters were used for detecting the NH and OH fluorescence signals, respectively. A DG535 digital box was used to trigger and synchronize all the lasers and cameras. The gate width of the ICCD camera was set to 50 ns for NH and 80 ns for OH and the time delay between two laser pulses was 100 ns. Besides, another OH-PLIF measurement was separately performed to capture the entire flame profiles in one single-shot image by using a larger laser sheet. A concave cylindrical lens (f = -40 mm) and a convex cylindrical lens (f = +500 mm) were used to form a laser sheet with an approximately 15 cm width in the measured area. The obtained entire flame profiles are used to evaluate the turbulent flame speeds in this work.

Besides, a two-component LDA system was employed to obtain the turbulent flow field information. The basic principle of the LDA technique and some information about this two-component LDA system are described in Section 2.1.3. To enable a 2D measurement, the 2D traversing system was used to carry the LDA laser scanning the target field both horizontally and vertically. For the data collection and analysis in the BSA system (introduced in Section 2.1.3), a burst mode sampling was selected for the high temporal resolution and two LDA channels for each component are operated in a coincidence way. The mean and root mean square (RMS) velocities were acquired for the entire flow field by scanning the field in a range of 10 mm to 150 mm above the jet exit with a step of 20 mm in an axial direction and 20000 data points were set to collect for each point. While a higher sampling rate (around 20 kHz) was required and set for achieving analysis of time-correlation and turbulent spectrum. Detailed information on the setting of data collection and analyzer is given in Paper IV.

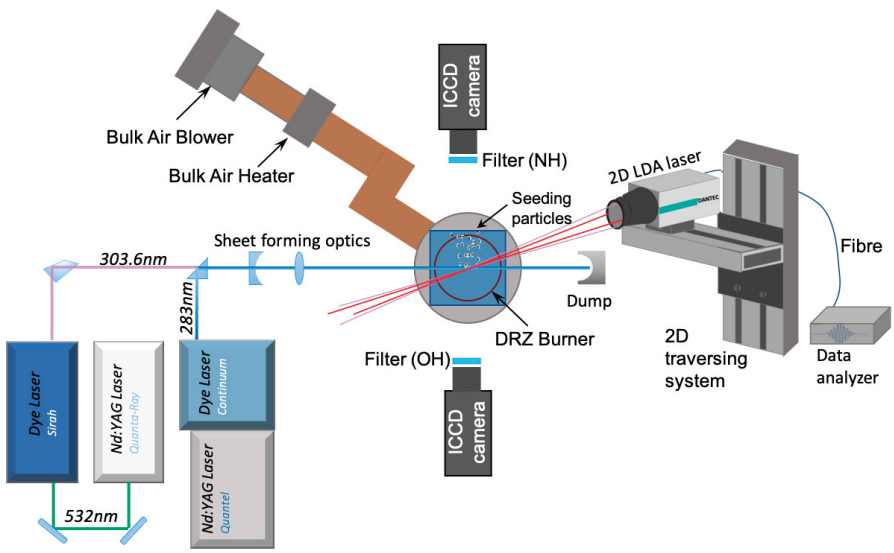

Figure 5.3: Schematic of experimental setups for the investigation at DRZ burner.

Table 5.1 presents the operating conditions as well as the corresponding scales for the tested cases in the current experiment. Cases are labelled as DRZα-β, in which α indicates ϕ for the jet flame and β indicates the jet velocity (m/s). For all cases, a pilot CH_4/air flame with ϕ = 1.0 and inlet velocity of around 0.9 m/s was used to provide a hot ambient area to help stabilize the central jet flame. The turbulent fluctuating velocity (u') and the integral scale (l_0) shown in the table are evaluated by the LDA measurement. Details on numerical simulation of the S_L, δ_L, and NH layer thickness ($\delta_{L,NH}$) for these cases can be found in Paper IV. Figure 5.4 shows a photograph of a turbulent premixed ammonia/air flame measured in the current experiment. Moreover, the thermal power for flames at the DRZ burner is up to 39 kW, which is comparable to that of a lab-scale gas turbine model combustor.

Table 5.1: Summary of the operating conditions and key parameters.

Cases	Φ	S_L cm/s	δ_L mm	$\delta_{L,NH}$ mm	u' m/s	l_0 mm	Re_t	η μm	u'/S_L	l_0/δ_L	Ka	Da	LDA
DRZ08-10	0.8	4.86	2.53	0.533			979	167	85	12	228	0.137	
DRZ10-10	1.0	7.86	1.83	0.529	4.11	29.3	837	188	52	16	94	0.306	√
DRZ12-10	1.2	8.72	1.71	0.983			808	193	47	17	78	0.364	
DRZ08-20	0.8	4.86	2.53	0.533			2041	116	147	14	476	0.095	
DRZ10-20	1.0	7.86	1.83	0.529	7.13	35.2	1745	130	91	19	197	0.212	√
DRZ12-20	1.2	8.72	1.71	0.983			1683	134	82	21	163	0.252	
DRZ08-30	0.8	4.86	2.53	0.533			3124	94	201	16	720	0.078	√
DRZ10-30	1.0	7.86	1.83	0.529	9.75	39.4	2670	106	124	22	298	0.174	√
DRZ12-30	1.2	8.72	1.71	0.983			2576	109	112	23	246	0.206	√

Figure 5.4: Photograph of a premixed ammonia/air turbulent flame at the DRZ burner.

5.2.1 Turbulent characteristics of the flow field

Part of the results from the LDA measurements are discussed in this section. The mean velocity distributions in the axial direction for flames with ϕ = 1.0 and jet velocity of 10, 20, 30 m/s are shown in Figure 5.5 (a). And the corresponding turbulence intensity profiles are shown in Figure 5.5 (b). The mean velocity for each case is normalized by the value at the first height (10 mm) above the jet exit, which is the maximum. Turbulence intensity (I) is calculated by:

$$I = \frac{\sqrt{\frac{1}{3}\left(\sigma_x^2 + \sigma_y^2 + \sigma_z^2\right)}}{\sqrt{\left(\bar{u}^2 + \bar{v}^2 + \bar{w}^2\right)}}$$

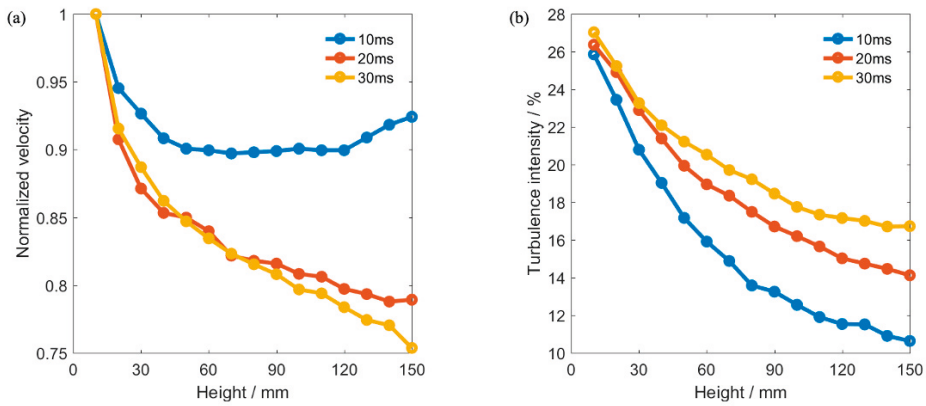

Figure 5.5: Distributions of normalized velocity and turbulence intensity along the axial direction for flames with ϕ = 1.0 and different jet velocities.

It can be seen that the axial velocity decreases monotonically with an increase in height. One exception appears for the case at 10 m/s, in which the axial velocity keeps almost the same from 60 mm above the jet exit. It can result from the low turbulent level and more homogeneous temperature distribution at the higher axial location for lower jet velocity. The turbulence intensity shows a similar level for all cases at the first height above the exit, and then shows a monotonic decrease but with different gradients for cases with different jet velocities. It can be seen that the higher jet velocity can maintain the turbulence axially in a larger area.

Figure 5.6 presents the turbulent energy spectrum for the case with a jet velocity of 30 m/s at four different heights. As the data collection is more than 5 seconds, the minimum energy spectrum frequency can down to 0.2 Hz, while the maximum frequency is limited by the sampling rate. The black dashed line plotted in the figure indicates the -5/3 slope for the wavenumber κ, corresponding to the Kolmogorov spectrum law. Results show that the energy spectrum for all heights follows the -5/3 slope from a certain frequency, which represents the starts of the inertial subrange of the turbulent flows.

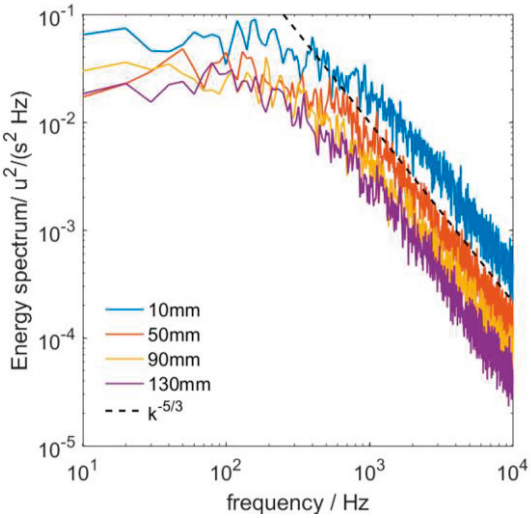

Figure 5.6: Turbulent energy spectrum for ϕ = 1.0 and 30 m/s cases at four different heights.

5.2.2 Turbulent flame structures

Single-shot images from simultaneous OH- and NH-PLIF measurements for cases with ϕ = 1.0 and jet velocities of 10, 20, and 30 m/s are shown in Figures 5.7, 5.8, and 5.9, respectively. Images shown in the right column are the overlapping results of the NH layer and the OH leading edge, which marks the edge of the OH radicals.

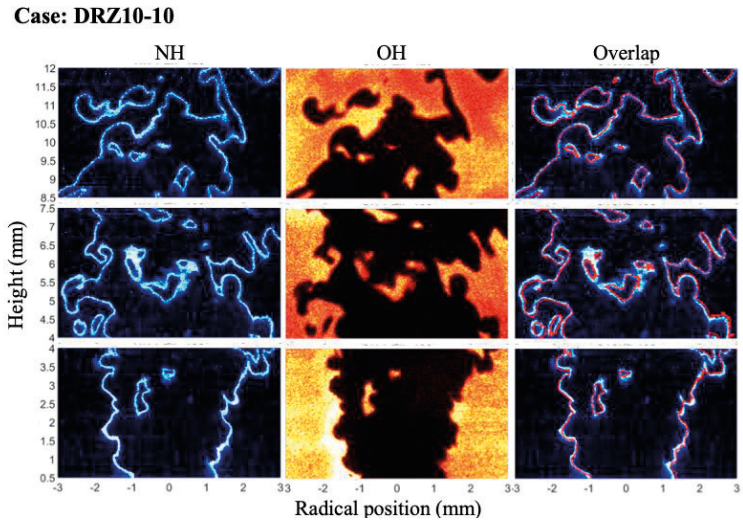

Figure 5.7: Instantaneous results of simultaneously OH-/NH-PLIF for case DRZ10-10.

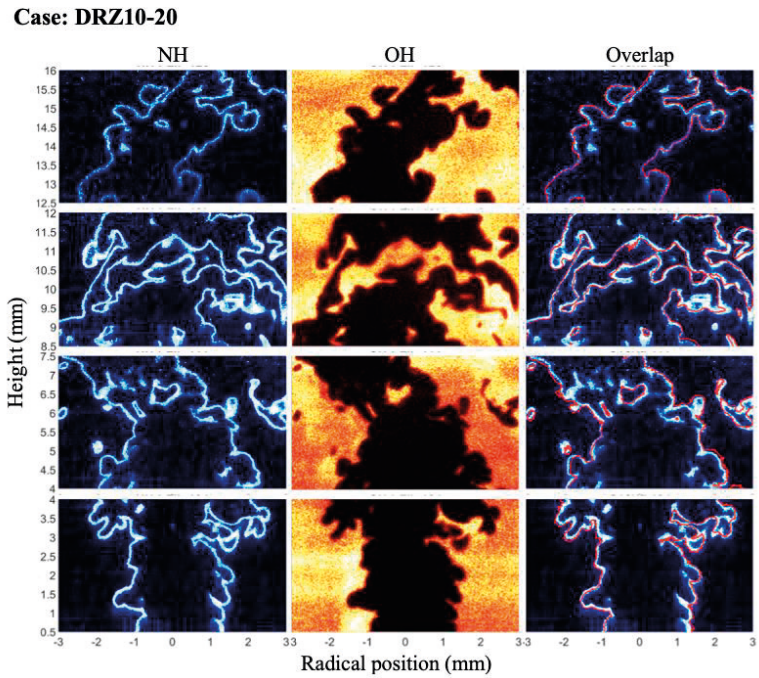

Figure 5.8: Instantaneous results of simultaneously OH-/NH-PLIF for case DRZ10-20.

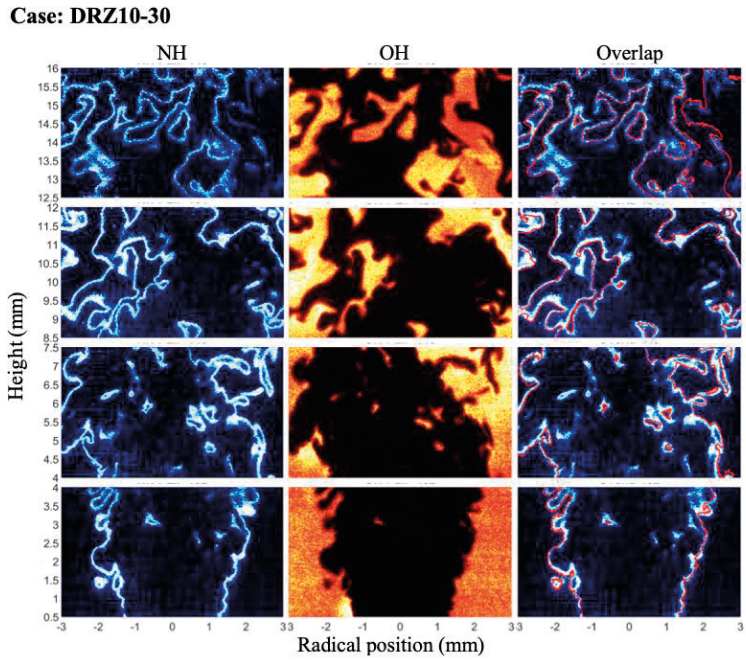

Figure 5.9: Instantaneous results of simultaneously OH-/NH-PLIF for case DRZ10-30.

From the NH single-shot images, one interesting characteristic can be observed is that the NH layers always keep thin even though most of the flames are located in the DRZ regime with high Ka. There is no broadening of the NH layer being observed in all cases. As increasing the jet velocity, more wrinkles are found in the flame structure, and different sizes of the isolated patchy islands are observed. Also, the correlation between NH and OH radicals can be inspected by the overlap image of the NH layer and the OH leading edge. It can be seen that the OH leading edge is always located inside the NH layer, indicating that NH and OH coexist in a very thin layer under high turbulent conditions. This phenomenon further reveals that the NH radical is a potential marker of the flame front for ammonia flames. And by a close inspection, the leading edge of the NH is found closer to the reactants side comparing to OH.

5.2.3 NH layer thickness

Although no significant change can be found in the thickness of the NH layer from the instantaneous NH-PLIF image, a quantitative analysis on the NH layer thickness is given here. A particular post-processing method on the results of NH-PLIF is needed, in which the ridge lines of the NH layer were extracted by the watershed transform [87] in a binarized NH image. The thickness of the layer is determined by the distance between the watershed ridge lines and the nearest point in the edge of the layer [88]. An example of the ridge lines extracted from the NH-PLIF image is shown in Figure 5.10 (a). Based on this method, profiles of the NH layer thickness normalized by $\delta_{L,NH}$ at several heights for various cases are plotted in Figure 5.10 (b). Only slight increases for the NH layer thickness can be found as increasing the jet velocity. In general, the thickness of NH layer remains unchanged for ammonia/air turbulent flames within a wide range of turbulent intensities.

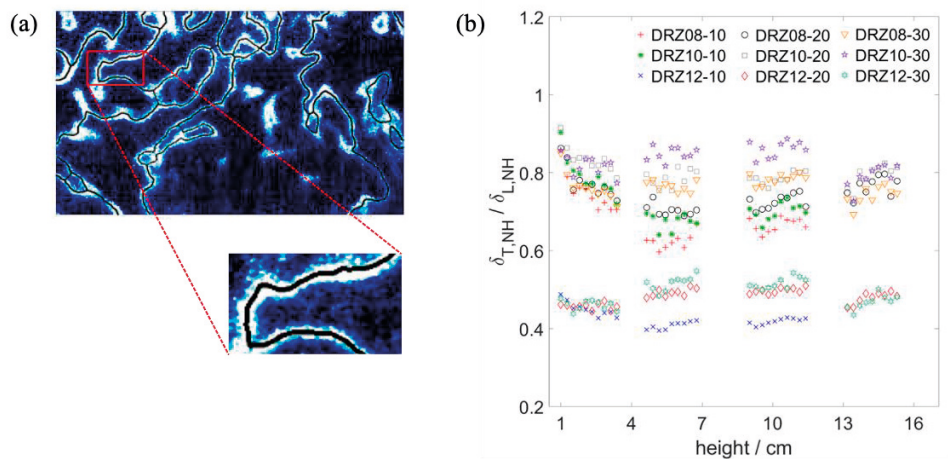

Figure 5.10: (a) Example of ridge lines extracted from the NH signals; (b) normalized NH layer thickness at several heights for various cases.

5.3 Investigation of turbulent inverse diffusion flames at high pressure

Although the lean premixed flames have significant advantages as discussed in the previous sections, diffusion flames are still extensively used in many practical combustion devices due to the better stability, safety, and wider operating range [89]. A special type of diffusion flame is the inverse diffusion flame (IDF), in which the oxidizer is injected into the centre of the surrounding fuel flow. IDF features less soot than normal diffusion flame (NDF) and locally exhibits characteristics of a partially premixed turbulent combustion. Studies on the characteristics of the IDFs have been conducted for many years and reported in many publications [90-94]. However, studies on IDFs at high-pressure conditions are rarely reported. Performing high-pressure test of combustion is crucial due to the fact that most combustion processes in high-load industrial combustors, e.g., gas turbines, internal combustors, etc., occurred at elevated pressures.

A coaxial IDF burner was assembled in a plenum and horizontally mounted in the high-pressure test rig in Lund University. Geometries of the burner can be found in Ref. [95] and more details on burner assembling and the high-pressure rig are described in Chapter 3. The complexity of the test rig causes difficulties for laser diagnostics. In the current study, OH-PLIF measurement was performed, and a schematic of the experimental setup is shown in Figure 5.11. Laser systems were arranged in a separate room next to test sections, and the beam was guided into the combustor through a window on the wall between the two rooms. An approximate 4 cm laser sheet was formed and horizontally passed through the test section with optical access. The fluorescence signal was detected by the ICCD camera through a reflecting mirror under the test section.

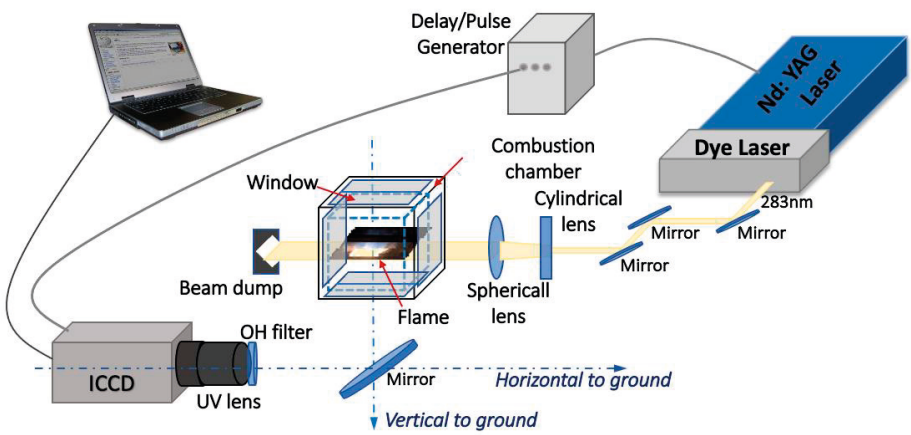

Figure 5.11: Experimental setup for investigation of IDFs at high pressure.

The velocity ratio (V_r) of air velocity to fuel velocity and Re of the central jet are used as parameters for characterizing such flames [96]. In the current experiment, the velocity of the fuel (methane) remains unchanged as 0.3 m/s while the central air velocity varies in a range of 60 – 180 m/s. Therefore, V_r and pressure in the combustor were used to indicate the flame operating conditions. Figure 5.12 presents OH-PLIF in single-shot and averaged results for three cases, in which the mean result is calculated from 1000 single-shots. The red box marks the measured area where the blue torch is mainly located, representing a partially premixed flame feature. When comparing the single-shot image of cases with the same V_r at 2 bar and 5 bar, more wrinkles can be found in the inner jet flame structure (marked by the white dashed circle) at high pressure. This phenomenon is also observed for the turbulent premixed flame at high pressure [97] which can be explained with the flame intrinsic instability could be the reason. In addition, local 'breaks' in the flame front can be found for the flame at 5 bar, which can be caused by either local quenching or feint breaks misled by 2D measurement. From the mean results, it can be also seen that the flame lift-off height becomes larger for higher pressure. Besides, the effect of Vr on flame structure, overall shape, and lift-off height can be observed by comparing the first and third cases. The flame is more wrinkled as increasing the V_r, which due to the turbulent area driven by the shear layer between jets is enhanced by a larger velocity ratio. No obvious difference is found for the flame lift-off height, while the height of the flame unburned region decreases with increasing V_r. More results and discussion of this work are presented in Paper VII.

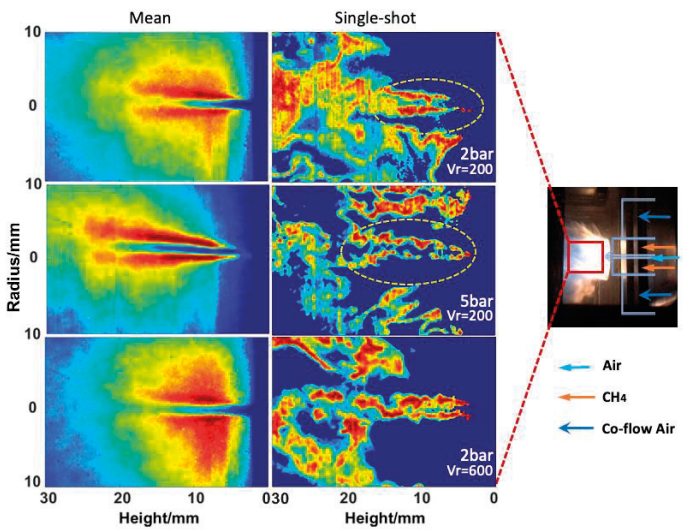

Figure 5.12: Single-shot and mean results of OH-PLIF for three different cases.

6 Summary and outlook

Throughout the thesis, various laser-based diagnostics techniques, as the main research tools, have been applied to study turbulent flames in different burners, aiming to achieve better performance and fuel flexibility for the gas turbine relevant burners, as well as to gain a deeper understanding of the mechanisms governing the turbulent and combustion interactions. The results lead to the following conclusions, and some suggestions for future work are listed below.

6.1 Summary and conclusions

The works presented in this thesis can be summarized as the following four parts, corresponding to the four different burners employed. All studies are related to gas turbine applications either directly or indirectly.

The first major part is focused on a lab-scale CECOST swirl burner, which is a gas turbine model combustor. At the first stage, experiments were performed for natural gas/air turbulent lean premixed flames to study the stability range, flame structure, and flame dynamics in the CECOST burner. By changing the equivalence ratio, the stability regimes ranging from the LBO limit to the flashback limit were identified for cases with different Reynolds numbers (Re). Simultaneous OH-/CH_2O-PLIF and high-speed OH^* chemiluminescence imaging were used to characterize the flame structure and the combustion dynamics. The LBO limit was observed to be nearly invariant for all Re, while the flashback occurred in different forms as the Re changes. The flame was prone to flashback at low and moderate Re, and no flashback was observed for Re > 17000, even when it approached the stoichiometry condition. Results of PLIF indicate that the flame is within the flamelet regime. The flame dynamics were analyzed for a flashback case, which showed that the flashback process under certain conditions can be highly dynamic and associated with low-frequency oscillations.

The subsequent study on the CECOST burner was conducted for the hydrogen-enriched methane/air turbulent premixed flames to enable and investigate the fuel flexibility. Three fuel mixtures of H_2/CH_4: 0/100, 25/75, and 50/50 (in vol.%) were studied at three different Re. Compared to the natural gas flames, completely different stability regimes were obtained for the hydrogen-enriched methane flames.

The LBO limits were found to be decreased slightly with increasing Re for the same fuel but significantly decreased when increasing the H_2 content in the fuel mixtures. Both Re and H_2 addition influenced the flashback limits, in which the flashback limit shifted to richer condition for higher Re for the methane flame cases, but flashback limits for the H_2 enrichment cases presented different trends as Re increasing. The transition of the flame shape from M to Π was only observed for the H_2 enriched cases, and it was found to be an essential factor for changing the flashback limits as well as the flashback mechanisms. The structures and stabilization of both the M- and Π-shaped flames were inspected and discussed using OH-PLIF and OH^* chemiluminescence results. The mean flow fields acquired by the PIV measurement for the cold-flows and both lean and rich methane/air flame cases were compared between low and high Re conditions. The centre recirculation zone (CRZ) was observed for almost all cases except the rich case at low Re, in which the absence of CRZ in the measured region resulted from the upstream propagation of the vortex breakdown, i.e., the occurrence of flashback. Besides, different mechanisms for flashback were observed for M- and Π-shaped flame, which were identified by time-sequence single-shots OH^* chemiluminescence images. It was concluded that the flashback with the CIVB mechanism occurred for all pure methane cases, while the boundary layer flashback occurred for all H_2 enriched cases.

In the second part, investigations were performed on a scaled Siemens DLE burner, which was modified to install an electrode in the RPL section, to study the rotating gliding arc (RGA) discharge plasma-assisted flames at atmospheric conditions. Results demonstrated that the application of the RGA discharge plays a significant role in flame stabilization and extending the LBO limit. A flame kernel, initiated by the plasma discharge was observed to interact with the Pilot fuel and air, which can help stabilizing the main flame similar to the reference operation by the RPL flame. NO_x emission levels of the flames were also examined by the exhaust emission probe sampling. It was found that the NO_x emission for the flame with RGA is higher than that without RGA but still less than that from the reference case with a RPL flame. Air or O_2 was injected through the RPL and studied individually. Better improvement in extending the LBO limit was found for the O_2 injection, and although the NO_x emissions for flames without RGA were sufficiently lower for both O_2 and air injection, the NO_x emission for the flame with RGA was significantly lower from the O_2 injection as compared to the air case.

In the third part of the thesis, a two-dimensional LDA measurement and the simultaneous NH- and OH-PLIF were performed to characterize turbulent premixed ammonia/air flames on a DRZ burner. Most of the operating flames in this work were located in the regime of the distributed reaction zone (DRZ). The thermal load for the measured flames was up to 39 kW, which is comparable to that of the gas turbine model combustors. The turbulent flow field information was discussed based on the LDA measurements. Results of the PLIF measurement indicate that

the NH and OH radicals can coexist in a thinner boundary and the leading edge of the NH layer was found to be closer to the reactants side than that of the OH layer. No significant broadening of the NH layer was observed in this work even in the extreme turbulent conditions, implying that eddies couldn't penetrate the NH layer.

In the fourth part of the thesis, a challenging experiment was carried out in the high-pressure test rig to study the turbulent inverse diffusion flames under elevated pressure conditions. High-speed OH^* chemiluminescence imaging and OH-PLIF measurement were performed. Effects of both the velocity ratio and pressure on the characteristics of the flame were discussed. More winkles in the flame fronts were observed at higher pressure. The higher velocity ratio resulted in a shorter height of the unburned flame region.

6.2 Outlook and future work

Based on the results presented in this thesis, several future works can be suggested:

- Regarding the investigations on the CECOST swirl burner, fuel flexibility, as a key issue in enabling the gas turbine combustor to operate in a wider range of fuels, need to be explored further. The available alternative fuels generally involve H_2 content such as syngas, diluents addition in the fuel like H_2O, CO_2, etc., and also renewable fuel such as ammonia. The causes for the flame shape transition, which also triggers different flashback mechanisms, are still unclear and further studies are needed. Besides, simultaneous PIV and OH-PLIF measurements with high repetition rates are needed in order to investigate the interaction between flames and turbulence, and simultaneous pressure measurement is also needed to identify the mechanisms of the flame oscillations.
- The gliding arc discharge plasma has been demonstrated as a promising method in assisting the flames in a gas turbine combustor. Multi-scalar optical measurements are required to explore the underlying plasma/combustion interaction mechanisms in a gas turbine relevant burner.
- Ammonia as a potential renewable fuel and energy carrier has gained growing attention recently. But the characteristics of ammonia flames are lacking basic understandings. For further studies on turbulent ammonia flames at a piloted jet burner, extensive experiments with both qualitative and quantitative measurements on the key species are required for providing valid data to chemical kinetics research and CFD modelling. Although the gradient of OH or NH layer (potential) can be a marker of the heat release zone for the ammonia flames, the best heat release indicator, just like HCO for methane flames, remains unknown. Besides, the effect of the preheating

temperature of the inlet flow on characteristics and structures of the turbulent premixed ammonia/air flames are of considerable interest to be investigated in the future.

References

[1] IEA, *World Energy Outlook 2020 IEA*, Paris.

[2] *The changing global energy mix: IEA 2020*. https://context.capp.ca/infographics/2018/infographic_global-energy-mix_iea-weo-2018.

[3] T.C. Lieuwen, V. Yang, *Combustion instabilities in gas turbine engines: operational experience, fundamental mechanisms, and modeling*, American Institute of Aeronautics and Astronautics, 2005.

[4] Y.D. Korolev, I.B. Matveev, *Nonsteady-state processes in a plasma pilot for ignition and flame control*, IEEE transactions on plasma science 34 (2006) 2507-2513.

[5] R.K. Hanson, J.M. Seitzman, P.H. Paul, *Planar laser-fluorescence imaging of combustion gases*, Applied Physics B 50 (1990) 441-454.

[6] A.C. Eckbreth, *Laser diagnostics for combustion temperature and species*, CRC press, 1996.

[7] F. Grisch, M. Orain, *Role of Planar Laser-Induced Fluorescence in Combustion Research*, AerospaceLab, (2009) p. 1-14.

[8] *Measurement Principles of PIV*. https://www.dantecdynamics.com/solutions-applications/solutions/fluid-mechanics/particle-image-velocimetry-piv/measurement-principles-of-piv/.

[9] Z. Zhang, *LDA application methods: laser Doppler anemometry for fluid dynamics*, Springer Science & Business Media2010.

[10] *BSA Flow Software*. https://www.dantecdynamics.com/components/bsa-flow-software/.

[11] J. Ballester, T. García-Armingol, *Diagnostic techniques for the monitoring and control of practical flames*, Progress in Energy and Combustion Science 36 (2010) 375-411.

[12] M. Lauer, T. Sattelmayer, *On the utilization of OH^* chemiluminescence as a measure for local heat release in turbulent flames*, Technische Universitat Munchen, (2011).

[13] R.M. Twyman, *ATOMIC EMISSION SPECTROMETRY*, *Principles and Instrumentation*, 2005, pp. 190-198.

[14] *Gas Sample Probe PSP4000-H/C/T*. https://www.mc-techgroup.com/en/ products-special-systems/gas-sampling/gas-sample-probes/40s1015.

[15] R. Paschotta, *YLF lasers*, Wiley-VCH, Encyclopedia of Laser Physics and Technology, October 2008.

[16] A. Holms, A. Quach, *Complementary Metal-Oxide Semiconductor Sensors*, (2010).

[17] A. Subash, *Laser-Based Investigations of Combustion Phenomena in Gas Turbine Related Burners*, Lund University2018.

[18] A. Lantz, *Application of Laser Techniques in Combustion Environments of Relevance for Gas Turbine Studies*, Lund University2012.

[19] T. Sattelmayer, M. Felchlin, J. Haumann, J. Hellat, D. Styner, *Second-generation low-emission combustors for ABB gas turbines: burner development and tests at atmospheric pressure*, (1992).

[20] K. Dobbeling, H.P. Knopfel, W. Polifke, D. Winkler, C. Steinbach, T. Sattelmayer, *Low-NO_x Premixed Combustion of MBtu Fuels Using the ABB Double Cone Burner (EV Burner)*, Journal of Engineering for Gas Turbines and Power 118 (1996) 46-53.

[21] C. Steinbach, T. Ruck, J. Lloyd, P. Jansohn, K. Döbbeling, T. Sattelmayer, T. Strand. *ABB's Advanced EV Burner—A Dual Fuel Dry Low NO_x Burner for Stationary Gas Turbines*. In: editor^editors. Turbo Expo: Power for Land, Sea, and Air; 1998: American Society of Mechanical Engineers. p. V003T006A049.

[22] P. Jansohn, T. Ruck, C. Steinbach, H.-P. Knöpfel, T. Sattelmayer, C. Troger. *Development of the advanced EV (AEV) burner for the ABB GTX100 gas turbine*. In: editor^editors. ASME 1997 Turbo Asia Conference; 1997: American Society of Mechanical Engineers Digital Collection. p.

[23] E. Hodzic, *Analysis of flow dynamics and flame stabilization in gas turbine related combustors*, Lund University, 2016.

[24] A.A. Subash, R. Collin, M. Aldén, A. Kundu, J. Klingmann. *Laser-Based Investigation on a Dry Low Emission Industrial Prototype Burner at Atmospheric Pressure Conditions*. In: editor^editors. ASME Turbo Expo 2016: Turbomachinery Technical Conference and Exposition; 2016: American Society of Mechanical Engineers Digital Collection. p.

[25] A. Skiba, *On the Structure of Premixed Flames Subjected to Extreme Levels of Turbulence*, 2017.

[26] A.A. Subash, R. Collin, M. Aldén, A. Kundu, J. Klingmann. *Investigation of Hydrogen Enriched Methane Flame in a Dry Low Emission Industrial Prototype Burner at Atmospheric Pressure Conditions*. In: editor^editors. Turbo Expo: Power for Land, Sea, and Air; 2017: American Society of Mechanical Engineers. p. V04AT04A056.

[27] E. Hodzic, S. Yu, A.A. Subash, X. Liu, X. Liu, R.-Z. Szasz, X.-S. Bai, Z. Li, M. Alden. *Numerical and Experimental Investigation of the CeCOST Swirl Burner*. In: editor^editors. ASME Turbo Expo 2018: Turbomachinery Technical Conference and Exposition; 2018. p.

[28] B. Zhou, *Advanced laser-based multi-scalar imaging for flame structure visualization towards a deepened understanding of premixed turbulent combustion*, Lund University2015.

[29] L.S. Langston, *Turbines, Gas, Reference Module in Earth Systems and Environmental Sciences*, Elsevier2014.

[30] K. Brun, R. Kurz, *Introduction to Gas Turbine Theory*, 3rd Edition ed., Solar Turbines Incorporated.

[31] C. Soares, *Gas turbines: a handbook of air, land and sea applications*, Elsevier2011.

[32] M.G. Michaud, P.R. Westmoreland, A.S. Feitelberg. *Chemical mechanisms of NO_x formation for gas turbine conditions*. In: editor^editors. Symposium (international) on Combustion; 1992: Elsevier. p. 879-887.

[33] J.P. Warnatz, D.D.U. Maas, a.R.W. Dibble, *Formation of nitric oxide, Combustion*, Springer1996, pp. 219-236.

[34] N. Syred, J.M. Beér, *Combustion in swirling flows: A review*, Combustion and Flame 23 (1974) 143-201.

[35] A.K. Gupta, D.G. Lilley, N. Syred, *Swirl Flows*, Abacus Press1984.

[36] N. Syred, *A review of oscillation mechanisms and the role of the precessing vortex core (PVC) in swirl combustion systems*, Progress in Energy and Combustion Science 32 (2006).

[37] N. Syred, N. Chigier, J. Beer. *Flame stabilization in recirculation zones of jets with swirl*. In: editor^editors. Symposium (International) on Combustion; 1971: Elsevier. p. 617-624.

[38] M. Vigueras-Zuñiga, A. Valera-Medina, N. Syred, *Studies of the precessing vortex core in swirling flows*, Journal of applied research and technology 10 (2012) 755-765.

[39] Y. Huang, V. Yang, *Dynamics and stability of lean-premixed swirl-stabilized combustion*, Progress in energy and combustion science 35 (2009) 293-364.

[40] Syred N, B. J., *The damping of precessing vortex cores by combustion in swirl generators*, Asttonautica Acta 17 (1972) 783–801.

[41] A. Valera-Medina, N. Syred, A. Griffiths. *Characterisation of large coherent structures in a swirl burner*. In: editor^editors. 46th AIAA Aerospace Sciences Meeting and Exhibit; 2008. p. 1019.

[42] T. Poinsot, D. Veynante, *Theoretical and numerical combustion*, RT Edwards, Inc.2005.

[43] N. Syred, A *review of oscillation mechanisms and the role of the precessing vortex core (PVC) in swirl combustion systems*, Progress in Energy and Combustion Science 32 (2006) 93-161.

[44] H.J. Sheen, W.J. Chen, S.Y. Jeng, T.L. Huang, C*orrelation of swirl number for a radial-type swirl generator*, Experimental Thermal and Fluid Science 12 (1996) 444-451.

[45] T. Lieuwen, V. McDonell, D. Santavicca, T. Sattelmayer, *Burner development and operability issues associated with steady flowing syngas fired combustors*, Combustion Science and Technology 180 (2008) 1169-1192.

[46] S. Menon. *CO emission and combustion dynamics near lean-blowout in gas turbine engines*. In: editor^editors. Turbo Expo: Power for Land, Sea, and Air; 2004. p. 153-160.

[47] Y. Sommerer, D. Galley, T. Poinsot, S. Ducruix, F. Lacas, D. Veynante, *Large eddy simulation and experimental study of flashback and blow-off in a lean partially premixed swirled burner*, Journal of Turbulence 5 (2004) N37.

[48] V. Hoferichter, *Boundary Layer Flashback in Premixed Combustion Systems*, Technische Universität München, 2017.

[49] M. Kroner , J. Fritz , T. Sattelmayer, *Flashback Limits for Combustion Induced Vortex Breakdown in a Swirl Burner*, Journal of Engineering for Gas Turbines and Power 125 (2003) 693-700.

[50] F. Kiesewetter, M. Konle, T. Sattelmayer, *Analysis of combustion induced vortex breakdown driven flame flashback in a premix burner with cylindrical mixing zone*, (2007).

[51] A.H. Lefebvre, D.R. Ballal, *Gas Turbine Combustion: Alternative Fuels and Emissions*, Third Edition, CRC Press2010.

[52] R. Pavri, G.D. Moore, *Gas turbine emissions and control*, Atlanta: GE Energy Services, (2001).

[53] P. Gokulakrishnan, M.S. Klassen, *NO_x and CO formation and control, Gas turbine emissions*, (2013) 175-208.

[54] S.J. Shanbhogue, S. Husain, T. Lieuwen, *Lean blowoff of bluff body stabilized flames: Scaling and dynamics*, Progress in Energy and Combustion Science 35 (2009) 98-120.

[55] I. Glassman, R.A. Yetter, N.G. Glumac, *Combustion*, Elsevier Science2014.

[56] Z.S. Li, B. Li, Z.W. Sun, X.S. Bai, M. Aldén, *Turbulence and combustion interaction: High resolution local flame front structure visualization using simultaneous single-shot PLIF imaging of CH, OH, and CH_2O in a piloted premixed jet flame*, Combustion and Flame 157 (2010) 1087-1096.

[57] M. Röder, T. Dreier, C. Schulz, *Simultaneous measurement of localized heat-release with OH/CH_2O–LIF imaging and spatially integrated OH^* chemiluminescence in turbulent swirl flames*, Proceedings of the Combustion Institute 34 (2013) 3549-3556.

[58] Y. Tong, *Experimental and Numerical Investigations of Flames Stabilized by Swirl Flow and Bluff-body: Flame Structures and Flame Instabilities*, Lund University, 2017.

[59] T.G. Reichel, C.O. Paschereit, *Interaction mechanisms of fuel momentum with flashback limits in lean-premixed combustion of hydrogen*, International Journal of Hydrogen Energy 42 (2017) 4518-4529.

[60] V. McDonell, G. Samuelsen, *Measurement of fuel mixing and transport processes in gas turbine combustion*, Measurement Science and Technology 11 (2000) 870.

[61] J.H. Stufflebeam, D.W. Kendrick, W.A. Sowa, T.S. Snyder, *Quantifying Fuel/Air Unmixedness in Premixing Nozzles Using an Acetone Fluorescence Technique*, Journal of Engineering for Gas Turbines and Power 124 (1999) 39-45.

[62] S.M. Starikovskaia, *Plasma assisted ignition and combustion*, Journal of Physics D: Applied Physics 39 (2006) R265-R299.

[63] A. Starikovskiy, N. Aleksandrov, *Plasma-assisted ignition and combustion*, Progress in Energy and Combustion Science 39 (2013) 61-110.

[64] D.H. Lee, K.-T. Kim, H.S. Kang, Y.-H. Song, J.E. Park, *Plasma-Assisted Combustion Technology for NO_x Reduction in Industrial Burners*, Environmental Science & Technology 47 (2013) 10964-10970.

[65] W. Kim, M.G. Mungal, M.A. Cappelli, *The role of in situ reforming in plasma enhanced ultra lean premixed methane/air flames*, Combustion and Flame 157 (2010) 374-383.

[66] T. Ombrello, X. Qin, Y. Ju, A. Gutsol, A. Fridman, C. Carter, *Combustion enhancement via stabilized piecewise nonequilibrium gliding arc plasma discharge*, AIAA journal 44 (2006) 142-150.

[67] A. Fridman, S. Nester, L.A. Kennedy, A. Saveliev, O. Mutaf-Yardimci, *Gliding arc gas discharge*, Progress in energy and combustion science 25 (1999) 211-231.

[68] A. Czernichowski, *Gliding arc: applications to engineering and environment control*, Pure and Applied Chemistry 66 (1994) 1301-1310.

[69] J. Zhu, Z. Sun, Z. Li, A. Ehn, M. Aldén, M. Salewski, F. Leipold, Y. Kusano, Dynamics, *OH distributions and UV emission of a gliding arc at various flow-rates investigated by optical measurements*, Journal of Physics D: Applied Physics 47 (2014) 295203.

[70] C. Kong, J. Gao, J. Zhu, A. Ehn, M. Aldén, Z. Li, *Effect of turbulent flow on an atmospheric-pressure AC powered gliding arc discharge*, Journal of Applied Physics 123 (2018) 223302.

[71] A.A. Subash, R. Whiddon, R. Collin, M. Aldén, A. Kundu, J. Klingmann, *Flame Investigation of a Gas Turbine Central Pilot Body Burner at Atmospheric Pressure Conditions Using OH PLIF and High-Speed Flame Chemiluminescence Imaging*, 2015.

[72] A.A. Subash, R. Collin, M. Aldén, A. Kundu, J. Klingmann, *Laser-Based Investigation on a Dry Low Emission Industrial Prototype Burner at Atmospheric Pressure Conditions*, 2016.

[73] A.A. Subash, R. Collin, M. Aldén, A. Kundu, J. Klingmann. *Experimental Investigation of the Influence of Burner Geometry on Flame Characteristics at a Dry Low Emission Industrial Prototype Burner at Atmospheric Pressure Conditions*. In: editor^editors. ASME Turbo Expo 2017: Turbomachinery Technical Conference and Exposition; 2017: American Society of Mechanical Engineers Digital Collection. p.

[74] S.R. Turns, *An Introduction to Combustion: Concepts and Applications*, McGraw-Hill2000.

[75] W.P. Jones, A. Tyliszczak, *Large Eddy Simulation of Spark Ignition in a Gas Turbine Combustor*, Flow, Turbulence and Combustion 85 (2010) 711-734.

[76] T. Jaravel, J. Labahn, B. Sforzo, J. Seitzman, M. Ihme, *Numerical study of the ignition behavior of a post-discharge kernel in a turbulent stratified crossflow*, Proceedings of the Combustion Institute 37 (2019) 5065-5072.

[77] V.E. Zakharov, V.S. L'vov, G. Falkovich, *Kolmogorov spectra of turbulence I: Wave turbulence*, Springer Science & Business Media2012.

[78] B. Hjertager, *Computational analysis of fluid flow processes - A compendium*, 2014.

[79] E. Baudoin, *Large eddy simulation of turbulent premixed and partially premixed combustion*, Lund University, 2010.

[80] S.B. Pope, *Turbulent Flows*, Measurement Science and Technology 12 (2001) 2020-2021.

[81] D. Ting, *Basics of engineering turbulence*, Academic Press2016.

[82] R. Borghi, *Turbulent combustion modelling*, Progress in Energy and Combustion Science 14 (1988) 245-292.

[83] N. Peters, *Turbulent combustion*, IOP Publishing, 2001.

[84] H. Kobayashi, A. Hayakawa, K.K.A. Somarathne, E.C. Okafor, *Science and technology of ammonia combustion*, Proceedings of the Combustion Institute 37 (2019) 109-133.

[85] C. Zamfirescu, I. Dincer, *Ammonia as a green fuel and hydrogen source for vehicular applications*, Fuel processing technology 90 (2009) 729-737.

[86] C. Brackmann, B. Zhou, Z. Li, M. Aldén, *Strategies for quantitative planar laser-induced fluorescence of NH radicals in flames*, Combustion Science and Technology 188 (2016) 529-541.

[87] F. Meyer, *Topographic distance and watershed lines*, Signal processing 38 (1994) 113-125.

[88] A.W. Skiba, T.M. Wabel, C.D. Carter, S.D. Hammack, J.E. Temme, J.F. Driscoll, *Premixed flames subjected to extreme levels of turbulence part I: Flame structure and a new measured regime diagram*, Combustion and Flame 189 (2018) 407-432.

[89] S. Mahesh, D. Mishra, *Study of the turbulent inverse diffusion flame in recessed backstep and coaxial burners*, Combustion, Explosion, and Shock Waves 47 (2011) 274-279.

[90] K.-T. Wu, R.H. Essenhigh. *Mapping and structure of inverse diffusion flames of methane*. In: editor^editors. Symposium (International) on Combustion; 1985: Elsevier. p. 1925-1932.

[91] G.W. Sidebotham, I. Glassman, *Flame temperature, fuel structure, and fuel concentration effects on soot formation in inverse diffusion flames*, Combustion and flame 90 (1992) 269-283.

[92] A. Sobiesiak, J.C. Wenzell, *Characteristics and structure of inverse flames of natural gas*, Proceedings of the Combustion Institute 30 (2005) 743-749.

[93] C. Kaplan, K. Kailasanath, *Flow-field effects on soot formation in normal and inverse methane–air diffusion flames*, Combustion and Flame 124 (2001) 275-294.

[94] L. Sze, C.S. Cheung, C.W. Leung, *Appearance, temperature, and NO_x emission of two inverse diffusion flames with different port design*, Combustion and flame 144 (2006) 237-248.

[95] Ł.J. Kapusta, C. Shuang, M. Aldén, Z. Li, *Structures of inverse jet flames stabilized on a coaxial burner*, Energy 193 (2020) 116757.

[96] L. Dong, C.S. Cheung, C.W. Leung, *Heat transfer characteristics of an impinging inverse diffusion flame jet–Part I: Free flame structure*, International journal of heat and mass transfer 50 (2007) 5108-5123.

[97] J. Wang, S. Yu, M. Zhang, W. Jin, Z. Huang, S. Chen, H. Kobayashi, *Burning velocity and statistical flame front structure of turbulent premixed flames at high pressure up to 1.0MPa*, Experimental Thermal and Fluid Science 68 (2015) 196-204.

Acknowledgements

Time flies! I can't imagine that I have lived in Lund for more than four years. On December 13rd 2016, I arrived at Arlanda airport alone, which was the first time I came to Sweden. I still remember the chorus that I met on the way to transfer the flight, in which girls wore white robes with candles above the heads and singing pretty songs. Later, I knew that the day was Lucia Day. Since that day, I started a new life in Sweden.

When you get here of this thesis, I am about to finish my journey of pursuing a doctorate, which has the joy of acquiring new knowledge, solving problems and harvesting results, but also has a lot of setbacks. In the meantime, I have many unforgettable memories over the past four years. I met and made new friends, married with my boyfriend who had been in love with me for many years, raised the first pet in my life, and learned to ski, etc. Here, I would like to express my most sincere gratitude to all those who have given me support, care, company and love during this journey.

At first, I want to thanks to my main supervisor, *Prof. Zhongshan Li*, who provided me the opportunity to start my PhD study in Lund University. Much appreciated for your supporting in the work, supervising me in different fields, and encouraging me when I faced problems. You always have many ideas for scientific questions, which often inspired me a lot although sometimes they were too much for me to keep up.

I would like to give great thanks to *Prof. Marcus Aldén*, for supporting me in many projects and solving issues I met. I admire that you are not only an outstanding scientist, but also an excellent leader of the division. Due to your proper management, I can study in such a good working environment and atmosphere.

Particular gratitude should be given to *Prof. Xuesong Bai*, for your patient guidance to me in the field of turbulent combustion. You spent a lot of time for the discussions on my work, papers and rebuttals, which were quite valuable to deepen my understanding on research problems. I admire your intelligent insights, and I appreciate you very much for your generosity to me.

To my co-supervisor, *Dr. Arman Ahamed Subash*, thanks for your supervising in the lab and supporting all of my works. I appreciate the time we spent together in the lab, where you have taught me a lot of skills. Your patience and optimism always make the people work with you feel relaxed and happy.

Many thanks should also be given to all of those who have worked with me. *To Dr. Christian Brackmann*, thanks for helping me align lasers in the lab. I benefit a lot from your scholarly expertise on laser applications. To *Dr. Andreas Ehn*, thanks for supporting me in the plasma project and the useful tutorial on how to present our work in a conference. I like your humour and the light-hearted way of communication. To *Dr. Robert-Zoltán Szász*, for your valuable discussions on analysing our experimental results and carefully revision comments on my papers. To *Michael Bertsch*, thank you for the good teamwork in the lab and sacrificing your movie time without any complaint when we need to work overtime. I enjoy the time we work together, the debate on research issues, and the discussion on views of life. I am sincerely happy for you to find the major what you really like and wish you all the best in your new journey of studying medicine. To *Dr. Bo Zhou*, *Dr. Yajun Zhou*, *Dr. Jinlong Gao*, *Dr. Senbin Yu*, *Dr. Xiao Liu*, *Yupan Bao*, *Qingshuang Fan*, and *Shijie Xu*, thanks for the good collaboration we had in the lab, in which I learned different things form each of you.

I feel very grateful to *Dr. Sven-Inge Möller* for the discussion we made about the experimental work, the valuable advice you gave, and your encouragement when I felt frustrated to the work. I'm also appreciating the help from *Minna Ramkull*, *Cecilia Bille*, *Igor Buzuk*, *Johan Evers*, and *Dr. Robert Collin*.

It is my great pleasure to share the same office with *Manu Mannazhi* for my whole PhD time. Thank you for being also my good friend. I enjoy every moment of chatting with you, and we talked about our daily life, hobbies, views on life issues, and even current affairs. You can always give me new inspiration and encourage me when I was down.

To *Dr. Christoffer Pichler* and *Joakim Jönsson*, thank you for being warm and kind to me when I just came to the division, helping me improve my spoken English with lots of patience, and all the good time we spent together, such as playing badminton, adventure swimming, trip to Ven island, etc. To *Dr. Dina Hot*, for your kind-hearted and encouragement to me. To *Maria Ruchkina*, for always being nice to me, lending me equipment, helping me overcome my fears and teaching me to try a diving during the Gordon conference. To *Prof. Joakim Bood*, for many enjoyable chats with you about Warriors and Stephen Curry. To *Dr. Frederik Ossler*, *Per Samuelsson*, *Ruike Bi*, *Saeed Derafshzan*, *Dr. Marco Lubrano Lavadera*, *Haisol Kim*, *Sandra Török*, *Panagiota Stamatoglou*, *Dr. Zhenkan Wang*, *Dr. Wubin Weng*, *Dr. Chengdong Kong*, *Dr. Pengji Ding*, *Yupan Bao*, *Dr. Karolina Dorozynska Dr. Thi Kim Cuong Le*, et al., I am also great thankful for all of your supporting in my work and generously sharing equipment with me.

I would also like to thank my best friends, *Ludovica Luise*, *Hara Mari*, *Leonardo Padial*, and *Anna Caterina Milanetto*, for many warm and unforgettable memories among us. We had lots of fun in Ystad, Kullaberg, Lomma beach, and to try tasty

food and fika together. Even though we are now living in different countries, we still keep contact, miss and care each other.

I feel very lucky to meet a group of lovely friends who bring me happiness and make my life colourful. To *Yupan Bao*, thanks for being my best friend, always supporting and caring me in both life and work since I came here, sharing feelings with me, teaching me how to ski, and helping me whenever I need. To my buddies, *Wubin Weng*, *Mengshu Hao*, *Shen Li*, *Zhenkan Wang*, *Jie Zhong*, thanks for the countless wonderful memories we have together in Lund and also in trips to many places, making delicious food together, and always being so reliable. To *Shichao Ren* and *Lai Wei*, thanks for being our close friends and neighbours in Sofiaparken together with *Yupan Bao* and *Yingzhe Xiong*, which was the best living experience in abroad for me that I couldn't imagine before. To *Jinlong Gao* and *Zhen Li*, thanks for always helping us and giving useful suggestions when we encountered problems in life and inviting us many times to your home for dinner. To *Chengdong Kong* and *Jie Niu*, thanks for preparing many tasty meals for us and organizing BBQ several times during summer. To *Meng Li*, thanks for always being so caring about me and the pleasant chat every time. Thanks for *Rui Li*, *Jian Wu*, *Pengji Ding*, *Xiao Cai*, *Yong Qian*, *Xinlu Han*, *Ruike Bi*, *Jianqing Huang*, *Yuhe Zhang*, et al. I will never forget the great time we enjoyed together in travels, activities like fishing, and celebrating Spring Festivals every year in abroad.

I would also like to express my special gratitude to the wonderful girls I met here. To *Kena Li*, *Haoran Yu*, *Qi Shi*, *Haiyue Gong*, *Juanzi Shi*, thanks for all of your company over all of my life in Lund. I never thought I could make such best friends like you before I came here. You are always being side of me, sharing my emotions, caring about me, and inspiring me to be better.

Moreover, many thanks should also be given to my good friends in Lund. They are, *Senbin Yu*, *Miao Zhang*, *Bo Zhou*, *Yiheng Tong*, *Huifang Geng*, *Huiting Ma*, *Fang Huang*, *Jie Zhang*, *Jun Li*, Jixing Ding, *Mengqiao Di*, *Siyuan Hu*, Xianshao Zou, *Yi Lu*, et al.

I would like to give my particular thanks to my best friends in China. To *Bingyan Hou*, *Jinrui Ma*, *Qian Yang*, *Min Li*, *Li Ji*, *Peilin Wei*, *Lu Wang*, *Shan Zhu*, *Wei Niu*, thanks for always encouraging me, keeping contact and being deeply concern about me, which give me a lot of support and strength.

I want to express my great thanks and love to my husband, *Qingshuang Fan*. You are my competent partner in both life and work. I can't imagine how difficult it would be to complete this thesis if without your supporting in all aspects. Thanks for your love, company, caring and respecting all my choices. Your charming personality makes me feel happier. I also want to thank my kitten, Chacha. Your arrival and company have brought us priceless joy and happiness and make us to be more responsible adults.

In the end, I would like to give the deepest gratitude to my mom and dad, *Jianling Liu* and *Dezhe Liu*. They provided me a family full of love and meticulous care and concern. Thank you for loving me so completely to make me grow up healthy and receive good education. Thank you for being enlightened parents, who always respect my freedom of making decisions and believe in and support the decision I made. I learned from you to be independent, be serious to work, be responsible, and always follow my heart. Special thanks to my late maternal grandpa, Qi Liu, for inspiring me to pursue science and your endless love for me. I am also very grateful to my aunt, uncles, cousins, and parents-in-law, for always supporting, concerning and caring about me.

最后，我要深深地感谢我亲爱的妈妈和爸爸。你们给我了一个充满爱的家和无微不至的照顾。谢谢你们如此毫无保留的爱着我，让我健康快乐地成长，接受好的教育。谢谢你们选择做开明的父母，尊重我做决定的权利，相信并支持我做的每一个决定。你们教会了我成为一个独立，认真，有担当的人，且永远听从自己的内心。这里，要特别地感谢我已过世的外公，是他激励着我在科研道路上一路追寻，而他对我的爱给了我不断前进的勇气。此外，非常感激我在家乡的姨妈，舅舅们，以及其他亲人们一直以来对我的关心和照顾，也非常感谢庆骊父母对我们在瑞典生活的支持和关心。

Summary of papers

Paper I

E. Hodzic, S. Yu, A. A. Subash, **X. Liu**, X. Liu, R. Z. Szasz, X. S. Bai, Z. S. Li and M, Aldén, "Numerical and experimental investigation of the cecost swirl burner", *In Proceedings of the ASME Turbo Expo 2018, Volume 4A: Combustion, Fuels and Emissions, GT2018-75760*

In this paper, the development process of the conceptual swirl burner developed at the Swedish National Centre for Combustion and Technology (CeCOST), is presented. Utilizing extensive computational fluid dynamics (CFD) analysis, both the lead time and cost in manufacturing of the different burner parts were significantly reduced. The performance maps bounded by the flashback and blow-off limits for the current configuration were obtained and studied in detail using advanced experimental measurements and numerical simulations. Utilizing high speed OH-chemiluminescence, OH/CH_2O-PLIF and Large Eddy Simulation (LES), details of the combustion process and flame-flow interaction are presented. The main focus is on three different cases, a stable case, a case close to blow-off and flashback condition. We show the influence of the flame on the core flow and how an increase in swirl may extend the stability limit of the anchored flame in swirling flow burners.

I took part in the performance of all the experimental campaign. I also contributed to the preparation of the experimental setup. For the manuscript preparation, I prepared the figure of the experimental setup and post processed the results of simultaneously OH- and CH_2O PLIF and high-speed OH chemiluminescence. E. Hodzic was responsible for this paper and designed the new CECOST swirl burner. A. A. Subash planned the experiment, built the experimental setup, participated in all the measurements and processed part of the experimental results. S. Yu prepared the operating conditions, took part in all the experiment, did the LES numerical study with X. Liu, and prepared the manuscript with E. Hodzic. All co-authors were involved in the discussion and the revision process.

Paper II

A. A. Subash, S. Yu, **X. Liu**, M. Bertsch, R. Z. Szasz, Z. S. Li, X. S. Bai, M. Aldén and D. Lörstad, "Flame investigation of a laboratory-scale CECOST swirl burner at atmospheric pressure conditions", *Fuel, Vol. 279, 118421, 2020*

In this paper, experimental and numerical studies were performed to understand the stabilization of lean premixed natural gas/air flames in the CECOST burner. The operability range, flame stabilization, and flashback were investigated employing simultaneous OH– and CH_2O-PLIF, and high-speed chemiluminescence imaging. Large eddy simulation (LES) was carried out for analysis of the vortex breakdown structures under non-reacting conditions. It was found that the vortex breakdown structures under isothermal conditions were insensitive to the Reynolds number (Re) for $Re \geq 10000$; however, the stability of the flames and operability range of the burner were highly sensitive to Re as well as to equivalence ratio. The LBO limit was found to be mainly a function of equivalence ratio while being nearly independent of the Reynolds number, whereas the occurrence of flashback showed distinct characteristics for different ranges of the Reynolds number.

A. A. Subash was responsible for this paper, planned the experiment, built the setup, post processed the results of chemiluminescence and PLIF, and prepared the manuscript. I participated in all the experimental campaign, helped A. A. Subash building the setup, acquired the data and was involved in the discussion and revision process. S. Yu did the LES for analysis of the vortex breakdown structures under non-reacting conditions in this paper and wrote the simulation part of the paper. The discussion on simulation part was corrected by M. Bertsch, R. Z. Szasz and X. S. Bai. All co-authors contributed to the rebuttal and the revision process of this paper.

Paper III

X. Liu, M. Bertsch, A. A. Subash, S. Yu, R. Z. Szasz, Z. S. Li, X. S. Bai, M. Aldén and D. Lörstad, "Investigation of turbulent premixed methane/air and hydrogen-enriched methane/air flames in a laboratory-scale gas turbine model combustor", *Accepted for publication in International Journal of Hydrogen Energy*

In this paper, hydrogen-enriched (0/25/50% in volume) methane/air premixed flames were investigated in a gas turbine model combustor under atmospheric conditions. The flame operability ranges were mapped at different Reynold numbers (Re), showing the dependence on Re and H_2 concentrations. The effects of equivalence ratio (ϕ), Re, and H_2 enrichment on flame structures were examined

employing OH-PLIF measurement. For CH_4/air cases, the M-shaped flame was stabilized; while for H_2-enriched cases, the flame transitions to a Π shape above a certain ϕ. This transition was observed to influence significantly the flashback limits. Flow fields of CH_4/air flames were compared between low and high Re cases employing high-speed PIV. By high-speed OH chemiluminescence imaging, the flashback events led by two mechanisms were observed. It was found that the flashback driven by combustion-induced vortex breakdown occurred only for CH_4 flames with M shape, whereas the boundary-layer flashback occurs for all H_2-enriched flames with Π shape.

As the first author of this paper, I planned this experiment with A. A. Subash, built the setup and conducted all the measurements. I mapped the stabilization regime for the three fuels, post-processed the results of PIV and OH chemiluminescence, and prepared the manuscript. A. A. Subash was responsible to this paper, helped building the setup, did the Abel inversion of the image and post-processed the PLIF data. M. Bertsch participated in all the experimental measurement, prepared the operation conditions, calculated the laminar flame speed, and prepared the statistical analysis for the two types of flashback event. R. Z. Szasz and X. S. Bai contributes to the analysis and discussion on the results. All co-authors were involved in the revision process.

Paper IV

Q. S. Fan, **X. Liu**, A. A. Subash, C. Brackmann, M. Aldén, X. S. Bai and Z. S. Li, "Experimental investigation of large-scale ammonia/air premixed flames under different turbulent intensity", *Manuscript to be submitted.*

In this paper, the combustion characteristics of premixed ammonia/air flames with power generation up to 39 KW at extremely turbulent conditions are presented. Simultaneous planar laser-induced fluorescence (PLIF) imaging of nitrogen monohydrate (NH) and hydroxyl (OH) radicals were performed to investigate the local flame structure and Laser Doppler Anemometry (LDA) measurement acted as a complement extracting relevant turbulent quantities from the complex flow field. An overall layout of completed flames was captured by the OH-PLIF to evaluate the turbulent burning velocity. Two methods based on linear density and volume density were taken to evaluate the effect of the flame front wrinkles on the propagation speed of the turbulent flames. All the selected cases are located in the regime of the thin reaction zone (TRZ) and distributed reaction zone (DRZ) with the maximum Karlovitz number (Ka) and turbulence levels (u'/S_L) equal to 720 and 201, respectively. The NH layer remains thin and continuous over a wide range of turbulent intensities and the thickness keeps constant statistically without any significant broadening by turbulent eddies. Spatial correlations of the NH and OH

radicals show that overlap always existed in a slim region where OH has a weaker signal intensity. The global consumption speed was obtained from the mean progress variable using OH contours and the ratio of turbulent to laminar burning velocity (S_T/S_L) shows a monotonous increase with the turbulence levels. The result of the area ratio (A_T/A_L) indicates that the increase of the turbulent burning velocity is mainly contributed to the enhanced turbulent diffusivity in the preheat region rather than the extended burning area caused by turbulent wrinkles at high Ka levels.

I planned this experimental campaign, built the experimental setup and conducted all the measurements together with Q. S. Fan. I was also involved in the discussion and analysis on the experimental results. Q. S. Fan post-processed the results of LDA and simultaneous NH-/OH-PLIF measurement and prepared the manuscript. C. Brackmann helped aligning the dye laser for the NH-PLIF measurement. X. S. Bai was responsible to this paper. X. S. Bai and Z. S. Li supervised this work. All co-authors helped correcting the writing.

Paper V

X. Liu, A. A. Subash, Y. P. Bao, T. Hurtig, Z. S. Li, A. Ehn, J. Larfeldt, D. Lörstad, T. Nilsson and C. Fureby, "Experimental investigation of plasma discharge effect on swirl flames at a scaled Siemens Dry Low Emission burner", *In Proceedings of the AIAA SciTech Forum, 2021.*

In this work, the effect of a Rotating Gliding Arc (RGA) plasma discharge on the flame in a scaled Siemens Dry Low Emission (DLE), SGT-750, burner was experimentally investigated under atmospheric combustion conditions. The central pilot section of the burner, named RPL (rich pilot lean), was redesigned with an integrated high voltage electrode to generate an RGA. The exhaust gas was sampled and analysed in terms of CO and NO_x emissions, and the CO emission data show that the RGA extends the lean blow-out limit (LBO). High-speed OH chemiluminescence imaging was employed to understand the transient behaviour of the flame in both conditions with and without RGA and also to study the process of flame re-stabilization by the assistance of the RGA. A flame kernel, initiated around the RGA channel, was observed to play an important role in the re-stabilizing process of the flame. Although the NO_x emission for the flame with RGA was found to be higher than that without RGA, it was still less than what previous data show for operating conditions with the RPL flame.

I contributed to building the experimental setup with A. A. Subash, participated in all the experimental measurements, post-processed the OH-chemiluminescence and combustion emission results, and prepared the manuscript and most of the figures. I was also involved in planning this experimental campaign with A. Ehn and A. A.

Subash. A. Ehn was responsible to this paper, supervised the campaign with C. Fureby, and prepared the high voltage electrode inside the burner section with T. Hurtig. Y. P. Bao built the setup for optical emission measurement, post-processed the spectra results and prepared the discussion on the spectra results in the manuscript. All co-authors were involved in the revision process.

Paper VI

A. A. Subash, **X. Liu**, Y. P. Bao, T. Hurtig, A. Ehn, J. Larfeldt and C. Fureby, "Experimental investigation of the influence of plasma discharge on flame characteristics at a Siemens Dry Low Emission industrial burner under atmospheric conditions", *Manuscript to be submitted.*

The current work presents results of experimental investigations performed to study the influence of a rotating gliding arc (RGA) discharges on swirl-stabilized methane (CH4) flames in a Siemens dry low emission (DLE) combustor under atmospheric conditions. The RPL section in the burner was redesigned with integrated electrodes to generate RGA discharges (having average powers of 75-82 W) for investigating the interaction between discharges and the main flame in the combustor. The discharges in the RPL were generated by injecting air and oxygen (O_2) to observe their effect on the plasma formation and flame stabilization. How the discharge impacts on the flame stabilization, LBO, and flame dynamics were investigated employing planar laser-induced fluorescence (PLIF) of OH radicals and high-speed imaging of OH chemiluminescence. Results indicate that the position and shape of the flame were significantly affected by the RGA discharges and injection of air/O_2. The lean blowout performance was improved by the assistance of RGA. This improvement was more apparent for injecting O_2 as compared to the air case. The emission of NO_x was increased by the plasma discharge in both air and O_2 cases and this increase was higher for the air cases. However, the emission is still well below the level observed standard operation when the RPL flame being used to stabilize the main flame.

I took part in the preparation of the experimental campaign, built the setup with A. A. Subash, participated in all the measurements and post-processed the results of the CO and NO_x emission. A. A. Subash planned this campaign with me and A. Ehn, post-processed the OH-PLIF and OH-chemiluminescence results, conducted the flame dynamics analysis and prepared the manuscript. Y. P. Bao operated the electric power supply equipment, built two kinds of the optical emission measurement setup, processed the spectra results, and prepared the discussion on it in the manuscript. A. Ehn was responsible to this paper, supervised this campaign with C. Fureby, and designed the high voltage electrode part assembling in the modified burner with T. Hurtig. All co-authors contributed to the revision process.

Paper VII

X. Liu, A. A. Subash, Q. S. Fan, C. Brackmann, J. Evers, M. Aldén and Z. S. Li, "Visualization of turbulent inverse diffusion flames at elevated pressure using OH-PLIF and OH^* chemiluminescence imaging", *In Proceedings of the 9th European Combustion Meeting, 2019.*

In this paper, a co-axial inverse jet burner was installed and tested in the high-pressure combustion rig (HPCR) at Lund University to investigate the characteristics of methane/air inverse diffusion flames (IDF) at elevated pressure. OH-PLIF and OH^* chemiluminescence imaging were employed to capture the instantaneous flame image. Flames were stabilized with a fixed fuel velocity (Vf) of 0.3m/s and flow rate of the co-flow air, while varying either the air to fuel velocity ratio (Vr) from 200 to 600, increase the inner air jet velocity or the pressure in the combustion chamber from 2bar to 5bar. The effect of pressure on the flame front structure and flame lift-off height are analyzed from single-shot and averaged OH-PLIF image. Results indicate that the inner flame structure changed with pressure. With same Vf and Vr, more wrinkles and larger curvature of the flame front were found in the inner flame structure at higher pressure. The effect of Vr on the flame front structure and overall flame shape were also observed. Wrinkles and flame front area were found to increase as Vr increased, by increasing the air jet velocity with a fixed Vf corresponding to a higher turbulence intensity. Moreover, the flame shape became narrower as Vr increased for a constant pressure.

I planned this experiment, built the setup, conducted all the measurements, post-processed the data and prepared the manuscript. A. A. Subash provided help in the preparation of the experimental setup and in the data processing. C. Brackmann helped aligning the dye laser for the OH-PLIF measurement. Q. S. Fan participated in the measurement and the result discussion. J. Evers was the engineer who is responsible to the high-pressure rig and helped operating the rig. Z. S. Li supervised this work and the writing of the manuscript.